Ricardo Miguel Tomás do Couto
Mestre em Biotecnologia

Development of Integrated Separation Processes with Green Solvents

Dissertação para obtenção do Grau de Doutor em
Química Sustentável

Orientador: Pedro Calado Simões, Professor Auxiliar,
Universidade Nova de Lisboa
Co-orientador: Susana Barreiros, Professora Associada,
Universidade Nova de Lisboa
Co-orientador: Rui Ruivo, Investigador Doutorado,
Universidade Nova de Lisboa

Júri:

Presidente: Prof. Doutora Ana Isabel Aguiar-Ricardo
Arguentes: Prof. Doutor Haiko Hense
Prof. Doutor Henrique Aníbal Santos de Matos
Prof. Doutor Carlos Alberto Mateus Afonso

Vogais: Prof. Doutor Pedro Miguel Calado Simões
Prof. Doutora Susana Filipe Barreiros
Doutor Rui Manuel Ruivo

FACULDADE DE CIÊNCIAS E TECNOLOGIA
UNIVERSIDADE NOVA DE LISBOA

Dezembro 2012

Development of Integrated Separation Processes with Green Solvents

Agradecimentos

Chegada a hora dos agradecimentos, tenho obrigatoriamente de começar por agradecer aos meus orientadores, que sempre me apoiaram e acreditaram em mim, Prof. Pedro Simões, Profª. Susana Barreiros e Dr. Rui Ruivo. Um muito obrigado muito especial por tudo o que me ensinaram.

Ao Dr. Luís Branco, por toda a ajuda nas medições de polaridades de líquidos iónicos e pela colaboração que conseguimos estabelecer, que continua ainda a dar frutos e se estende para lá do âmbito desta tese.

À Tânia Carvalho, que foi uma ajuda preciosa na preparação das primeiras membranas de Ion-Jelly®, e a quem devo um grande agradecimento.

Ao João Fernandes, meu colega de gabinete que me passou o testemunho de aluno de doutoramento do Prof. Pedro Simões, e com quem tive também oportunidade de aprender muitos conceitos de engenharia química.

E ao Pedro Lisboa, a quem passo agora o testemunho de aluno de doutoramento do Prof. Pedro Simões com muito gosto. Foi com muito prazer que no início ensinei e mais tarde partilhei todas as ideias malucas que fomos tendo. Parabéns pela instalação da unidade piloto! (Quando é que começamos a produção de cerveja?).

A todos os alunos que foram passando pelo laboratório e foram deixando contributos valiosos para os diversos trabalhos: Beatriz Afonso, Anabela Santos, Filipe Calixto, Tiago Reis, Murilo Nascimento, Elvis Ramos.

Ao Pedro Vidinha, que me iniciou no mundo dos supercríticos e me contagiou com o entusiasmo pela ciência.

Ao Alexandre Paiva, companheiro de laboratório e de aventuras. Temos de inventar uma nova aventura em breve!

Aos "colegas do lado", presentes e passados, com quem vamos partilhando espaço e ferramentas: Teresa Casimiro, Márcio Temtem, Mara, Eunice, Telma, Rita Restani, Vanessa, Raquel, Ana Paninho, Anita, etc… de certeza que me estou a esquecer de alguém!

A todas as pessoas do 427 que ainda não mencionei: Sílvia Rebocho, Rita Rodrigues, Rita Craveiro, Diana Garcia, Andreia Pimenta, Carmen Montoya e vários outros que por lá foram passando.

À Catarina Pereira e Ana Pereira pelas pausas para café nos últimos tempos.

À Fundação para a Ciência e Tecnologia, pela bolsa de doutoramento SFRH/BD/36618/2007.

Ao meu agrupamento de escuteiros, Agrupamento 337 – Caldas da Rainha, com quem muito aprendi, e que é sempre um prazer acompanhar ao longo de todos estes anos a dar pontapés no im do impossível.

Aos meus amigos de sempre, Filipe Ramires, João Pedro Gomes, André Pontes, Ricardo Barata, Vanessa Nascimento, João Lopes, Ana Lucena, Leonardo Mendes, Diana Fernandes, Vítor Silva, etc., etc.

À minha família, por ser uma Família e estar lá sempre que preciso. E à minha avó, que já não me vê Doutor…

Resumo

Esta tese explora o fraccionamento de misturas com solventes não convencionais, como dióxido de carbono supercrítico ($scCO_2$) e líquidos iónicos à temperatura ambiente (RTILs), e desenvolve novos processos integrados que acoplam estes solventes com membranas.

Explorou-se a possibilidade de usar membranas de osmose reversa para fraccionamentos em $scCO_2$ com uma mistura modelo de ácido oleico e esqualeno. Todas as membranas testadas foram selectivas para o ácido oleico. Testou-se o efeito de acoplar a membrana a um processo de extracção supercrítica tendo-se atingido um enriquecimento combinado de 1.6 vezes.

Os RTILs foram usados para fraccionar a mistura modelo de ácido oleico e esqualeno. Escolhendo adequadamente o anião e catião do RTIL é possível modelar o fraccionamento. Com [EMIM][$MDEGSO_4$] a selectividade para ácido oleico foi 2.96 e com [BMIM][NTf_2] foi de 0.86. Desenvolveu-se um método indirecto de sondar as polaridades dos RTILs usando solventes orgânicos comuns e o corante de Reichardt, permitindo a construção de uma escala de polaridades. Mostrou-se que os RTILs mais polares têm menores selectividades para o ácido oleico.

Desenvolveram-se membranas suportadas de líquidos iónicos e aplicaram-se no fraccionamento de misturas modelo. Estas membranas apresentaram selectividades negligenciáveis no fracionamento da mistura modelo de ácido oleico e esqualeno, mas apresentaram bons resultados no fraccionamento dos produtos e reagentes de uma reacção de transesterificação, retendo completamente o glicerol e produzindo um permeado com uma fracção mássica de ésteres metílicos de 0.85.

Desenvolveu-se um novo tipo de membranas de gel, usando gelatina como polímero de suporte para RTILs. Apesar de estas membranas não serem capazes de fraccionar a mistura modelo de ácido oleico e esqualeno, foram capazes de atingir um factor de separação de ésteres metílicos em relação ao glicerol numa reacção de transesterificação de 166. Estas membranas foram também testadas na separação de gases, mas as selectividades obtidas foram muito baixas.

Palavras Chave: CO_2 Supercrítico, Líquidos Iónicos, Membranas, Processos Verdes, Integração de Processos, Ion-Jelly®

Abstract

This thesis explores the fractionation of mixtures with unconventional solvents, like supercritical carbon dioxide ($scCO_2$) and room temperature ionic liquids (RTILs), and develops new integrated processes which couple these solvents with membranes.

It was explored the feasibility of using reverse osmosis membranes for fractionations in $scCO_2$ with a model mixture of oleic acid and squalene, and it was found that all membranes tested were selective towards oleic acid. The effect of coupling the membrane to a supercritical fluid extraction (SFE) process was also tested, achieving a combined enrichment in squalene of 1.6 times.

RTILs were used to fractionate the model mixture oleic acid and squalene. By appropriately choosing the anion and cation of the RTIL it was possible to model the fractionation. With [EMIM][$MDEGSO_4$] a selectivity towards oleic acid of 2.96 was achieved, and with [BMIM][NTF_2] the selectivity was 0.86.

An indirect method of probing the polarities of RTILs is developed using common organic solvents and Reichardt's dye and a polarity scale is built. It was found that the most polar RTILs have lower selectivities towards oleic acid.

Supported ionic liquid membranes were developed and applied in the fractionation of model mixtures. These membranes had negligible selectivities for fractionating the model mixture of oleic acid and squalene, but presented good results when fractionating the products and reactants of a transesterification reaction, retaining completely glycerol and producing a permeate with 0.85 mass fraction of methyl esters.

A new type of gel membranes was developed, using gelatine as a support polymer for RTILs. Although these membranes were not able to fractionate the model mixture of oleic acid and squalene, they were able to achieve a separation factor of methyl esters in detriment of glycerol of 166. These membranes were also tested for the separation of gases, but the selectivities obtained were very low.

Keywords: Supercritical CO_2, Ionic Liquids, Membranes, Green Processes, Process Integration, Ion-Jelly

Table of Contents

Figures Index

Tables Index

Abbreviations List

$\alpha_{i/j}$ – Selectivity of component *i* over component *j*

β – Geometric parameter

Δl – Change in length

ΔP – Pressure drop

ε - Strain

$\mu_{i/j}$ – Number of moles of component *i* per number of moles of component *j*

µL - Microliter

µm – Micrometer

λ_{max} - Wavelength of the maximum of the long-wavelength

$\tilde{\nu}_{max}$ – Wavenumber

σ – Stress

A – Cross-sectional area

A – Membrane area

A^+ - Generic cation

Å - Angstrom

AC – Cellulose acetate membrane

ACN - Acetonitrile

AD – Polyamide AD membrane

[ALIQUAT] – Tri-octyl-methyl-ammonium

[BDMIM] - 1-butyl-2,3-dimethyl-imidazolium

BES - 2-[N,N-bis(2-hydroxyethyl)amino]ethanesulfonate

[BF_4] – Tetrafluroborate

[BMIM] - 1-butyl-3-methyl-imidazolium

[BMPyr] - 1-butyl-3-methylpyrrolidinium

BPR - Back Pressure Regulator

c (page 50) – Speed of Light

C (page 47) - Concentration

ºC – Celsius Degree

[C_2] - (2-hydroxyethyl)-ethyl-dimethyl-ammonium

[C_2OHMIM] - 1-(2-hydroxyethyl)-3-methyl-imidazolium

[C_3OMIM] – 1-(2-Methoxyethyl)-3-methyl-imidazolium

[C_5O_2MIM] - 1-[2-(2-Methoxyethoxy)-ethyl]-3-methyl-imidazolium

[$(C_6)_3C_{14}$P] - Trihexyl-tetradecyl-phosphonium

[C_{10}MIM] - 1-decyl-3-methyl-imidazolium

C14:0 – Myristic acid

C16:0 – Palmitic acid

C16:1 – Palmitoleic acid

C18:0 – Stearic acid

C18:2 – Linoleic acid

ca. – circa

CH_4 - Methane

$CHCl_3$ – Chloroform

CHES - 2-(Cyclohexylamino)-ethanesulfonate

[Cl] - Chloride

cm – Centimeter

cm^2 – Square centimeter

cm^3 – Cubic centimeter

CO_2 – Carbon dioxide

CT – Charge transfer

CV*i* - Check-Valves

Da – Dalton

[DCA] – Dicyanamide

[DMG] - Dimethylguanidinium

[EMIM] - 1-ethyl-3-methyl-imidazolium

$E_T(30)$ – Reichardt's empirical scale of solvent polarity

E_T^N – Normalized scale of solvent polarity

EtOH - Ethanol

[$EtSO_4$] - Ethylsulfate

EPV - Electro-Pneumatic Valve.

F – Applied force

FID – Flame ionization detector

g - Gram

GC – Gas chromatography

h – Planck's constant

H_2 - Hydrogen

HPLC – High performance liquid chromatography

I.D. – Internal diameter

i.e. – *id est*; in other words

IJ – Ion-jelly

IL – Ionic liquid

i-PrOH - isopropanol

IUPAC – International Union of Pure and Applied Chemistry

K –Kelvin Degree

K_D – Partition coefficient

KPa – Kilopascal

l – Membrane thickness

L - Length

m – Meter

m^2 – Square meter

m^3 – Cubic meter

[$MDEGSO_4$] - 2-(2-methoxyethoxy)-ethylsulfate

MFM - Mass flow meter

mg - Milligram

min - Minute

mL - Milliliter

mm – Millimeter

mM – Millimolar

MO – Methyl oleate

mol – Moles

MOPSO - 2-hydroxy-3-(4-morpholino)propanesulfonate

MPa – Megapascal

[MSO_4] – Methanesulfonate

N – Newton

N_2 - Nitrogen

N_A – Avogadro's constant

nm - nanometer

[NTf_2] - Bis(trifluoromethylsulfonyl)-imide

O_2 - Oxygen

OA – Oleic acid

[OMIM] - 1-octyl-3-methyl-imidazolium

P – Membrane permeability

Pa - Pascal

[PF_6] – Hexafluorophosphate

p_{feed} – Pressure in the feed compartment

PI - Pressure Indicator

P_{perm} – Pressure in the permeate compartment

PTI - Pressure and Temperature Indicator

PTV – Programmed temperature vaporizing

R – Generic substituent

Ref. - Reference

RO – Reverse Osmosis

RTIL – Room temperature ionic liquid

s - Second

$scCO_2$ - Supercritical carbon dioxide

SEM – Scanning electron microscopy

S/F – Solvent-to-feed mass flow ratio

SFE – Supercritical fluid extraction

SG – Thin-Film SG membrane

SILM – Supported ionic liquid membrane

SQ – Squalene

t - Time

THF - Tetrahydrofuran

TMS - Tetramethylsilane

TUHH - Technische Universität Hamburg-Harbug

UV/Vis – Ultraviolet/Visible

V*i* - Valves

V_{feed} – Volume of the feed compartment

Vol. – Volume

V_{perm} – Volume of the permeate compartment

vs. - Versus

wt% - Weight percent

w/w – Weight per weight

X^- - Generic anion

$X_{i/j}$ – Mole fraction of component *i* in component *j*

Chapter 1

Introduction

1.1 Thesis Outline

This thesis explores the fractionation of mixtures with unconventional solvents, like supercritical carbon dioxide ($scCO_2$) and room temperature ionic liquids (RTILs), and develops new integrated processes which couple these solvents with membranes.

In Chapter 1 is given a general introduction to the main themes discussed in this thesis. It starts with the characteristics of one of the main solvents, $scCO_2$, and a brief state of the art of applications of $scCO_2$ is also given. The main separation process, membrane separation, is also explained, and the previous applications of membranes in $scCO_2$ are explored. It follows with the other main class of solvents, RTILs. Their characteristics and applications are reviewed, as well as a brief overview of some of the applications in $scCO_2$. And finally, the Introduction ends with a state of the art of the recent developments in supported ionic liquids membranes (SILMs) and gel membranes.

In Chapter 2 is explored the feasibility of using reverse osmosis membranes for fractionations in $scCO_2$. The influence of pressure, temperature and pressure drop across the membranes in the permeability of the membranes is tested. Next, these are tested for the fractionation of a model mixture of oleic acid and squalene in $scCO_2$. The effect of coupling the membrane to a supercritical fluid extraction (SFE) process is also tested.

Chapter 3 and 4 explore the characteristics of RTILs and their ability to fractionate mixtures, which would otherwise be difficult to separate. In Chapter 3 RTILs are used to fractionate the same model mixture used in Chapter 2, and in Chapter 4 an attempt to build a polarity scale of RTILs is made as a way of rationalising and explaining the results obtained in Chapter 3.

Finally, the knowledge obtained in the previous Chapters is used in Chapter 5 to develop SILMs and apply them in $scCO_2$ in the fractionation of the model mixture tested in Chapters 2 and 3. Due to the poor results obtained in this attempt, a new type of gel membranes was developed, using gelatine as a support polymer for RTILs. These new membranes are tested in $scCO_2$ for the fractionation of the model mixture of oleic acid and squalene and for the fractionation of products and reagents of a transesterification reaction. Furthermore, these membranes are also tested for the separation of gases.

This thesis concludes with Chapter 6, which includes the general conclusions of the thesis and several possibilities of future work.

1.2 - Supercritical Fluids

In August 12, 1822, Baron Cagniard de la Tour described for the first time an experiment where he would heat a fluid far beyond its boiling point, inside a closed vessel. He introduced alcohol at 36º in a cannon barrel and a silex sphere, and sealed it. By gradually heating it, and making the sphere roll back and forth inside the barrel, he could listen to the sound the sphere would make at different temperatures. At first, he would hear the splashing sound that the sphere would make when traversing the liquid-vapour interface, but when the temperature would rise enough, that sound would disappear. And thus, the critical point of a substance was for the first time acknowledged [1].

A pure component is considered to be in a supercritical state if its temperature and its pressure are higher than the critical values, which for carbon dioxide, the supercritical fluid used in this work, are 304.15 K and 7.38 MPa, respectively [2].

At critical conditions for pressure and temperature, there is no sudden change of component properties. This is depicted in Figure 1.1 by the broken line. The variation of properties with conditions of state is monotonous, when crossing the broken line, with the exception of the critical point itself [2].

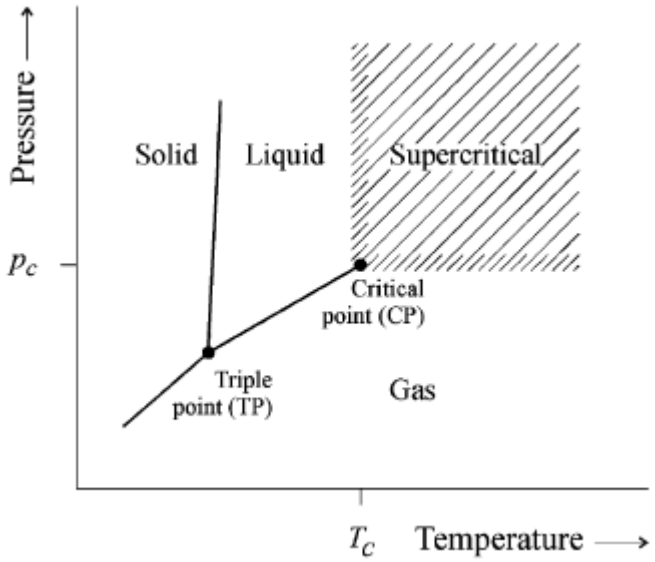

Figure 1.1 – Generic phase diagram of a common pure substance, including the supercritical region. CP: critical point, TP: triple point, T_c: critical temperature, P_c: critical pressure [2].

Supercritical carbon dioxide ($scCO_2$) has been widely studied and applied in a range of processes, from separations [3], to reaction medium [4], [5], and even as a building block in reactions [6].

1.2.1 – Fractionations with Supercritical Carbon Dioxide

Extraction of compounds from natural sources is the most widely studied application of supercritical fluids (SCFs) with several hundreds of published scientific papers. Indeed, SFE has immediate advantages over traditional extraction techniques: it is a flexible process due to the possibility of continuous modulation of the solvent power/selectivity of the SCF, allows the elimination of polluting organic solvents and of the expensive post-processing of the extracts for solvent elimination. Carbon dioxide is the most popular SFE solvent because it is safe, readily available and has a low cost. It allows supercritical operations at relatively low pressures and near-room temperatures. The only serious drawback of SFE is the higher investment costs if compared to traditional atmospheric pressure extraction techniques. However, the base process scheme (extraction plus separation) is relatively cheap and very simple to be scaled up to industrial scale [3].

SFE of solids is the most studied application since the most frequently required separation process is the extraction/elimination of one or more compound families from a solid natural matrix [3]. Some examples include the extraction of lipids from cyanobacteria [7], extraction of essential oils from plants [8], [9], extraction of lycopene from tomatoes [10] and the decaffeination of coffee [11]. It has been carried out in a commercial scale for more than three decades, in processes like the decaffeination of coffee beans and black tea leaves and the production of hop extracts [3].

1.3 - Membranes

In a membrane process, a stream is fed into the membrane, where it is divided into a retentate and a permeate stream (Figure 1.2). In this process, either retentate or permeate streams could be the product of interest, depending on the objective of the separation. If the objective is to concentrate a product, then the retentate is the stream of interest, but if the objective is to purify one of the components of the mixture, then both retentate or permeate streams could yield the product of interest [12].

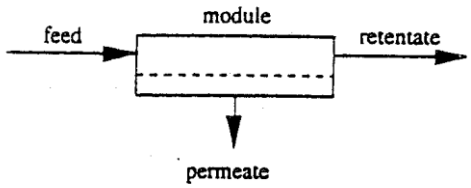

Figure 1.2 – Schematic representation of a membrane process [12].

A membrane process can also be seen as a barrier (the membrane) separating two phases, where transference of some compounds can occur from one phase to the other (Figure 1.3).

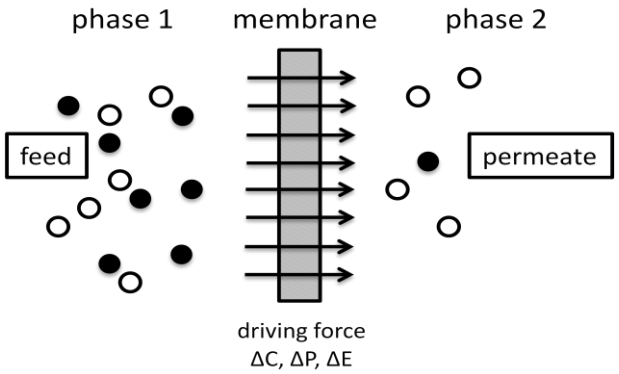

Figure 1.3 – Schematic representation of a two-phase system separated by a membrane (adapted from [12]).

The performance or efficiency of a membrane is defined by two parameters, the selectivity and the flow through the membrane. The latter is defined as the volume flowing through the membrane per unit of time. Volume flow can also be easily converted to mass or mole flow. The selectivity of the membrane can be represented by the retention factor (R) or the separation factor (α). The retention factor is given by:

$$R = \frac{C_f - C_p}{C_f} = 1 - \frac{C_p}{C_f} \tag{1.1}$$

Where C_f is the concentration of the solute in the feed phase and C_p is the concentration of the solute in the permeate phase. R is a dimensionless factor, and varies from 0% (no retention) to 100% (full retention). The separation factor is given by:

$$\alpha_{i/j} = \frac{y_i/x_i}{y_j/x_j} \tag{1.2}$$

with $y_{i,j}$ and $x_{i,j}$ the mass fraction of component i, j in the permeate and retentate streams, respectively. When the separation factor is greater than 1, the selectivity is towards component i, and when it is lower than 1, the selectivity is towards component j. If $\alpha = 1$, then there is no separation [12].

Membranes can be classified according to their morphology, or according to the separation which is possible to achieve with it. According to morphology, membranes can be symmetric or asymmetric. If they are symmetric, they can be homogeneous (non-porous) or heterogeneous

(porous). If they are asymmetric, then they are generally made from a very dense and thin top layer, supported by a porous and thicker layer. This combination allows to achieve the high selectivity of the dense layer with the high permeability of the porous layer [12].

The range of particle sizes that can permeate the different kinds of membranes are summarized in Table 1.1.

Table 1.1 – Range of permeations possible to obtain according to particle size, for different membranes. (Adapted from [13]).

Membrane	Particle Size Range
Particle Filtration	> 1 µm
Microfiltration	0.1 – 10 µm
Ultrafiltration	< 0.1 µm – 5 nm
Nanofiltration	≈ 1 nm
Reverse Osmosis	< 1 nm
Electrodialysis	< 5 nm
Dialysis	< 5 nm

1.3.1 - Applications in Supercritical Carbon Dioxide

One of the greatest advantages of using membranes with supercritical fluids is that separations can be made without pressure loss. Otherwise, CO_2 would have to be decompressed in order for solutes to precipitate, with major energy losses associated.

The association of a membrane to the supercritical fluid extraction process was already suggested by several authors. Three kinds of potential applications have been studied: (i) solvent recovery after SFE extraction step; (ii) carbon dioxide extraction coupled with cross-flow or countercurrent-flow filtration; (iii) fractionation of solutes. Semenova *et al.* [14] studied the separation of $scCO_2$ and ethanol mixtures with an asymmetric polyimide membrane and obtained a separation factor ($\alpha_{ethanol/CO2}$) of 8.7. For the separation of $scCO_2$ / iso-octane mixtures, a separation factor of 12.8 was obtained by Ohya *et al.* [15]. Sartorelli *et al.* [16] used two different inorganic membranes to separate low volatile compounds from $scCO_2$ extracts. Retention factors between 80 to 90 % were obtained; the main point to control is, according with the authors, the mechanical stability and chemical resistance to carbon dioxide of the membrane to be used. Pietsch *et al.* [17] proposed to use a reverse osmosis membrane to recover caffeine from a high pressure decaffeination process.

Regeneration of $scCO_2$ from caffeine loaded gas phases was achieved by commercial nanofiltration membranes, with a ZrO_2-TiO_2 thin layer [18], and later with silica and microporous silicalite membrane filters, obtaining a retention factor of 98% [19]. But a caffeine retention factor of 100% was possible to observe at a temperature of 308 K and a pressure equal to or lower than 12 MPa, with a microporous silicalite membrane [19]. Carlson *et al.* applied reverse osmosis membranes (thin layer SC membrane) to separate efficiently limonene (94 % retention factor) from $scCO_2$ extracts [20]. Reverse osmosis membranes have also been used to separate lemongrass essential oil from $scCO_2$ with a retention factor up to 90% [21], or polyphenols from $scCO_2$ after extraction from cocoa seeds with retention factors higher than 90% [22].

The use of hollow fiber microporous membrane contactors in supercritical fluid extraction processes has been reported in the literature [23]-[25]; improved mass transfer efficiency due to a reduced shell-side fiber bypassing is claimed by the authors. Sarrade *et al.* [26] proposed the coupling of $scCO_2$ extraction with nanofiltration separation to extract and purify low molecular weight compounds (up to 1500 Da). A nanofiltration tubular membrane resistant enough to endure supercritical conditions was applied to two different processes: (i) the fractionation of triglycerides from fish oil and (ii), the purification of β-carotene issued from either carrot oils or carrot seeds. The coupled process led to good quality extracts.

Goetheer *et al.* proposed to use an inorganic microporous membrane for the separation of catalyst from products in homogeneous catalysis in $scCO_2$, for the hydrogenation of 1-butene to n-butane, with a derivative of Wilkinson's catalyst [27]. And finally, two nanofiltration and one reverse osmosis membrane were studied for the purification of modified triglycerides, by retention of triglycerides and permeation of reaction subproducts (fatty acid esters and/or fatty acid lipids), achieving retention factors of triglycerides up to 100% [28].

1.4 – Room Temperature Ionic Liquids

Room temperature ionic liquids (RTILs) are salts which are liquid up to 373 K. The first example was described as early as 1914, ethylammonium nitrate, although for a long time this class of compounds was known as molten salts [29]. These can have organic or inorganic cations and anions. Some common examples are given in Figure 1.4

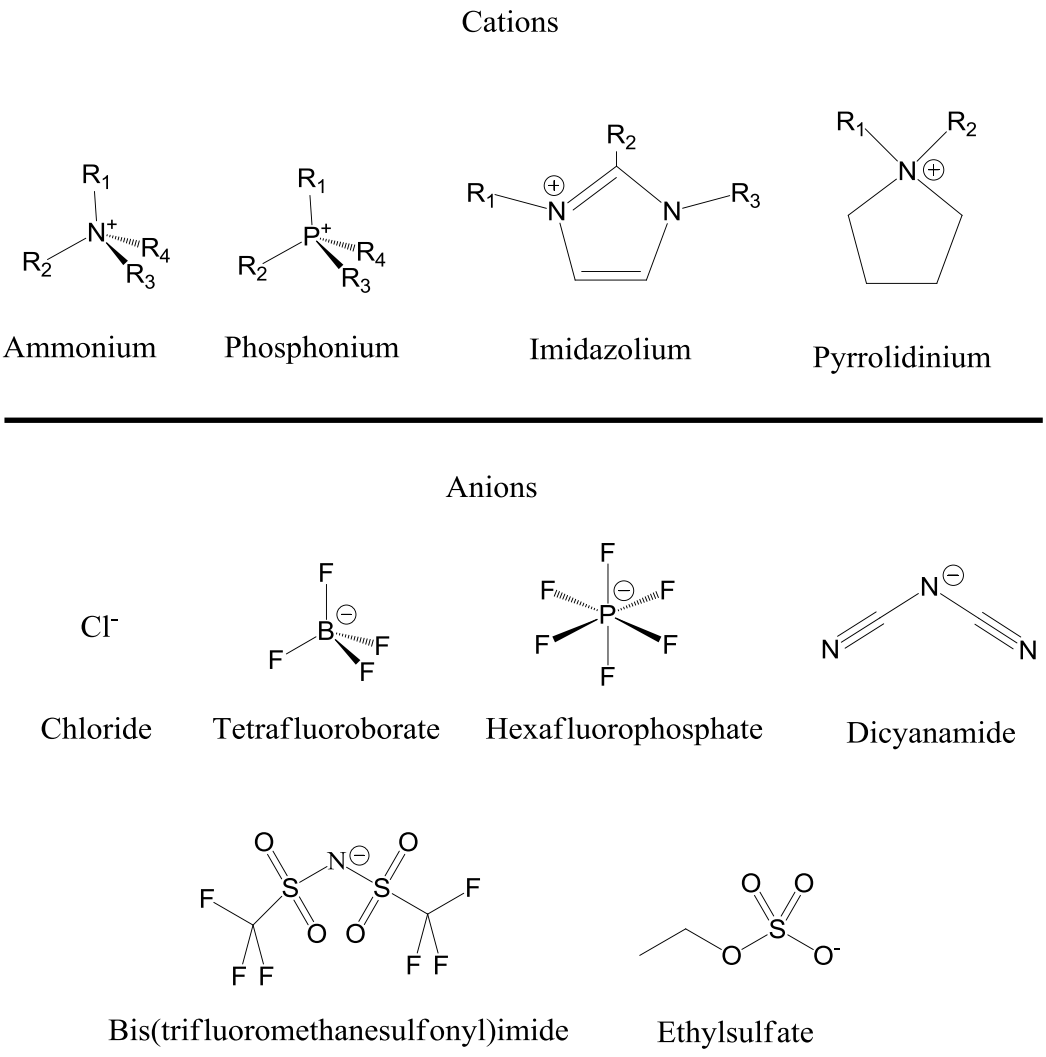

Figure 1.4 – Structures of some common ionic liquids cations and anions.

RTILs have proven to be effective in a large number of applications, ranging from extractions to reactions. In fact they have been used, for example, in the separation of olefins from paraffins [30], of several azeotropic mixtures [31], of poly- and disaccharides by means of an IL biphasic system [32], of alkali and alkaline earth cations [33] or in the separation of various gases [34]-[36]. In the field of extractions, they have been used pure in the extraction of free fatty acids from soybean oil [37], of biofuels and biofeedstocks from aqueous solutions [38], or in combination with other solvents, like an aqueous biphasic system (ABS), which uses both RTILs and a high charge-density inorganic salt (K_2CO_3) to extract lipolytic enzymes [39]. Special techniques can also be employed to improve the extraction efficiency of RTILs, for example, ultrasound-assisted extraction was successfully applied to the extraction of alkaloids [40]. Other applications include hydrolysis of cellulose and dissolution of its components [41], or the fabrication of electrolytes for lithium batteries [42].

Many studies have been made with ionic liquids and $scCO_2$. The phase equilibria for many systems has been determined, and it was found that, as a general rule, CO_2 has high solubility in RTILs, but RTILs are not soluble in $scCO_2$. This behavior renders it viable to use $scCO_2$ to extract solutes from RTILs [43]. It is also possible to purify RTILs by using $scCO_2$ extraction, which can remove water and organic impurities [44]. Other applications have also been explored, for example, RTILs have been used as effective solvents in extractive distillation for the separation of an azeotropic mixture containing tetrafluoroethylene and carbon dioxide [45]. Still another example is the combination of RTILs with $scCO_2$ as reaction mediums. This was accomplished for lipase catalysis, with RTILs stabilizing the enzyme and $scCO_2$ extracting the products of the reaction [46] and for continuous-flow rhodium-catalysed hydroformylation of long chain alkenes, achieving selectivities to the desired linear aldehyde of 92% and minimum rhodium loss, using a xantphos-derived ligand attached to an imidazolium salt [47].

1.5 – Supported Ionic Liquid Membranes and Gel Membranes

It has been recognized for a long time that RTILs have the potential to recover solutes or fractionate mixtures which are not easy to separate/fractionate with conventional solvents. The immobilization of RTILs in membranes, creating supported ionic liquid membranes (SILMs), has been developed as a way to facilitate the application of RTILs in industrial environments. SILMs have several advantages, allowing to operate with an extremely large specific membrane area (membrane area per unit volume) without dispersing the extractant in the feed phase; extraction and re-extraction take place simultaneously, involving a minimal amount of extractant, which is constantly regenerated and with the additional possibility of tuning the selectivity of the extractant phase to a defined solute by adequate selection of the solid supporting membrane [48].

One of the major applications studied for SILMs is the separation of gases. Very diverse pairs of ionic liquids and membranes have been tested. Imidazolium ionic liquids immobilized in Viton membranes achieved a separation factor for CO_2/CH_4 around 59 [49]. Nafion membranes with imidazolium ionic liquids achieved an ideal separation factor for CO_2/CH_4 of 26 [50]. The permeability of hydrogen (H_2), oxygen (O_2), nitrogen (N_2), and carbon monoxide (CO) was studied for 1-butyl-3-methylimidazolium ([BMIM]), 1-decyl-3-methylimidazolium ([C_{10}MIM]], trioctylmethylammonium ([$(C_8)_3$CN]) and octylpyridinium ([OPy]) cations with the anion bis(trifluoromethylsulfonyl)-imide ([NTf_2]) supported on nanofiltration membranes and the best selectivity of H_2/CO (5.5) was obtained for [BMIM][NTf_2] at 0.3 MPa [51]. A ceramic nanofiltration membrane with an immobilized silane functionalized ionic liquid was studied for the separation of CO_2 from CO, obtaining a separation factor of 25 at 323 K [52]. Imidazolium

RTILs supported in polyvinylidene fluoride porous membrane were used to separate CO_2 from N_2, being possible to achieve a separation factor of 86.5 with [BMIM][BF_4] at 303.15 K [53]. With imidazolium RTILs immobilized in polyethersulfone membranes, the best selectivities were found for the RTIL 1-ethyl-3-methylimidazolium trifluoromethanesulfone ([EMIM][CF_3SO_3]) (CO_2/N_2: 28; CO_2/CH_4: 16; SO_2/N_2: 337; SO_2/CH_4: 196) [53]. Also for imidazolium RTILs immobilized in polyethersulfone membranes, but now with fluoroalkyl substituents, the best selectivity it was possible to achieve was of 27 for the pair CO_2/N_2 [54]. The influence of anions trifluoromethanesulfone ([CF_3SO_3]), dicyanamide ([DCA]) and [NTf_2], in the separation of gases was studied with the cation [EMIM], and the best selectivities were obtained with [DCA] (CO_2/N_2: 61; CO_2/CH_4: 20) [55]. With ILs based in pyridinium and ammonium immobilized in α-alumina inorganic supports, the best selectivity was for the pair CO_2/CH_4 with a value of 30 for [BMPy][BF_4] [56].

The effect of increasing the alkyl chain length in 1-alkyl-3-methylimidazolium RTILs supported in polymeric membranes was investigated and it was found out that the permeability increases with increasing alkyl chain length, and also that permeability decreases with increasing viscosity. In this same study it was possible to obtain selectivities for the pairs CO_2/N_2 and CO_2/CH_4 of 32 and 161, respectively [57].

Camper *et al.* in 2006 developed a model to predict solubility of gases in imidazolium RTILs based on the molar volume of the RTILs and estimated gas permeability and gas pair separation selectivity for ideal CO_2/N_2 and CO_2/CH_4 separations. At the time, they concluded that there appears to be more potential for RTIL-based membranes in CO_2/N_2 separations than in CO_2/CH_4 [58]. In a later paper, Scovazzo summarized literature data and some new data for SILM permeabilities and selectivities for the gas pairs CO_2/N_2, CO_2/CH_4, O_2/N_2, ethylene/ethane, propylene/propane, 1-butene/butane, and 1,3-butadiene/butane, finding little room for improving the reported permeabilities, but some space for increasing the selectivities [59].

Other applications of SILMs include applications as diverse as separation of arsenate and arsenite from aqueous media [60], enzymatic synthesis in an active membrane using ionic liquids as catalyst support [61], removal of phenol from wastewater [62], vapor permeation of benzene/cyclohexane [63], transport of salicylic acid [64], or the removal of butan-1-ol from fermentation broths of *Clostridium acetobutylicum* in order to avoid the decrease of the population [65].

SILMs have also been used for the fractionation of organic compounds, for example, a porous polyvinylidene fluoride film membrane was used with a feed solution of heptanes and a receiving solution of hexadecane for the transport of aromatic hydrocarbons, benzene, toluene and p-xylene, with the best selectivity being obtained for benzene [66]. Víllora *et al.*, in a series of papers, started by showing that it was possible to fractionate the substrates and products of a transesterification reaction (vinyl butyrate, 1-butanol, butyl butyrate and butyric acid) through SILMs based on 1-n-alkyl-3-methylimidazolium cations combined with [BF_4], [PF_6] and [NTf_2] anions [67]. From this study, they found that the hydrophilic nature of ILs was a key parameter for the selective separation of those compounds, and thus developed new membranes based on a hydrophilic anion, dicyanamide, concluding that both the permeability of the compounds and the permselectivity of the membrane were enhanced with the use of dicyanamide based ionic liquids [68]. Then, they went on to study the permeability of sixteen different organic compounds (vinyl esters, aliphatic esters, alcohols and carboxylic acids) through SILMs containing [BF_4] based ionic liquids ([BMIM][BF_4] and [OMIM][BF_4]). It was found that permeability increased as the alkyl chain length decreased for the same organic functional group. In addition, significant permeability differences were found between the different organic functional groups [69].

Despite the fact that gel polymers with RTILs have been studied for some time to prepare electrolytes for lithium batteries [70], [71], it was only recently that they have been proposed as membranes for the separation of gases. The efforts in the development of gel membranes have been triggered by limitations of SILMs on the trans-membranes pressures that are possible to apply. In fact, it was demonstrated that trans-membrane pressures as low as 0.2 MPa can result in displacement of RTIL from SILMs [57].

Polymeric gel membranes have been prepared with addition of 20 to 80 wt.% of 1-butyl-3-methylimidazolium trifluoromethanesulfonate ([BMIM][CF_3SO_3]), to Pebax® 1657 and Pebax® 2533. Although permeability and selectivity of Pebax® 2533 are not notably affected by the addition of RTIL, Pebax® 1657 shows a significant increase in the gas permeability, but a slight decrease in the permselectivity for most gas pairs [72]. A series of cross-linked poly(vinylimidazolium)-RTIL gel membranes was synthesized and evaluated for ideal CO_2/N_2, CO_2/CH_4, and CO_2/H_2 room-temperature separation performance, and the effect of free RTIL ([EMIM][NTf_2]) loading on CO_2 separation performance was evaluated by varying RTIL loading at three levels (45, 65, and 75 wt. %). A higher loading of free RTIL increased CO_2 permeability dramatically, but had no effect on CO_2/N_2 or CO_2/CH_4 permeability selectivity. It had, however a significant improvement on CO_2/H_2 permeability selectivity [73]. A triblock copolymer self-assembled in CO_2-selective RTILs (poly(styrene-block-ethylene oxide-block-

styrene)) was synthesized and used with three RTILs based in the 1-n-hexyl-3-methylimidazolium ([HMIM]) cation and [NTf_2], [BF_4], and [PF_6] anions. The ideal CO_2/CH_4 separation factors were studied and ranged from 9.0 to 9.9 [74].

To the best of our knowledge, this work proposes for the first time the application of either SILMs or gel membranes in $scCO_2$.

1.6 – References

[1] C. de la Tour; Exposé de quelques résultats obtenus par l'action combinée de la chaleur et de la compression sur certains liquides, tels que l'eau, l'alcool, l'éther sulfurique et l'essence de pétrole rectifiée; Ann. Chim. Phys. 21, (1822) 127-132.

[2] G. Brunner, Gas Extraction, Springer, Berlin, 1994.

[3] E. Reverchon, I. De Marco; Supercritical Fluid Extraction and Fractionation of Natural Matter; J. of Supercritical Fluids 38 (2006) 146-166.

[4] H. Taher, S. Al-Zuhair, A. Al-Marzouqi, Y. Haik, M. Farid; A Review of Enzymatic Transesterification of Microalgal Oil-Based Biodiesel Using Supercritical Technology; Enzyme Research Volume 2011, Article ID 468292, doi:10.4061/2011/468292

[5] R. Couto, P. Vidinha, C. Peres, A. Ribeiro, O. Ferreira, M. Oliveira, E. Macedo, J. Loureiro, S. Barreiros; Geranyl Acetate Synthesis in a Packed-Bed Reactor Catalyzed by Novozym in Supercritical Carbon Dioxide and in Supercritical Ethane; Ind. Eng. Chem. Res. 2011, 50, 1938–1946.

[6] V. Bonifácio, V. Correia, M. Pinho, J. Lima, A. Aguiar-Ricardo; Blue emission of carbamic acid oligooxazoline biotags; Materials Letters 81 (2012) 205–208.

[7] Mendes, R. L.; Reis, A. D.; Palavra, A. F.; Supercritical CO_2 extraction of c-linolenic acid and other lipids from Arthrospira (Spirulina)maxima: Comparison with organic solvent extraction; Food Chemistry 99 (2006) 57–63.

[8] Simões, P.C.; Nunes da Ponte, M.; Matos, H.; Gomes de Azevedo, E.; *in* Proceedings of the Second International Symposium on High Pressure Chemical Engineering, Erlangen, 1990, p. 401.

[9] Della Porta, G.; Porcedda, S.; Marongiu, B.; Reverchon, E.; Isolation of eucalyptus oil by supercritical fluid extraction, Flavour Fragr. J. 14 (1999) 214–218.

[10] Cadoni, E.; De Giorgi, M.R.; Medda, E.; Poma, G.; Supercritical CO_2 extraction of Lycopene and β-carotene from ripe tomatoes; Dyes Pigments 44 (2000) 27–32.

[11] Zosel, K.; *Separation with Supercritical Gases: Practical Applications*; Angew. Chem. Int. Ed. Eng. 17 (10) (1978) 702 – 709.

[12] M. Mulder; Basic principles of membrane technology; Kluwer Academic Publishers; 2nd edition; Dordrecht; The Netherlands; 1996.

[13] J. Coulson and J. Richardson; Chemical Engineering, Volume 2 – Particle Technology and Separation Processes; 5th edition; Oxford; 2002.

[14] S.I. Semenova, H. Ohya, T. Higashijima, Y. Negishi, Separation of supercritical CO_2 and ethanol mixtures with an asymmetric polyimide membrane, J. Membr. Sci. 74 (1992) 131-139.

[15] H. Ohya, T. Higashijima, Y. Tsuchiya, H. Tokunaga, Y. Negishi, Separation of supercritical CO_2 and iso-octane mixtures with an asymmetric polyimide membrane, J. Membr. Sci. 84 (1993) 185-189.

[16] L. Sartorelli, G. Brunner, Membrane separation of extracts from supercritical carbon dioxide, in: Proceedings of the 5th International Symposium on Supercritical Fluids, Atlanta, USA, 2000, 22.

[17] A. Pietsch, W. Hilgendorff, O. Thom, R. Eggers; Basic investigation of integrating a membrane unit into high-pressure decaffeination processing; Separation and Purification Technology 14 (1998) 107–115.

[18] C. Tan, Y. Chiu, Regeneration of supercritical carbon dioxide by membrane at near critical conditions, J. Supercrit. Fluids 21 (2001) 81-89.

[19] C. Tan, H. Lien, S. Lin, H. Cheng, K. Chao; Separation of supercritical carbon dioxide and caffeine with mesoporous silica and microporous silicalite membranes, J. of Supercritical Fluids 26 (2003) 55-62.

[20] L.H.C. Carlson, A. Bolzan, R.A.F. Machado, Separation of d-limonene from supercritical CO_2 by means of membranes, J. of Supercritical Fluids 34 (2005) 143-147.

[21] L. Sarmento, R. Machado, A. Bolzan, C. Spricigo, J. Petrus; Use Of Reverse Osmosis Membranes For The Separation Of Lemongrass Essential Oil And Supercritical CO_2; Brazilian Journal of Chemical Engineering; 21 (02) (2004) 285–291.

[22] L. Sarmento, R. Machado, J. Petrus, T. Tamanini, A. Bolzan; Extraction of polyphenols from cocoa seeds and concentration through polymeric membranes; J. of Supercritical Fluids 45 (2008) 64–69.

[23] J.R. Robinson, M.J. Sims, Method and System for Extracting a Solute from a Fluid Using Dense Gas and a Porous Membrane, US Patent 5490884 (13 February 1996).

[24] G.D. Bothun, B.L. Knutson, H.J. Strobel, S.E. Nokes, Mass transfer in hollow fiber membrane contactor extraction using compressed solvents, J. Membr. Sci. 227 (2003) 183–196.

[25] A. Gabelman, S.-T. Hwang, W.B. Krantz, Dense gas extraction using a hollow fiber membrane contactor: experimental results vs. model predictions, J. Membr. Sci. 257 (2005) 11-36.

[26] S. Sarrade, G.M. Rios, M. Carlès, Supercritical CO_2 extraction coupled with nanofiltration separation: Applications to natural products, Sep. Purif. Technol. 14 (1998) 19-25.

[27] E. Goetheer, A. Verkerk, L. van den Broeke, E. de Wolf, B. Deelman, G. van Koten, J. Keurentjes; Membrane reactor for homogeneous catalysis in supercritical carbon dioxide; Journal of Catalysis 219 (2003) 126–133.

[28] J. de Moura, L. Gonçalves, L. Sarmento, J. Petrus; Purification of structured lipids using SCCO2 and membrane process; Journal of Membrane Science 299 (2007) 138–145.

[29] C. Angell, Y. Ansari, Z. Zhao; Ionic Liquids: Past, present and future; Faraday Discuss., 154 (2012) 9–27.

[30] G. Belluomini, J. Pendergast, C. Domke, B. Ussing; Performance of Several Ionic Liquids for the Separation of 1-Octene from n-Octane; Ind. Eng. Chem. Res. 2009, 48, 11168–11174.

[31] A.B. Pereiro, J.M.M. Araújo, J.M.S.S. Esperança, I.M. Marrucho, L.P.N. Rebelo; Ionic Liquids in Separations of Azeotropic Systems A Review, J. Chem. Thermodynamics 46 (2012) 2–28.

[32] K. Tonova; Separation of poly- and disaccharides by biphasic systems based on ionic liquids; Separation and Purification Technology 89 (2012) 57–65.

[33] C. Hawkins, S. Garvey, M. Dietz; Structural variations in room-temperature ionic liquids: Influence on metal ion partitioning modes and extraction selectivity; Separation and Purification Technology 89 (2012) 31–38

[34] M.B. Shiflett, A. Yokozeki, Separation of CO_2 and H_2S using Room-Temperature Ionic Liquid [bmim][PF6], Fluid Phase Equilibria 294 (2010) 105–113.

[35] S.M. Mahurin, J.S. Lee, G.A. Baker, H. Luo, S. Dai, Performance of Nitrile-Containing Anions in Task-Specific Ionic Liquids for Improved CO2/N2 Separation, Journal of Membrane Science 353 (2010) 177–183

[36] S.M. Mahurin, J.S. Yeary, S. Baker, D.-e. Jiang, S. Dai, G.A. Baker, Ring Opened Heterocycles: Promising Ionic Liquids for Gas Separation and Capture, Journal of Membrane Science 401– 402 (2012) 61– 67

[37] M. Manic, V. Najdanovic–Visak, Z. Visak, M. Nunes da Ponte; Extraction of Free Fatty Acids from Soybean Oil using Ionic Liquids or Poly(ethyleneglycol)s; AIChE Journal 57 (5) (2011) 1344–1355.

[38] L. Simoni, A. Chapeaux, J. Brennecke, M. Stadtherr; Extraction of Biofuels and Biofeedstocks from Aqueous Solutions Using Ionic Liquids; Computers and Chemical Engineering 34 (2010) 1406–1412.

[39] F. J. Deive, A. Rodríguez, A. B. Pereiro, J. M. M. Araújo, M. A. Longo, M. A. Z. Coelho, J. N. Canongia Lopes, J. M. S. S. Esperança, L. P. N. Rebelo and I. M. Marrucho; Ionic liquid-based aqueous biphasic system for lipase extraction; Green Chem., 2011, 13, 390-396.

[40] L. Yang, H. Wang, Y. Zu, C. Zhao, L. Zhang, X. Chen, Z. Zhang; Ultrasound-assisted extraction of the three terpenoid indole alkaloids vindoline, catharanthine and vinblastine from Catharanthus roseus using ionic liquid aqueous solutions; Chemical Engineering Journal 172 (2011) 705– 712.

[41] J. van Spronsen, M. Tavares Cardoso, G. Witkamp, W. de Jong, M. Kroon; Separation and Recovery of the Constituents from Lignocellulosic Biomass by using Ionic Liquids and Acetic Acid as Co-Solvents for Mild Hydrolysis; Chemical Engineering and Processing 50 (2011) 196–199.

[42] J. Kim, A. Matic, J. Ahn, P. Jacobsson; An imidazolium based ionic liquid electrolyte for lithium batteries; Journal of Power Sources 195 (2010) 7639–7643.

[43] S. Keskin, D. Kayrak-Talay, U. Akman, O. Hortaçsu; A review of ionic liquids towards supercritical fluid applications; J. of Supercritical Fluids 43 (2007) 150–180.

[44] J. Andanson, F. Jutz, A. Baiker; Purification of ionic liquids by supercritical CO2 monitored by infrared spectroscopy; J. of Supercritical Fluids 55 (2010) 395–400.

[45] M. Shifletta, A. Shiflett, A. Yokozeki; Separation of tetrafluoroethylene and carbon dioxide using ionic liquids; Separation and Purification Technology 79 (2011) 357– 364.

[46] Y. Fan, J. Qian; Lipase catalysis in ionic liquids/supercritical carbon dioxide and its applications; Journal of Molecular Catalysis B: Enzymatic 66 (2010) 1–7

[47] T. Kunene, P. Webb, D. Cole-Hamilton; Highly selective hydroformylation of long-chain alkenes in a supercritical fluid ionic liquid biphasic system; Green Chem., 2011, 13, 1476-1481.

[48] L. C. Branco, J. G. Crespo and C. A. M. Afonso; Studies on the Selective transport of Organic Compounds by Using Ionic Liquids as Novel Supported Liquid Membranes; Chem. Eur. J. 2002, 8,No . 17, 3865-3871.

[49] P. Uchytil, J. Schauer, R. Petrychkovych, K. Setnickova, S.Y. Suen; Ionic liquid membranes for carbon dioxide-methane separation; Journal of Membrane Science 383 (2011) 262– 271.

[50] S. Yoo, J. Won, S. Kang, Y. Kang, S. Nagase; CO2 separation membranes using ionic liquids in a Nafion matrix; Journal of Membrane Science 363 (2010) 72–79.

[51] Q. Gan, D. Rooney, M. Xue, G. Thompson, Y. Zou; An experimental study of gas transport and separation properties of ionic liquids supported on nanofiltration membranes; Journal of Membrane Science 280 (2006) 948–956.

[52] O. Vangeli, G. Romanos, K. Beltsios, D. Fokas, C. Athanasekou, N. Kanellopoulos; Development and Characterization of Chemically stabilized Ionic Liquid Membranes-Part I: Nanoporous ceramic Supports; Journal of Membrane Science 365 (2010) 366–377.

[53] J. Yingying, W. Youting, W. Wenting, L. Lei, Z. Zheng, Z. Zhibing; Permeability and Selectivity of Sulfur Dioxide and Carbon Dioxide in Supported Ionic Liquid Membranes; Chinese Journal of Chemical Engineering, 17(4) (2009) 594-601.

[54] J. Bara, C. Gabriel, T. Carlisle, D. Camper, A. Finotello, D. Gin, R. Noble; Gas separations in fluoroalkyl-functionalized room-temperature ionic liquids using supported liquid membranes; Chemical Engineering Journal 147 (2009) 43–50.

[55] P. Scovazzo, J. Kieft, D. Finan, C. Koval, D. DuBois, R. Noble; Gas separations using non-hexafluorophosphate [PF6]$^-$ anion supported ionic liquid membranes; Journal of Membrane Science 238 (2004) 57–63.

[56] D.D. Iarikov, P. Hacarlioglu, S.T. Oyama, Supported Room Temperature Ionic Liquid Membranes for CO_2/CH_4 Separation; Chemical Engineering Journal 166 (2011) 401–406.

[57] L. Neves, J. Crespo, I. Coelhoso; Gas permeation studies in supported ionic liquid membranes; Journal of Membrane Science 357 (2010) 160–170.

[58] D. Camper, J. Bara, C. Koval, R. Noble; Bulk-Fluid Solubility and Membrane Feasibility of Rmim-Based Room-Temperature Ionic Liquids; Ind. Eng. Chem. Res. 2006, 45, 6279-6283.

[59] P. Scovazzo; Determination of the upper limits, benchmarks, and critical properties for gas separations using stabilized room temperature ionic liquid membranes (SILMs) for the purpose of guiding future research; Journal of Membrane Science 343 (2009) 199–211.

[60] R. Güell, C. Fontàs, E. Anticó, V. Salvadó, J. Crespo, S. Velizarov; Transport and separation of arsenate and arsenite from aqueous media by supported liquid and anion-exchange membranes; Separation and Purification Technology 80 (2011) 428–434.

[61] M. Mori, R. Gomez Garcia, M.P. Belleville, D. Paolucci-Jeanjean, J. Sanchez, P. Lozano, M. Vaultier, G. Rios; A new way to conduct enzymatic synthesis in an active membrane using ionic liquids as catalyst support; Catalysis Today 104 (2005) 313–317.

[62] S. Nosrati, N.S. Jayakumar, M.A. Hashim; Performance evaluation of supported ionic liquid membrane for removal of phenol; Journal of Hazardous Materials 192 (2011) 1283–1290.

[63] M. Matsumoto, K. Ueba, K. Kondo; Vapor permeation of hydrocarbons through supported liquid membranes based on ionic liquids; Desalination 241 (2009) 365-371.

[64] N. Kouki, R. Tayeb, R. Zarrougui, M. Dhahbi; Transport of salicylic acid through supported liquid membrane based on ionic liquids; Separation and Purification Technology 76 (2010) 8–14.

[65] M. Kohoutova, A. Sikora, Š. Hovorka, A. Randova, J. Schauer, M. Tišma, K. Setnickova, R. Petrickovic, S. Guernik, N. Greenspoon, P. Izak; Influence of ionic liquid content on properties of dense polymer membranes; European Polymer Journal 45 (2009) 813–819.

[66] M. Matsumoto, Y. Inomoto, K. Kondo; Selective separation of aromatic hydrocarbons through supported liquid membranes based on ionic liquids; Journal of Membrane Science 246 (2005) 77–81.

[67] A.P. de los Ríos, F.J. Hernández-Fernández, F. Tomás-Alonso, M. Rubio, D. Gómez, G. Víllora, On the importance of the nature of the ionic liquids in the selective simultaneous separation of the substrates and products of a transesterification reaction through supported ionic liquid membranes, J. Membr. Sci., 307 (2008) 233–238.

[68] F. Hernández-Fernández, A. de los Ríos, F. Tomás-Alonso, D. Gómez, G. Víllora; Improvement in the separation efficiency of transesterification reaction compounds by the use of supported ionic liquid membranes based on the dicyanamide anion; Desalination 244 (2009) 122–129.

[69] A. de los Ríos, F. Hernández-Fernández, M. Rubio, D. Gómez, G. Víllora; Highly selective transport of transesterification reaction compounds through supported liquid membranes containing ionic liquids based on the tetrafluoroborate anion; Desalination 250 (2010) 101–104.

[70] M. Rao, X. Geng, Y. Liao, S. Hu, W. Li; Preparation and performance of gel polymer electrolyte based on electrospun polymer membrane and ionic liquid for lithium ion battery; Journal of Membrane Science 399– 400 (2012) 37– 42.

[71] C. Sirisopanaporn, A. Fernicola, B. Scrosati; New, Ionic Liquid-Based Membranes For Lithium Battery Application; Journal of Power Sources 186 (2009) 490–495.

[72] P. Bernardo, J. C. Jansen, F. Bazzarelli, F. Tasselli, A. Fuoco, K. Friess, P. Izak, V. Jarmarova, M. Kacirkova, G. Clarizia; Gas transport properties of Pebax®/room temperature ionic liquid gel membranes; Separation and Purification Technology 97 (2012) 73–82.

[73] T. Carlisle, G. Nicodemus, D. Gin, R. Noble; CO_2/Light Gas Separation Performance of Cross-linked Poly(vinylimidazolium) Gel Membranes as a Function of Ionic Liquid Loading and Cross-linker Content; Journal of Membrane Science 397– 398 (2012) 24– 37.

[74] I. Yoon, S. Yoo, S. Park, J. Won; CO_2 separation membranes using ion gels by self-assembly of a triblock copolymer in ionic liquids; Chemical Engineering Journal 172 (2011) 237– 242.

Chapter 2

Reverse Osmosis Membranes

2.1 - Introduction

Supercritical fluid extraction (SFE), using supercritical carbon dioxide ($scCO_2$), can substitute traditional organic solvent extraction processes due to several advantages: contamination of the product does not occur; mass transport is highly facilitated owing to favourable transport properties (high mass and thermal diffusivities coupled with low viscosities); and the solvent parameters are tuneable by the operating conditions employed. One of the most promising applications of supercritical fluids is the extraction of high value natural compounds from residues of the food industry [1]. Squalene (Figure 2.1) is one of these compounds, used as a health-food or refined to squalane, a product used in pharmaceuticals and cosmetics. It has also been identified as a possible adjunctive in cancer therapy and during vaccination [2]. For the past decades the main source of squalene has been the liver oil of deep-sea sharks, where it is present in concentrations of 40 to 80% by weight. Strong environmental concerns with regard to the protection of the marine life, however, have focused the attention onto other sources, in particular to the residues from olive oil processing industries. Such residues, stemming from the olive oil deodorizer distillation, can contain up to 40% by weight of squalene and 30 to 40% by weight of free fatty acids. Supercritical carbon dioxide processing of such residues can be of interest to recover "vegetal" squalene [3]. However, this process poses technical difficulties that are mainly associated with the very similar solubilities of squalene and the free fatty acids in supercritical carbon dioxide [4]. Although it was possible to fractionate squalene from every other free fatty acid, the difficulty remains mainly in the separation of oleic acid (Figure 2.1), which is also the main fatty acid present in olive oil residues. In a previous work, a significant enrichment in squalene could be obtained with reverse osmosis membranes, but with the drawback of a lower total permeate flux [5]. Furthermore, this study was performed only at 313 K and 18 MPa, because these conditions were found to be the best for the fractionation of squalene from free fatty acids in $scCO_2$ [4]. However, for membrane separations other conditions of pressure and temperature could prove more suitable for this fractionation. So, in this chapter is explored the separation of squalene from oleic acid with reverse osmosis membranes at pressures ranging from 18 to 22 MPa and temperatures of 313 and 323 K. Permeability measurements to carbon dioxide were also performed to the membranes tested.

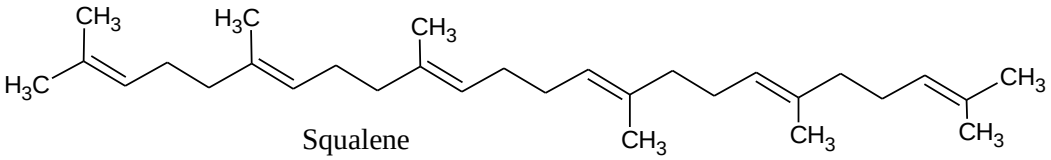

Squalene

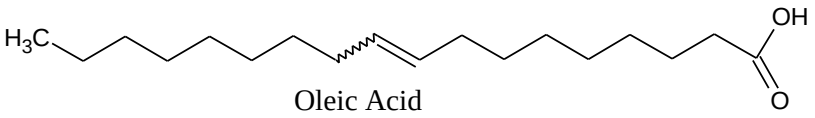

Oleic Acid

Figure 2.1 – Molecular structures of squalene and oleic acid.

SFE of olive oil residues can be an interesting alternative to the recovery of "vegetal" squalene, and has also been previously investigated [5]. One of the main drawbacks of this process is the relatively similarity of solubilities of squalene and free fatty acids in scCO2. Despite that, it was possible to extract 88% of the mass of squalene fed to the column by CO_2 at 18 MPa and 313 K and a solvent-to-feed mass flow ratio (S/F) of *ca.* 40. The squalene content of raffinate and extract streams was 10 and 63.5 wt%, respectively. Although both processes (SFE in a countercurrent packed column and membrane separation) have so far presented satisfactory results, it had never been tried to couple both processes. As it is foreseeable that the coupling of both processes would result in a better enrichment than any of the processes taken separately, it is also explored that hypothesis in this chapter.

2.2 – Materials and Methods

Carbon dioxide was supplied with a purity of 99.995% by Air Liquide. Squalene was supplied by Sigma (98% by weight). Oleic Acid, supplied by Riedel-de Haën, was of technical grade (79.9 % by mass); other major fatty acids present included myristic acid (C14:0) at 2.0 %, palmitoleic acid (C16:1) at 5.2 %, palmitic acid (C16:0) at 5.6 %, stearic acid (C18:0) at 1.0 %, and linoleic acid (C18:2) at 6.4 %.

2.2.1 - scCO$_2$ Fractionation Experiments

The flow scheme of the high pressure apparatus for the membrane separations and fractionations experiments with scCO$_2$ is presented in Figure 2.2. In the membrane separations experiments, gaseous CO_2 flows from a storage vessel into a gas compressor (model 5542121, Nova Swiss, Switzerland), where the working pressure is attained, and then into a Kenics static mixer (Chemineer, USA, model 37-04-065) with an internal diameter of 4.928 mm, length of 178 mm, and 21 helical mixing elements. The liquid feed is introduced in the apparatus by

means of a liquid pump (Minipump, LDC Analytical, FL, U.S.A.). The carbon dioxide and the oil mixture are put in contact in a "tee" joint just prior to the static mixer entrance. The gas and liquid phase flows pass co-currently through the static mixer where mixing of the two phases occur. At the liquid to gas flow ratios used in this work the static mixer is equivalent to one equilibrium stage of separation due to the co-current operation. Thus, in this way it is ensured that the gas phase leaving the static mixer ensemble and flowing to the membrane cell is saturated in oil at pressure and temperature operating conditions. The remaining liquid that is not solubilised in the CO_2 phase is collected after the static-mixer in a separation vessel.

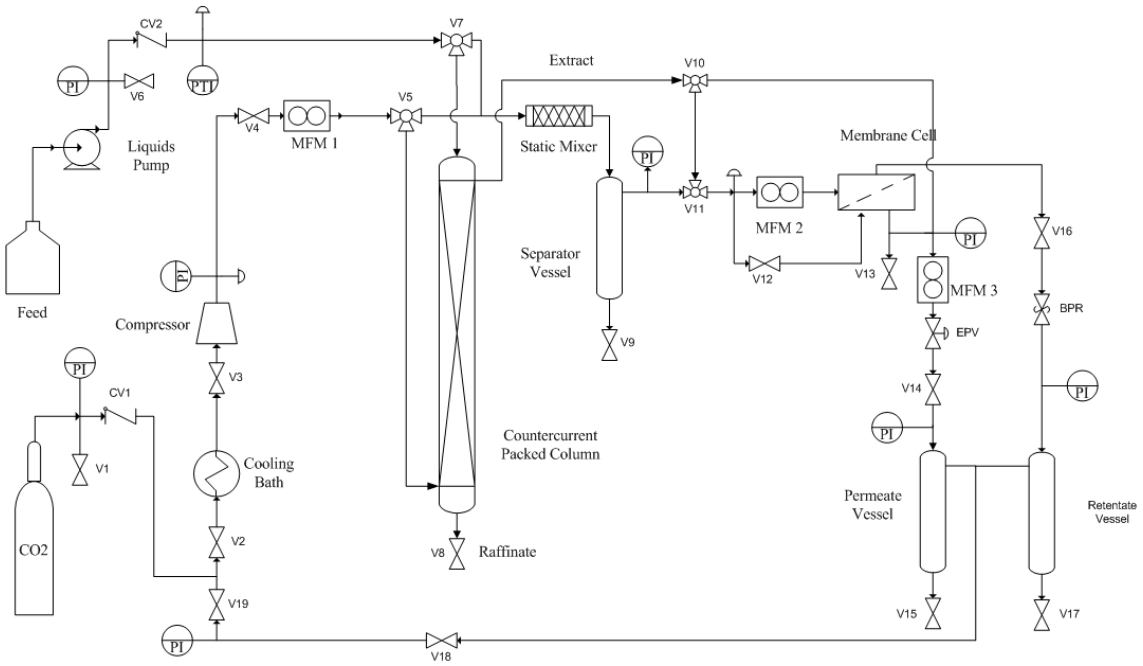

Figure 2.2 – Flow scheme of the high pressure apparatus for the fractionation experiments with $scCO_2$. MFM: Mass Flow Meter; V*i*: Valves; PI: Pressure Indicator; PTI: Pressure and Temperature Indicator; CV*i*: Check-Valves; BPR: Back Pressure Regulator; EPV: Electro-Pneumatic Valve.

For the experiments with the membrane coupled to the countercurrent packed column, instead of the CO_2 flowing into the static mixer, it flows to the bottom of the column, leaving by the top with the extract solubilised, flowing then through valves V10 and V11 to the mass flow meter placed before the membrane test cell (MFM2). Liquid feed, on the other hand, is pumped directly to the top of the column, and trickles to the bottom, where the raffinate is collected.

The membrane module consists of a small flat sheet membrane test cell of 40 mm diameter, manufactured in stainless steel 316. Figure 2.3 shows a scheme of this module and a picture of its assembly. It has entrance and exit ports in both the retentate and the permeate sides. The

ports in the retentate side are assembled with a 90º rotation relatively to the permeate ports. The retentate and the permeate sides are both connected via a bypass valve (V12) which is kept open before starting the experiments to prevent undesired pressure differences across the membrane, which could damage it. On the retentate side, the pressure is controlled by a back-pressure regulator valve (model 27-1700, Tescom Europe GmbH & Co., Germany) and the outlet stream is depressurized into a collection vessel where the retentate liquid precipitates. On the permeate side, the pressure is controlled by a micrometric valve (V14) (60-11HF4V, HiP, USA) and the outlet stream is depressurized into a collection vessel where the permeate liquid precipitates. Gaseous CO_2 is then collected from both retentate and permeate collection vessels and further recirculated. The working temperature in the entire installation is maintained by heating cables (HSS - 450ºC, Horst GmbH, Germany) and respective temperature controllers. The working temperature is maintained by a flange heating jacket (HFH10, Horst GmbH, Germany).

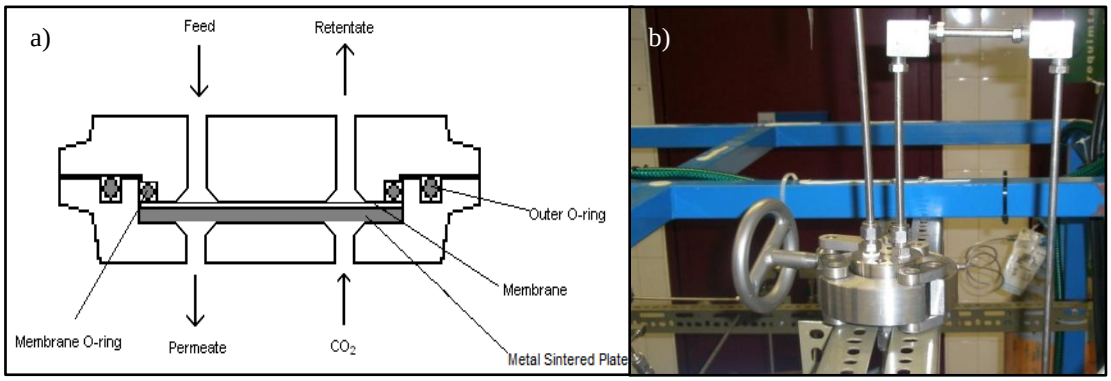

Figure 2.3 – Stainless steel flat sheet membrane test cell. a) Scheme of the module; b) Picture of the module assembled in the apparatus.

Membranes used in this work were reverse osmosis membranes made of Cellulose Acetate (YMCFSP3001), Polyamide AD (YMADSP3001), Thin-Film SG (YMSGSP3001) and Polyamide AG (YMAGSP3001) from GE Osmonics, USA. Teflon AF 2400 PEI was gently offered by the Technische Universität Hamburg-Harbug (TUHH).

The continuous countercurrent packed column is a high-pressure column (2.4 cm of internal diameter and 2 m high) filled with Sulzer EX structured gauze packing. The general characteristics of the packing elements are listed in Table 2.1.

Table 2.1 – Geometric characteristics of *Sulzer EX* gauze packing used in this work

Packing Type	Sulzer EX
Packing Material	Stainless Steel
Height (mm)	54
Diameter (mm)	24
Surface Area (m^2/m^3)	1710
Void Fraction	0.86
Crimp Height (mm)	1.6
Channel Base (mm)	4
Side of Corrugation (mm)	2.9
Channel Flow Angle from the Horizontal (degrees)	45

It operates as a stripping column with the pre-heated liquid feed introduced above the packing section at the top of the column by means of a liquid metering pump. Fresh carbon dioxide is introduced at the bottom of the column with the help of a compressor and heated to the desired temperature by heating cables. An expansion valve located downstream from the gas outlet flow automatically controls the pressure inside the column. Carbon dioxide and dissolved solutes after exiting the extraction column by the top (the so-called extract stream) are separated in a vessel by pressure expansion. The carbon dioxide is then recycled back to the extraction column.

The liquid level inside the extraction column is maintained at a constant position by manually opening a valve at the bottom of the column. The column is thus operated with the carbon dioxide stream as the continuous phase and the oil as the dispersed phase. During an extraction run samples of the raffinate and extract streams are collected at precise time intervals. These samples are subsequently weighed, and then analyzed to determine their squalene content.

2.2.3 - Sample analysis

The samples obtained either in the fractionations only with membranes or with the membrane coupled with SFE column were analyzed for their content in squalene and oleic acid by gas chromatography (GC). The fatty acids were methylated to the respective methyl ester forms, by reaction with diazomethane, prepared according to the method described elsewhere [6], prior to the GC analysis. Squalane was used as the internal standard. The chromatograph was a Thermo Quest Trace GC 2000 with a FID detector; a DB-1 column, 30 m x 0.25 mm and 0.25 μm film thickness, from J&W Scientific Inc. was used. Hydrogen was used as carrier at 100 KPa (constant pressure). The starting oven temperature was 448 K (0 min), a ramp of 4 $K \cdot min^{-1}$ until

543 K (0 min), followed by a ramp of 10 $K \cdot min^{-1}$ until 553 K with a final holding time of 10 minutes.

2.3 - Results

2.3.1 - $scCO_2$ Permeabilities

The first approach in studying the applicability of commercial reverse osmosis membranes was to test their permeability to $scCO_2$, to evaluate the feasibility of their application in high pressure conditions.

In Figure 2.4 are shown the permeabilities to $scCO_2$ for the membrane Polyamide AD at 313 K and two pressures (18 and 20 MPa). In these experiments the pressure drop across the membrane would be increased by opening a micrometric valve in the permeate side, and the correspondent permeate flow would be measured. There is no difference in permeability at 18 or 20 MPa and no hysteresis was observed.

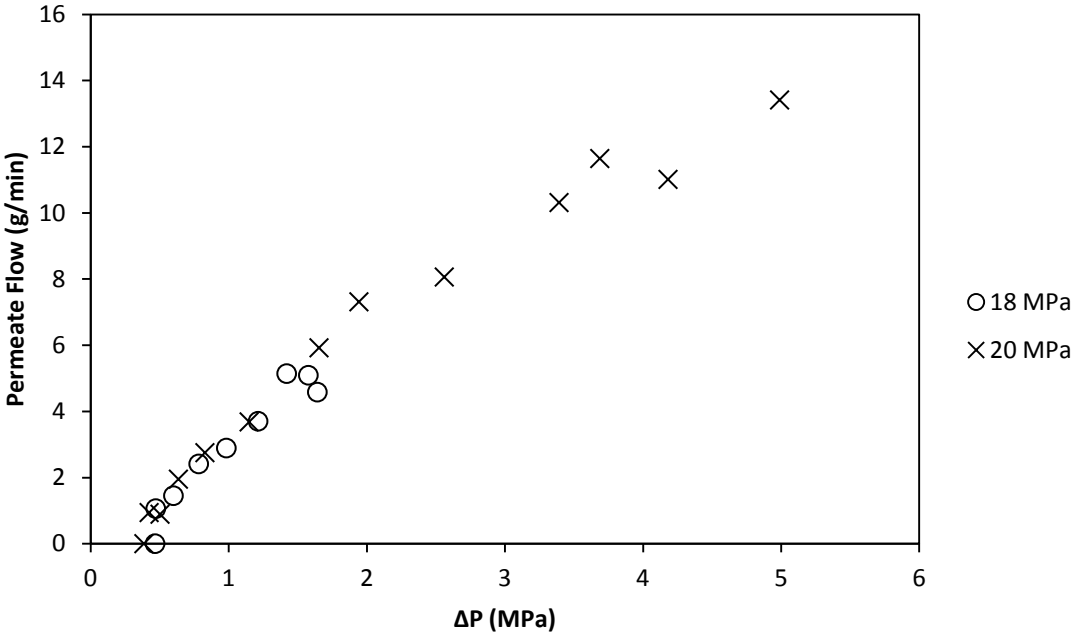

Figure 2.4 – $scCO_2$ permeabilities for Polyamide AD membrane at 313 K and two pressures.

In Figure 2.5 are shown the permeabilities to $scCO_2$ for the membrane Polyamide AG at 313 K and three pressures (15, 18 and 20 MPa). In this case only slightly higher permeabilities are observed for 15 MPa.

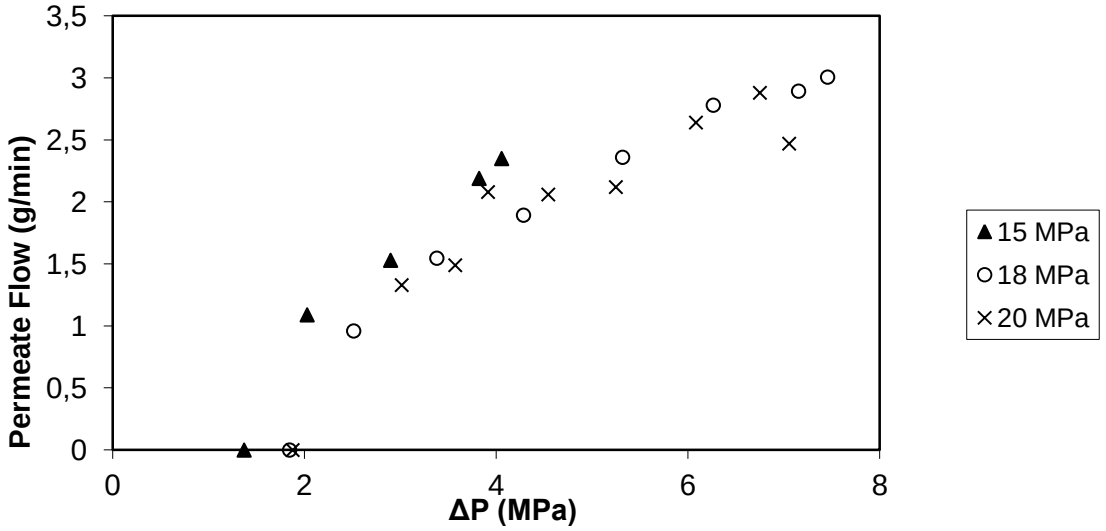

Figure 2.5 – $scCO_2$ permeabilities for Polyamide AG membrane at 313 K and several pressures.

In Figure 2.6 are shown the permeabilities to $scCO_2$ for the membrane Teflon Af 2400 at 313 K and two pressures (18 and 20 MPa). No significative differences in permeabilities are observed in this case. For this membrane two experiments at 18 MPa were conducted, which are coincidental, in consecutive days. The membrane was kept assembled and pressurized overnight. From this observation it is possible to attest the reproducibility of the method and also that there was no degradation of the membrane.

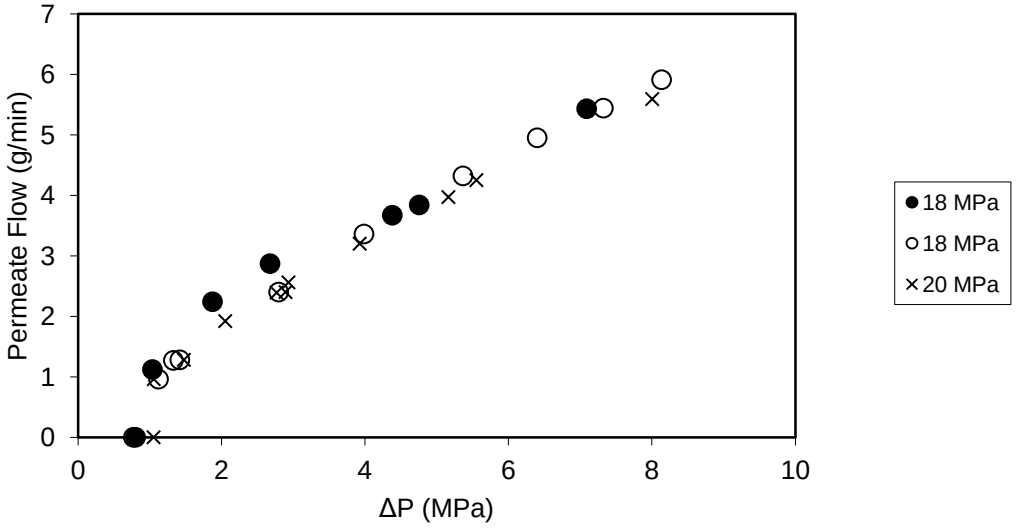

Figure 2.6 – $scCO_2$ permeabilities for Teflon Af 2400 membrane at 313 K and two pressures.

In Figure 2.7 are shown the permeabilities to $scCO_2$ for the membrane Cellulose Acetate at 313 K and two pressures (18 and 22 MPa). Both curves are coincidental. This membrane presented the highest pressure drops, up to 12 MPa, attained in all the experiments.

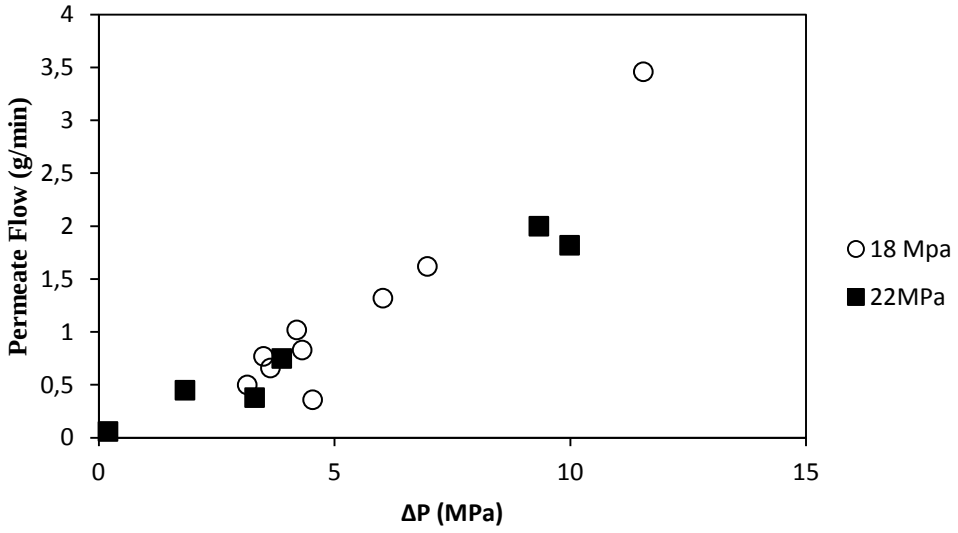

Figure 2.7 – $scCO_2$ permeabilities for Cellulose Acetate membrane at 313 K and two pressures.

In Figure 2.8 are shown the permeabilities to $scCO_2$ for the membrane Thin-Film SG at 313 K and two pressures (18 and 22 MPa). This membrane presented the lowest pressure drops of all the membranes studied in this work. Though in this plot the permeabilities at 22 MPa seem slightly higher than those at 18 MPa, this is only an apparent difference stemming from the plot scale, due to the low pressure drops observed.

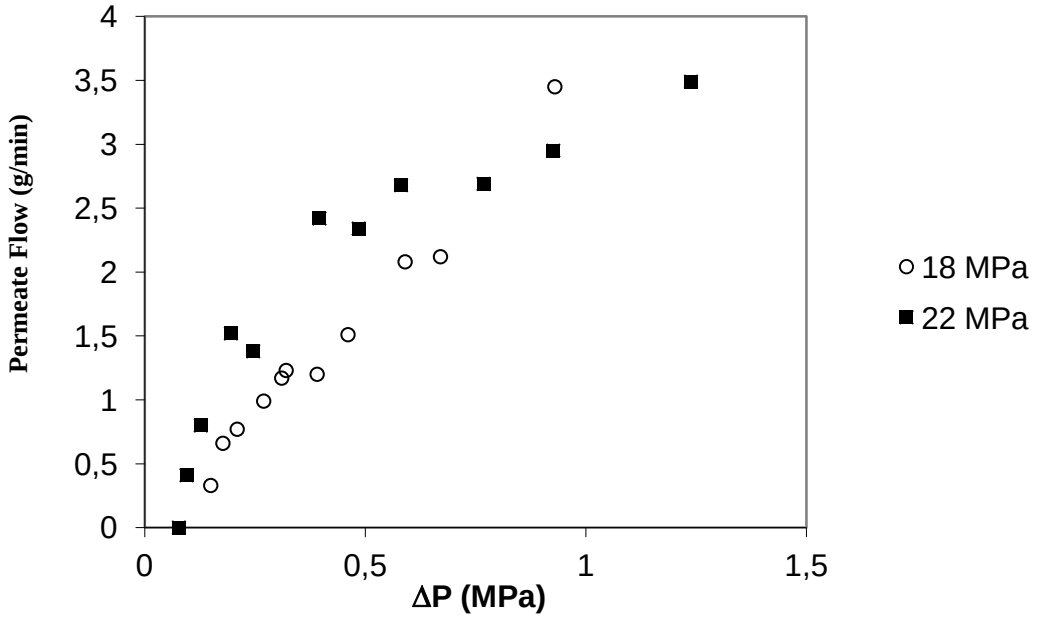

Figure 2.8 – $scCO_2$ permeabilities for Thin-Film SG membrane at 313 K and two pressures.

In Figure 2.9 are shown the permeabilities to $scCO_2$ for the membranes Thin-Film SG, Polyamide AD, Teflon Af 2400, Polyamide AG and Cellulose Acetate at 313 K and 18 MPa. As

can be seen, Polyamide AD and Thin-Film SG present the highest permeabilities, while Cellulose Acetate presents the lowest. Nevertheless, with all the membranes was possible to attain considerable pressure drops. Even for the Thin-Film SG membrane, which presents the lowest pressure drops, these are still considerable. These high pressure drops allow these membranes to be used in high pressure separations, using the pressure drop across the membrane as driving force for the separations, although the differences in permeate flow might influence the performance of these membranes.

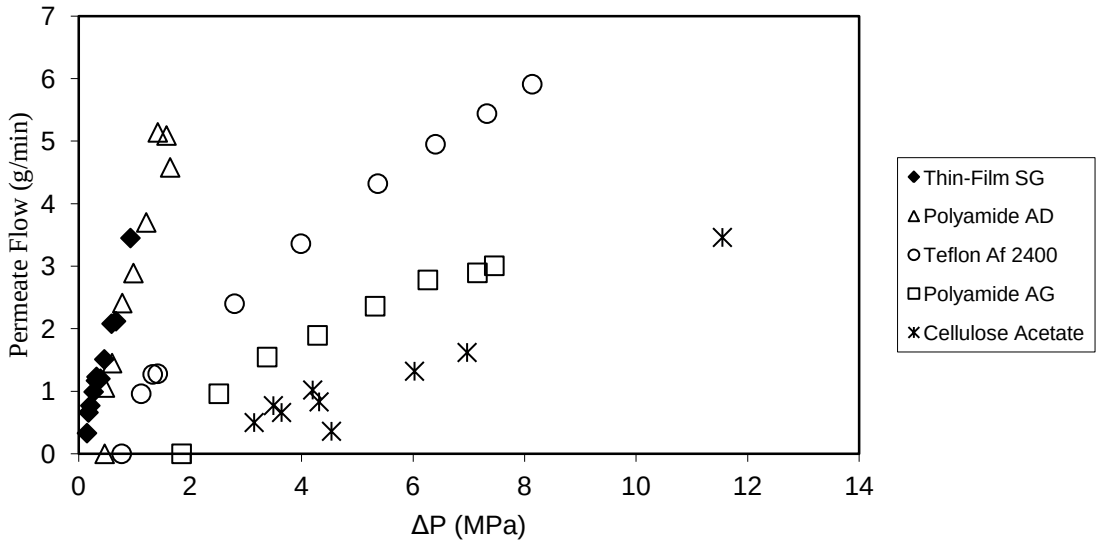

Figure 2.9 – $scCO_2$ permeabilities for Polyamide AD, Polyamide AG, Teflon Af 2400 and Cellulose Acetate membranes at 313 K and 18 MPa.

The same membranes tested in this work had already been tested in a previous work at the Technische Universität Hamburg-Harbug (TUHH), although only at one condition of pressure and temperature (18 MPa, 313 K)[5]. In Figures 2.10 and 2.11 are presented the results obtained in both works. In Figure 2.10 are presented the results which are more similar, those obtained for Polyamide AD and Thin-Film SG. In the case of Polyamide AD the results are exactly coincidental, while for Thin-Film SG those obtained at TUHH are slightly higher.

In Figure 2.11 are presented the results obtained for Teflon Af 2400, Polyamide AG and Cellulose Acetate membranes in both works. These are the results which are most dissimilar, with those obtained at TUHH consistently higher than the ones obtained in this work. However, the trend observed in both works is the same, i.e., Teflon Af 2400 presents the highest permeabilities, while Cellulose Acetate presents the lowest. In the case of Teflon AF, the one used at TUHH was 2x coated and the one used in this work was 1x coated.

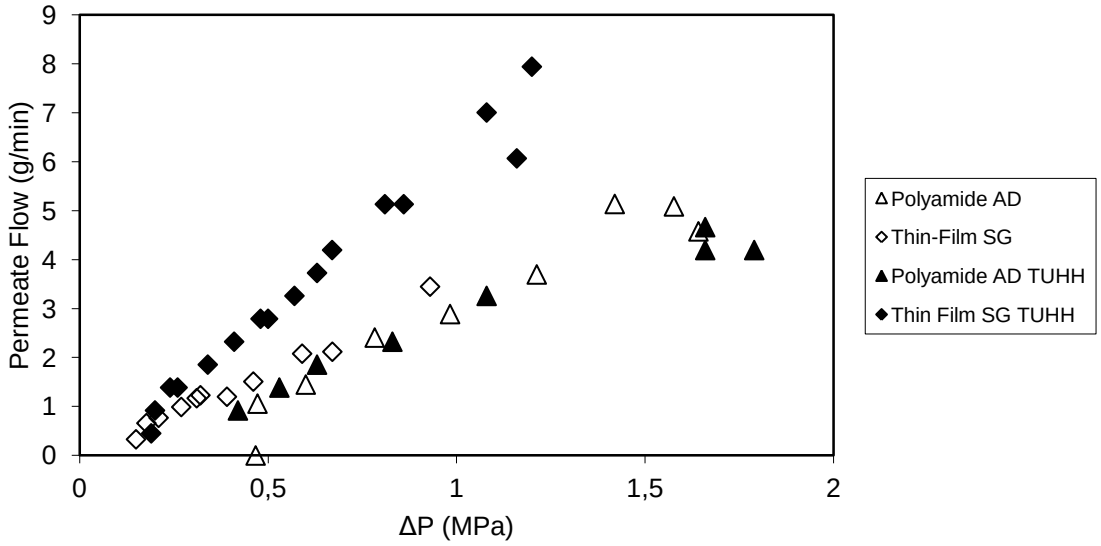

Figure 2.10 – $scCO_2$ permeabilities for Polyamide AD and Thin-Film SG membranes at 313 K and 18 MPa, obtained in this work (open symbols) and obtained at TUHH (closed symbols).

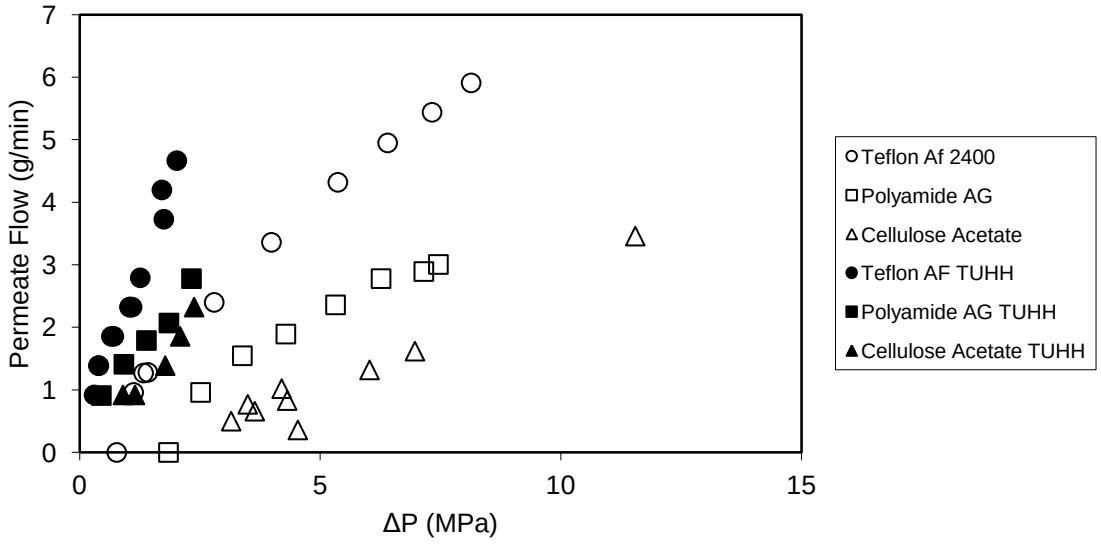

Figure 2.11 – $scCO_2$ permeabilities for Teflon Af, Polyamide AG and Cellulose Acetate membranes at 313 K and 18 MPa, obtained in this work (open symbols) and obtained at TUHH (closed symbols).

2.3.2 - Fractionation Experiments

The performance of these membranes for fractionation of a model mixture was expressed in terms of selectivity of one component towards the other, $\alpha_{SQ/OA}$, defined as:

$$\alpha_{SQ/OA} = \frac{y_{SQ}/x_{SQ}}{y_{OA}/x_{OA}} \quad (1.1)$$

with $y_{SQ,OA}$ and $x_{SQ,OA}$ the mass fraction of squalene and oleic acid in the permeate and retentate streams, respectively.

In Figure 2.12 are presented the selectivities obtained for combinations of two pressures (18 and 22 MPa) and two temperatures (313 and 323 K) with the membrane Polyamide AD in the separation of the model mixture oleic acid/squalene (50% w/w). In this plot are also represented the respective densities of CO_2 at these conditions, and the fraction of permeate collected. The permeate fraction is defined as the total mass collected in the permeate over the total mass fed to the membrane. It is seen that at all combinations of pressure and temperature this membrane is selective towards oleic acid. The selectivity of oleic acid towards squalene plotted here increases with increasing temperature, but decreases with increasing pressure. Relating these selectivities to CO_2 density, we can see that there is a direct relation, i.e., with higher CO_2 density, the selectivity increases. We can also see that the permeate fraction ranges from 0.2 to 0.4, but higher selectivities to oleic acid are also connected to lower permeate fractions.

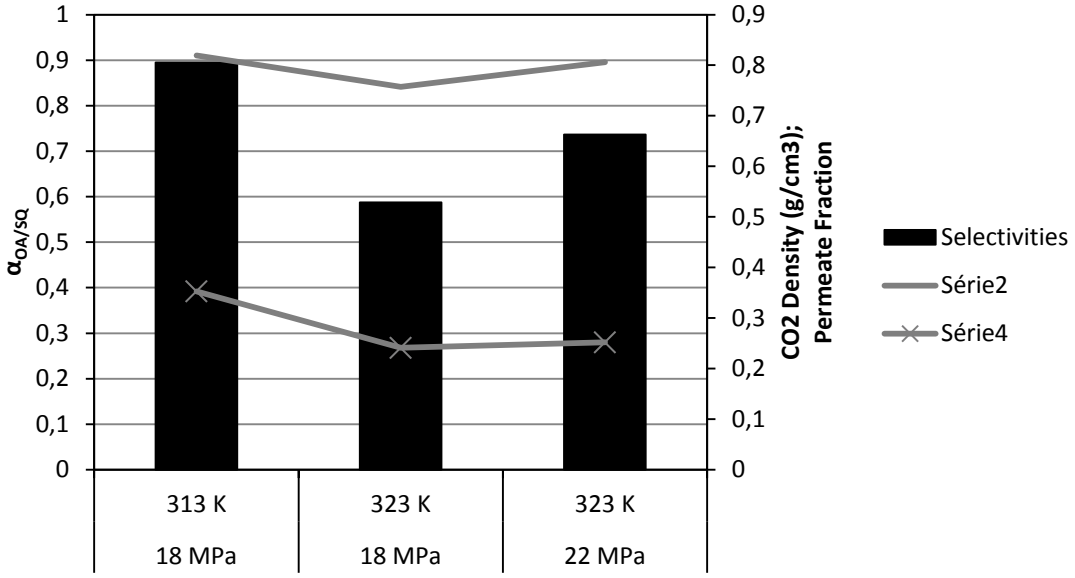

Figure 2.12 – Squalene selectivities and corresponding CO_2 densities for Polyamide AD membrane.

In Figure 2.13 are presented the selectivities obtained for combinations of two pressures (18 and 22 MPa) and two temperatures (313 and 323 K) with the Cellulose Acetate membrane in the separation of the model mixture oleic acid/squalene (50% w/w). In the three cases studied the selectivity is always towards oleic acid, with $\alpha_{SQ/OA}$ values below 0.5. Comparing with the Polyamide AD membrane (Figure 2.12), the selectivity values of squalene over oleic acid are always lower for the Cellulose Acetate membrane. Now, the relation between selectivity and CO_2 density remains valid for the two experiments at 18 MPa, but the same is not true for the experiment at 22 MPa. In this case, though CO_2 density is between those of the two cases at 18

MPa, the selectivity is actually slightly lower than the lowest selectivity of the previous cases. So, in this case the selectivity must be governed more by the morphology of the membrane than by CO_2 density.

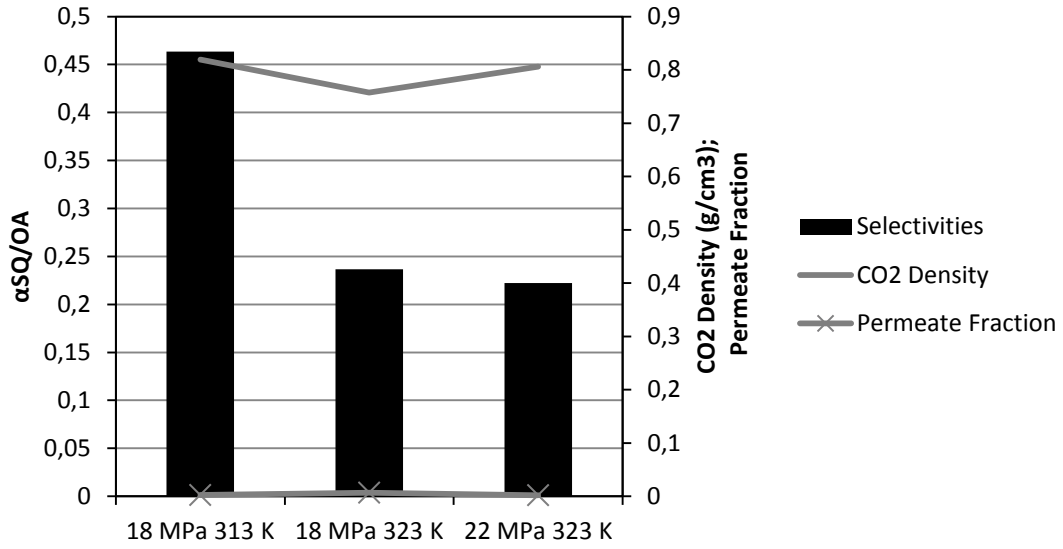

Figure 2.13 – Squalene selectivities and corresponding CO_2 densities for Cellulose Acetate membrane.

In Figure 2.14 are presented the selectivities of squalene towards oleic acid obtained for combinations of two pressures (18 and 22 MPa) and two temperatures (313 and 323 K) with the Thin-Film SG membrane in the separation of the model mixture oleic acid/squalene (50% w/w). In this case it is seen that the selectivity is inversely related with CO_2 density, but always with selectivities below 1 (selective towards oleic acid). Again, selectivities towards oleic acid are accompanied by lower permeate fractions.

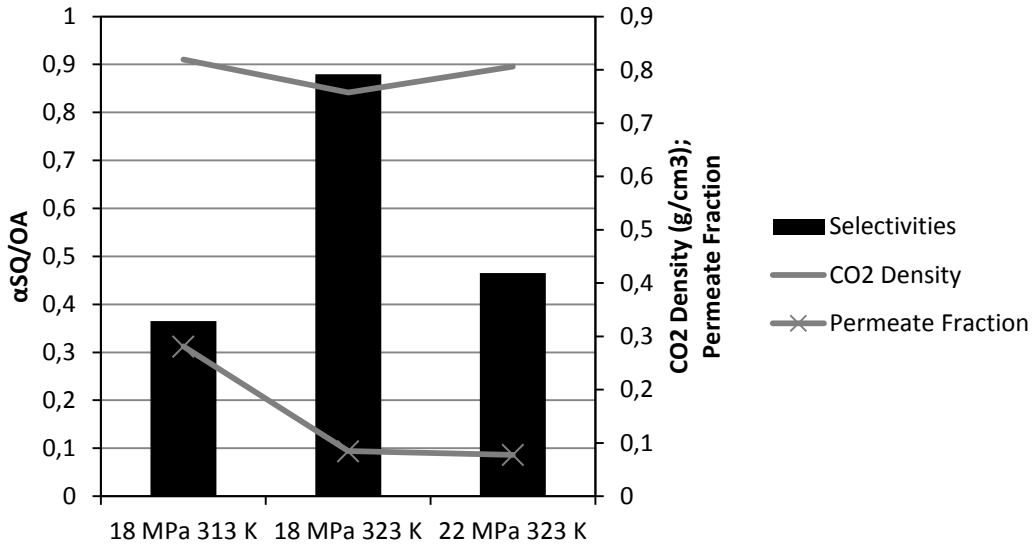

Figure 2.14 – Squalene selectivities and corresponding CO_2 densities for Thin-Film SG membrane.

With the Teflon AF 2400 membrane there was no permeation of the model mixture, or it permeated so little that no sample was possible to obtain in order to analyze. In Figure 2.15 are presented the selectivities at 18 MPa and 313 K for the model mixture of oleic acid/squalene (50% w/w) for the three membranes tested. At these conditions, the Thin-Film SG membrane presents the highest selectivity towards oleic acid, and Polyamide AD the lowest.

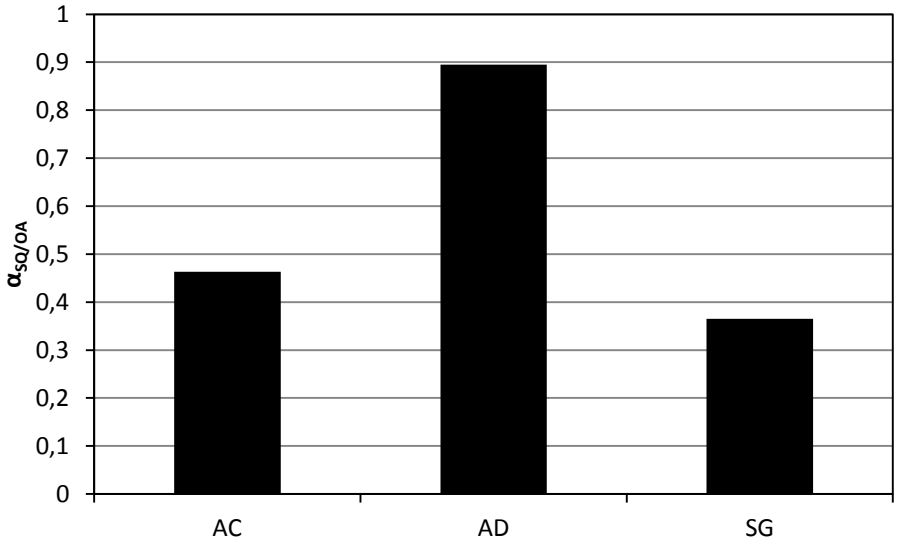

Figure 2.15 – Squalene selectivities at 18 MPa and 313 K for three membranes. AC: Cellulose Acetate; AD: Polyamide AD; SG: Thin-film SG

In Figure 2.16 are presented the selectivities at 18 MPa and 323 K for the model mixture of oleic acid/squalene (50% w/w) for the three membranes tested. Again, all membranes were selective towards oleic acid, with Thin-Film SG the less selective and Cellulose Acetate the most selective.

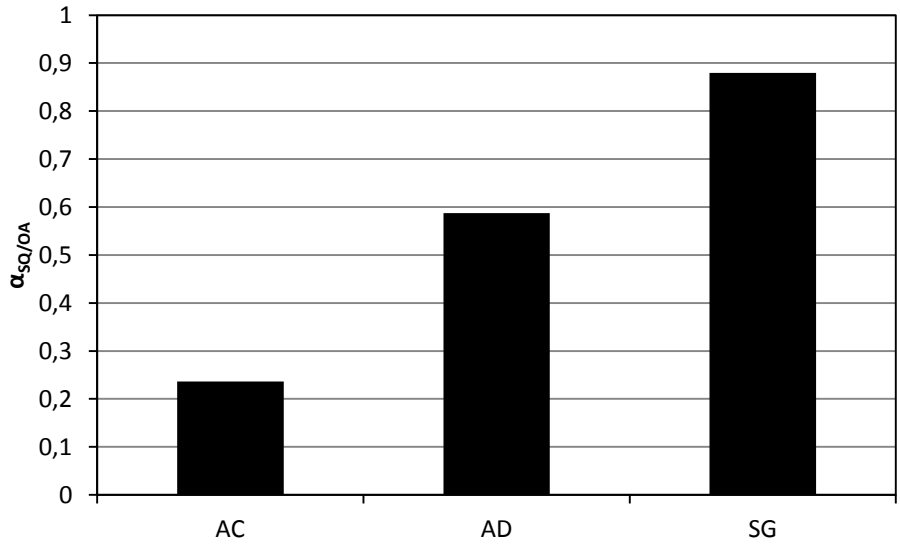

Figure 2.16 – Squalene selectivities at 18 MPa and 323 K for three membranes. AC: Cellulose Acetate; AD: Polyamide AD; SG: Thin-film SG

In Figure 2.17 are presented the selectivities at 22 MPa and 323 K for the model mixture of oleic acid/squalene (50% w/w) for the three membranes tested. As with the previous cases, all the membranes showed selectivity towards oleic acid. In this case, the membrane of polyamide AD is the less selective towards oleic acid while Cellulose Acetate is the most selective.

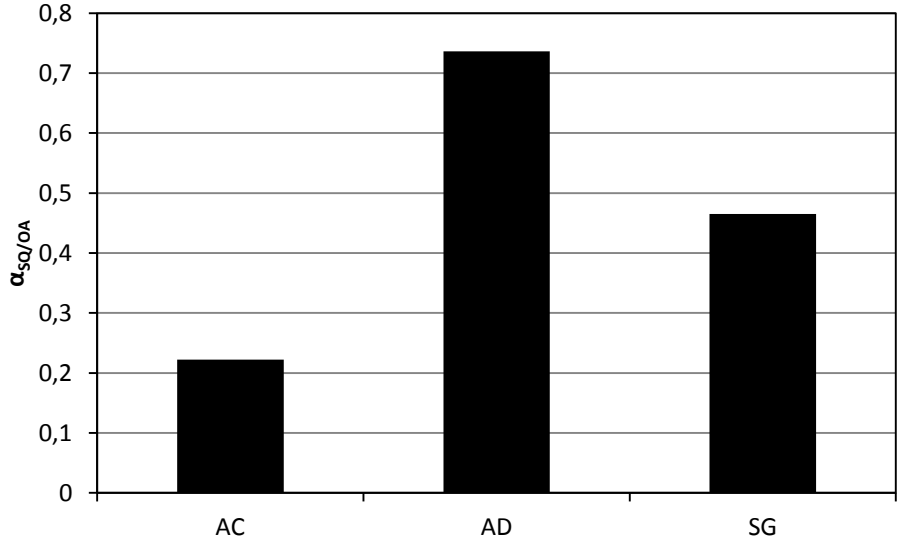

Figure 2.17 – Squalene selectivities at 22 MPa and 323 K for three membranes. AC: Cellulose Acetate; AD: Polyamide AD; SG: Thin-film SG

Overall, Polyamide AD can be considered the membrane less selective towards oleic acid, and Cellulose Acetate is the most selective towards oleic acid. However, the higher selectivity has the drawback of lower permeate fraction. In Table 2.2 are presented all the values obtained of selectivity and permeate fraction for the three membranes tested at the different pressure and temperature conditions, along with the respective CO_2 density.

Table 2.2 – Selectivity of squalene towards oleic acid, CO_2 densities and permeate fractions for Cellulose Acetate, Polyamide AD and Thin-Film SG at different pressure and temperature conditions.

	Pressure (MPa)	Temperature (K)	$\alpha_{SQ/OA}$	CO_2 Density (g/cm^3)	Permeate Fraction
AC	18	313	0.46	0.820	0.002
	18	323	0.24	0.757	0.007
	22	323	0.22	0.806	0.002
AD	18	313	0.89	0.820	0.085
	18	323	0.59	0.757	0.241
	22	323	0.74	0.806	0.252
SG	18	313	0.36	0.820	0.281
	18	323	0.88	0.757	0.085
	22	323	0.47	0.806	0.078

2.3.3 - Membrane Separation coupled with Supercritical Fluid Extraction

It was also studied the fractionation of the model mixture oleic acid/squalene in a continuous countercurrent packed column followed by separation of the extract flowing out of the top of the column with the membrane module coupled in line, in order to have a continuous process. For this system it was chosen to operate at 18 MPa and 313 K, the best conditions obtained in previous studies [5]. As it was known that the column extract at these conditions is enriched in squalene, it was chosen to use the Polyamide AD membrane, as this is the membrane which presented the best selectivities towards squalene.

Figure 2.18 presents the results obtained for the model mixture of oleic acid/squalene (50% w/w), with a feed flow of 1.2 g/min and a CO_2 flow of 40 g/min, resulting in a solvent to feed (S/F) ratio of 33.3. As expected, the extract obtained from the column is enriched in squalene to about 60%, and the membrane can further enrich this extract to about 80% in the permeate.

Comparing these results to the ones obtained previously for each system in separate (column [5] and membrane), we can see that the column has a similar behavior to the one observed previously, as expected, but the membrane presents now a significative enrichment in squalene. However, the membrane now started with a mixture with a composition in squalene slightly higher (60% vs. 50%), due to the enrichment in the column, leading to a final composition in squalene of 80%. This corresponds to a final composition 1.6 times richer in squalene.

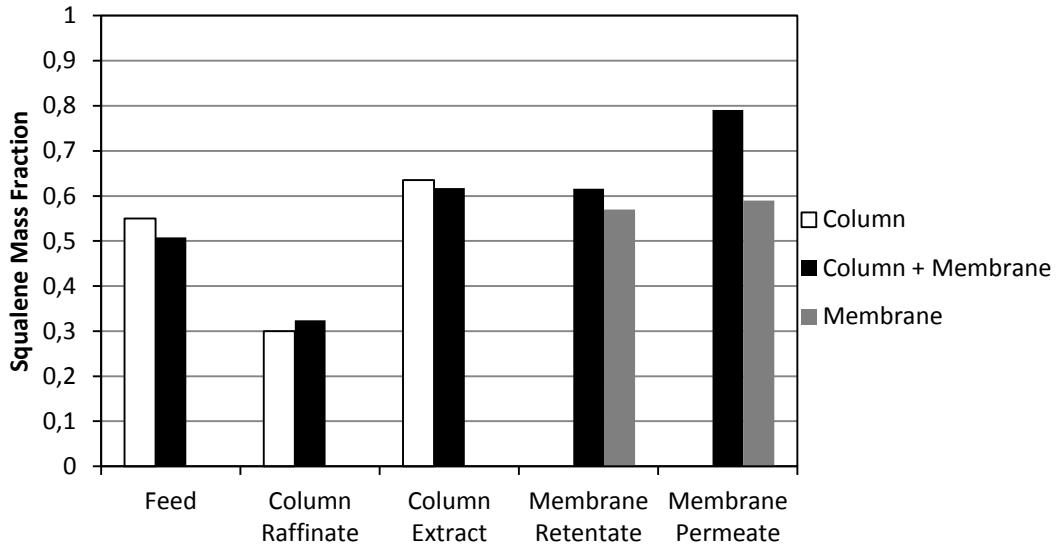

Figure 2.18 – Squalene mass fractions obtained with the coupling of Polyamide AD membrane with SFE column, at 313 K, 18 MPa, CO_2 flow of 40 g/min and feed flow of 1.2 g/min.

The same experiment was duplicated with a feed composition higher in squalene (70% w/w) and higher feed and CO_2 flow rates but a resulting S/F of only 20. Results are presented in Figure 2.19. As the feed composition is now higher in squalene, the resulting enrichment obtained in the column is now lower and the consequent separation obtained in the membrane is also negligible. These observations reveal that deviations from the optimal operation conditions result not only in lower fractionations but in complete loss of selectivity.

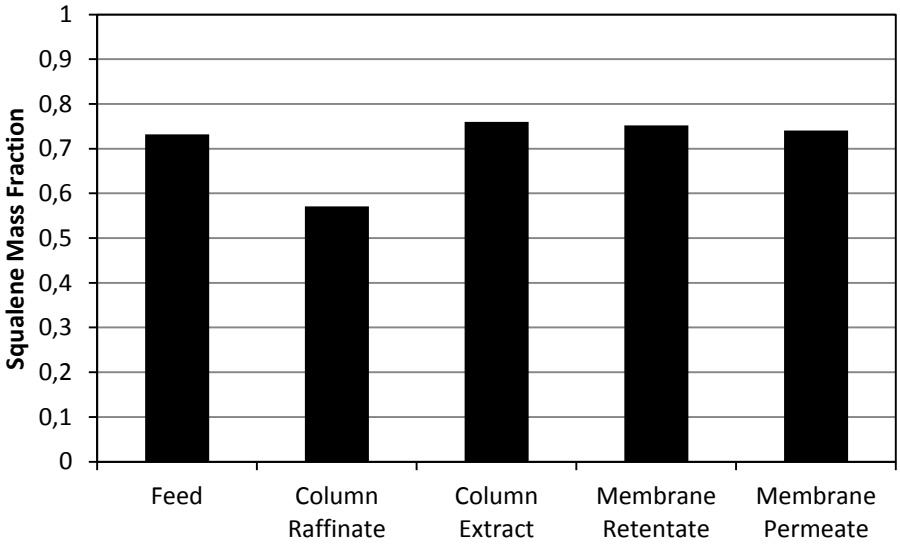

Figure 2.19 – Squalene mass fractions obtained with the coupling of Polyamide AD membrane with SFE column, at 313 K, 18 MPa, CO_2 flow of 90 g/min and feed flow of 4.5 g/min.

2.3.4 - Fractionation of Raffinate Model Mixture with Membranes

It was attempted to fractionate a model mixture identical to the one obtained in the column raffinate by a membrane, but several technical difficulties arose to implement the process; when these difficulties were overcame and it was possible to obtain a permeate flow through the membrane, the fractionation was negligible. The results obtained are presented in Table 2.3. The first problem which was needed to overcome was associated with the simulation of the raffinate fraction. This fraction is essentially model mixture with CO_2 dissolved. So, in the first attempts, model mixture would be placed inside a pressure vessel and connected to a pump. CO_2 pressure in the range 4-6 MPa would be added to the vessel in order to simulate the raffinate fraction, and the valve connecting the vessel with the pump would be open. However, the combined effect of CO_2 pressure and lowered viscosity would result in the model mixture passing immediately through the pump, without possibility of regulating the flow. This practical impossibility was assumed and the pump was removed from the system. Now remained the problem of reduced time of contact of the model mixture with the membrane. To try to overcome this problem, the exit valve on the retentate side of the membrane (valve V16 in Figure 2.2) would be closed, to force the model mixture to remain in contact with the membrane for longer periods of time.

For both Polyamide AG and Thin-Film SG membranes is seen that closing the retentate valve results in higher amounts of permeate collected, while when this valve is open the permeate collected is negligible. However, no separation results from this operation.

As for the Polyamide AD membrane, the permeate fraction collected is considerable and very similar in amount either with the retentate valve open or closed. This was also the only case in which it was possible to observe a slight fractionation. However, the fractionation values are so low that they can be considered negligible.

Table 2.3 – Results obtained in the fractionation of raffinate model mixture with membranes.

Membrane	Retentate Pressure (MPa)	Permeate Pressure (MPa)	Retentate Valve	Permeate Mass (g)	Squalene Fraction in Feed	Squalene Fraction in Permeate
AG	4	2	Open	----------		
	4	2	Closed	7.34	0.59	0.59
SG	4	2	Open	0.99	0.59	0.59
	5	2	Closed	2.60	0.59	0.59
AD	4	2	Open	28.79	0.58	0.55
	4.4	2.4	Closed	26.19	0.59	0.6

2.4 - Conclusions

In this work were explored the permeabilities to $scCO_2$ of several reverse osmosis membranes. It was found, for the same membrane, that permeability is not dependent on the pressure applied on the retentate side of the membrane, in the range of 18 to 22 MPa. It was also observed that, for 18 MPa and 313 K the membranes tested presented the same trend as that observed in a previous work [5], although with lower permeabilities.

For the membranes tested, it was found that all membranes are selective towards oleic acid, with polyamide AD being the less selective and cellulose acetate the more selective, although with lower permeate fractions obtained.

By coupling SFE in a countercurrent packed column with separation in Polyamide AD membrane it was possible to obtain an enrichment in squalene of 1.6 times.

When trying to simulate the separation of the retentate of the column with membranes, it was very difficult to achieve results due to the impossibility of pumping liquids with high amounts of dissolved gas, and to the low contact times of the model mixture with the membrane in these conditions. In the cases in which it was possible to obtain permeate fraction, either there was no selectivity or this was negligible.

2.5 - References

[1] G. Brunner, Gas Extraction, Springer, Berlin, 1994.

[2] L. Reddy, P. Couvreur; Squalene: A natural triterpene for use in disease management and therapy; Advanced Drug Delivery Reviews 61 (2009) 1412–1426.

[3] O. Catchpole, P. Simões, J. Grey, E. Nogueiro, P. Carmelo, M. Nunes da Ponte, Fractionation of Lipids in a Static Mixer and Packed Column Using Supercritical Carbon Dioxide, Ind. Eng. Chem. Res. 39 (12) (2000) 4820-4827.

[4] R.M. Ruivo, R.M. Couto, P.C. Simões, High Pressure Phase Equilibria of the Ternary System Oleic Acid / Squalene / Carbon Dioxide, J.Chem.Eng.Data. 52 (2007) 566-570.

[5] R. Ruivo, R. Couto, P. C. Simões; Supercritical carbon dioxide fractionation of the model mixture squalene/oleic acid in a membrane contactor; Separation and Purification Technology 59 (2008) 231–237.

[6] B.S. Furniss, A.J. Hannaford, P.W.G. Smith, A.R. Tachtell, Vogel's Textbook of Practical Organic Chemistry, fifth ed., Longmann Scientific & Technical, England, 1989.

Chapter 3

Ionic Liquids Screening[1]

1 Chapter published previously as: Rui Ruivo, Ricardo Couto, Pedro C. Simões; Screening of ionic liquids as promising separation agents of oil mixtures for application in membranes; Separation and Purification Technology 76 (2010) 84–88.

3.1 - Introduction

Chapter 2 explored the feasibility of coupling supercritical carbon dioxide extraction together with reverse osmosis membranes to improve the fractionation efficiency of squalene from the free fatty acids in olive oil residues. It was observed that the enrichment in the permeate side is mainly towards oleic acid. However, higher selectivities had the drawback of less permeate fraction collected.

A promising alternative is the use of supported ionic liquid membranes (SILM). SILM are composed of membranes in which a room temperature ionic liquid (RTIL) is immobilized. They have been successfully employed in the separation of organic compounds such as hydrocarbons, alcohols, amines and esters [1]-[5], owing to the high stability and non-volatile character of RTIL and their advantage with regard to tailor-made design for specific separation tasks. RTIL can be customized by an almost unlimited combination of cation-anion pairs to be selective for a specific compound in an extraction process. Thus, the use of supported ionic liquid membranes may be particularly interesting for the separation of squalene from free fatty acids in olive oil residues.

The purpose of this work was to screen and identify potential ionic liquids to be used in conjunction with the reverse osmosis membranes studied in Chapter 2, in order to create SILMs, which will be described in Chapter 5. With this aim in view, the same model mixture of oleic acid and squalene (50% w/w) used in Chapter 2, resembling the olive oil residues, was studied with a range of ionic liquids, chosen in order to assess the role of different cation (imidazolium, phosphonium and ammonium) and anion (tetrafluoroborate, hexafluorophosphate, bistriflamide, dicyanamide, nitrate, ethylsulfate, methanesulfonate, 2-(2-methoxyethoxy)-ethylsulfate) types on the extraction efficiency (Figure 3.1).

CATIONS

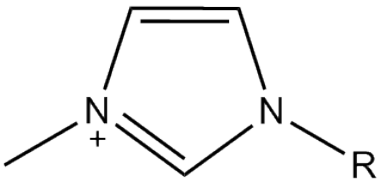

1-R-3-methyl-imidazolium

R= ethyl, butyl, octyl, decyl, 2-hydroxyethyl

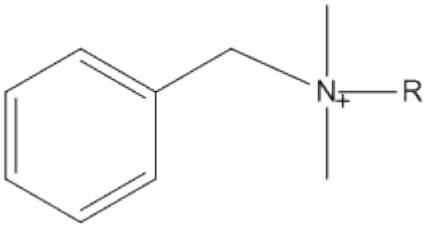

R-benzyl-dimethyl-ammonium

R= $C_{12}H_{25}$ (dodecyl), $C_{14}H_{29}$ (tetradecyl)

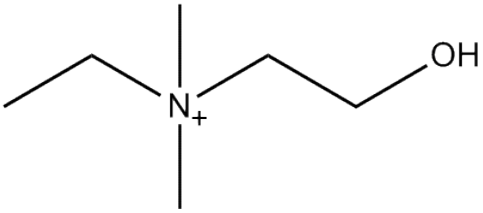

(2-hydroxyethyl)-ethyl-dimethyl-ammonium

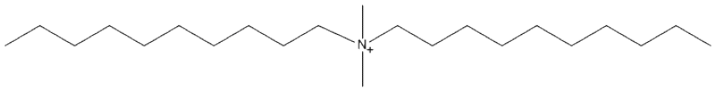

didecyl-dimethyl-ammonium

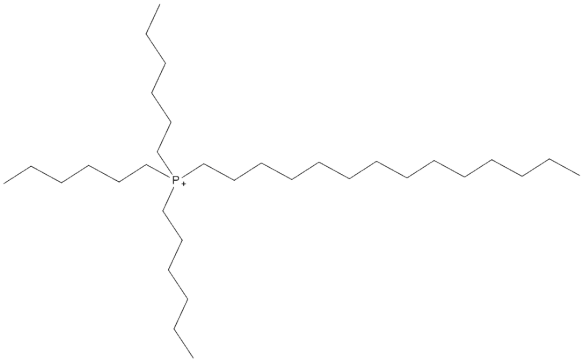

Trihexyl-tetradecyl-phosphonium

ANIONS

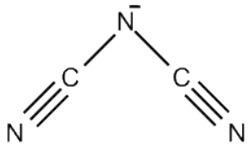

Dicyanamide

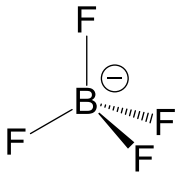

Tetrafluoro-borate

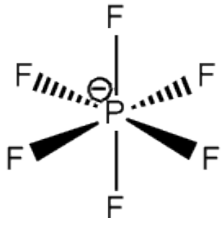

Hexafluoro-phosphate

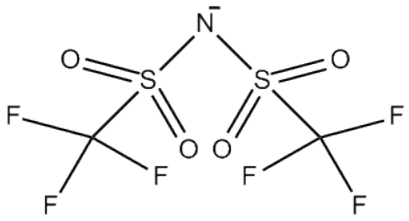

Bis(trifluoromethylsulfonyl)imide

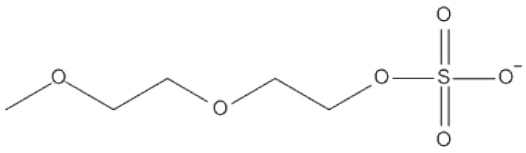

2-(2-methoxyethoxy)-ethylsulfate

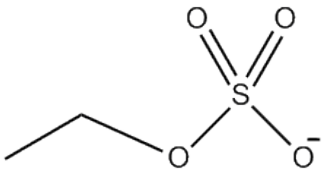

Ethylsulfate

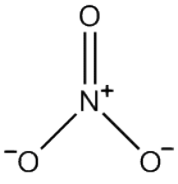

Nitrate

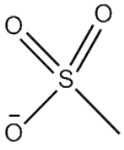

Methanesulfonate

Figure 3.1 - Molecular structures of the ionic liquids cations and anions studied in this work.

3.2 - Materials and Methods

Carbon dioxide was supplied with a purity of 99.995% by Air Liquide. Squalene was supplied by Sigma (98% by weight). Oleic Acid, supplied by Riedel-de-Haën, was of technical grade (79.9 % by mass); other major fatty acids present included myristic acid (C14:0) at 2.0 %, palmitoleic acid (C16:1) at 5.2 %, palmitic acid (C16:0) at 5.6 %, stearic acid (C18:0) at 1.0 %, and linoleic acid (C18:2) at 6.4 %.

The ionic liquids 1-ethyl-3-methyl-imidazolium ethylsulfate ([EMIM][$EtSO_4$], trade name ECOENG 212), 1-ethyl-3-methyl-imidazolium 2-(2-methoxyethoxy)-ethylsulfate ([EMIM][$MDEGSO_4$], trade name ECOENG 21M) and 1-ethyl-3-methyl-imidazolium methanesulfonate ([EMIM][MSO_4], trade name ECOENG 110) were purchased from Solvent Innovation (≥ 98% purity), trihexyl-tetradecyl-phosphonium tetrafluoroborate ([$(C_6)_3C_{14}P$][BF_4]) was purchased from Fluka (purity ≥95%), 1-decyl-3-methyl-imidazolium tetrafluoroborate ([$C_{10}MIM$][BF_4]), 1-octyl-3-methyl-imidazolium hexafluorophosfate ([OMIM][PF_6]), 1-octyl-3-methyl-imidazolium tetrafluoroborate ([OMIM][BF_4]), 1-butyl-3-methyl-imidazolium bis(trifluoromethylsulfonyl)-imide ([BMIM][NTf_2]), 1-butyl-3-methyl-imidazolium hexafluorophosfate ([BMIM][PF_6]), 1-butyl-3-methyl-imidazolium dicyanamide ([BMIM][DCA]), 1-(2-hydroxyethyl)-3-methyl-imidazolium tetrafluoroborate ([C_2OHMIM][BF_4]), 1-octyl-3-methyl-imidazolium dicyanamide ([OMIM][DCA]) and 1-butyl-3-methyl-imidazolium tetrafluoroborate ([BMIM][BF_4]) were purchased from Solchemar (>98% purity). All were used as received. The ionic liquids (2-hydroxyethyl)-ethyl-dimethyl-ammonium bis(trifluoromethylsulfonyl)-imide [C_2][NTf_2], didecyl-dimethyl-ammonium nitrate and alkyl-benzyl-dimethyl-ammonium nitrate ($C_6H_5CH_2N^+(CH_3)_2R^-NO_3$; R = 40% $C_{12}H_{25}$ + 60% $C_{14}H_{29}$) were synthesised according with previously published synthetic route [6].

Gas chromatography (GC) analysis was carried out as described in Chapter 2.

3.2.1 - Apparatus and Method.

Equal volumes of the model mixture oleic acid + squalene 50% (w/w) and ionic liquid were mixed at ambient temperature, shaken and left to separate for 48 hours. After separation, the oil and ionic liquid phases were collected separately. The relative composition of oleic acid and squalene in the two resulting phases was determined by GC analysis. RTIL are generally regarded as green solvents due to their non-volatile character. Yet, this makes difficult the separation and recovery of non-volatile or thermo-sensitive products from the RTIL. Supercritical carbon dioxide ($scCO_2$) was used in this work to recover a representative sample from the solutes dissolved in the ionic liquids for subsequent GC analysis. The recovery process is based on the principle that $scCO_2$ is soluble in RTIL, but RTIL are not soluble in $scCO_2$ [7].

Thus, the substances dissolved in the RTIL are transferred from RTIL to the supercritical fluid, from which these substances can then be recovered via depressurization [8]. The recovery method was accomplished in the high pressure apparatus schematically shown in Figure 3.2. It consists of a stainless steel cell of internal volume of 20 cm^3, and a CO_2 cylinder connected to a compressor. Pressure and temperature are measured by a pressure transducer (with an accuracy of ± 0.1 MPa) and an internal PT-100 sensor (precision of ±1 K), respectively. Sampling is performed through an HPLC valve.

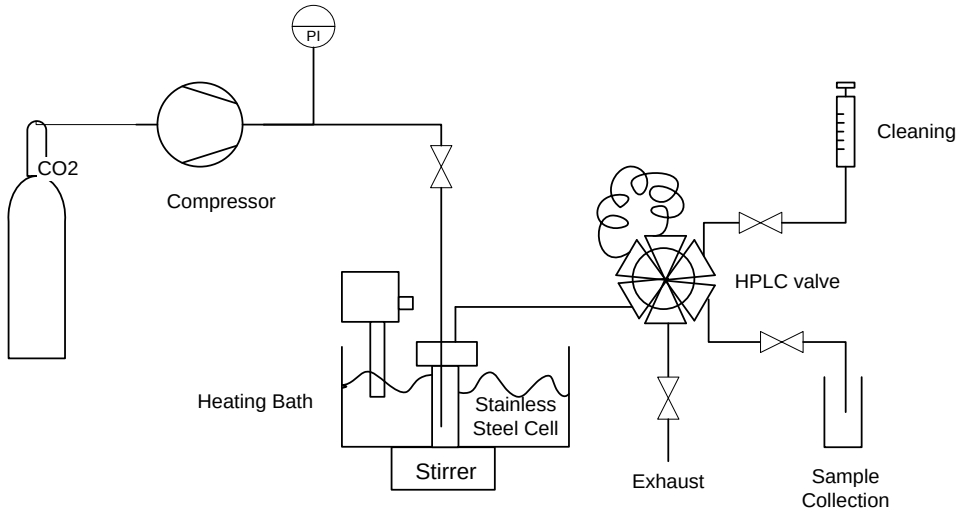

Figure 3.2 - High pressure apparatus for the extraction of solutes from the ionic liquid and oil phases.

Each phase is fed to the high pressure cell and later pressurized with carbon dioxide at 25 MPa and 313K for one hour, so that oleic acid and squalene partitionate to the CO_2 phase. These conditions of pressure and temperature were chosen so that the solubilities of squalene and oleic acid in $scCO_2$ were similar. Therefore, the relative composition of the sample solubilised in the CO_2-rich phase is identical to the original composition in the oil or ionic liquid phase. A sample from the gas phase is collected through an HPLC valve, by bubbling in hexane, for full recovery of dissolved substances. Samples are subsequently analysed by GC.

To validate the experimental method and guarantee that the composition of the sample extracted by $scCO_2$ was identical to the composition in the liquid phase introduced in the extraction cell, a blank experiment was carried out where a given amount of the model mixture oleic acid + squalene was extracted by $scCO_2$. The composition of the oil extracted by $scCO_2$ and analyzed by GC was the same as the original composition of the model mixture, therefore validating the method.

3.3 - Results and Discussion

For the most part of the ionic liquids studied, the volume of the ionic liquid phase was not observed to change during the contact and mixing with the model mixture of squalene + oleic acid, indicating a low co-solubility of the phases. The exceptions were [EMIM][$EtSO_4$] where a relative expansion of the oil phase was observed, and [EMIM][$MDEGSO_4$] and [C_{10}MIM][BF_4], where it was observed an expansion of the ionic liquid phase. No quantitative measurement of the volume expansion was possible to be made at the time of the experiments.

For some of the tested RTILs no separation was achieved, either because complete miscibility was observed (alkyl-benzyl-dimethyl-ammonium nitrate, [OMIM][DCA] and [EMIM][MSO_4]) or because solidification occurred (didecyl-dimethyl-ammonium nitrate).

The results obtained for the fractionation of the oleic acid / squalene mixture for the RTIL where separation was achieved are shown in Table 3.1 in terms of the partition coefficient (K_D) of oleic acid to the respective ionic liquid phase. The partition coefficient was calculated from the relative compositions of oleic acid in the ionic liquid and oil phases as determined by GC, with the following equation:

$$K_D = C_{oleic\ acid|ionic\ liquid\ phase} / C_{oleic\ acid|oil\ phase} \quad (3.1)$$

Table 3.1 - Partition coefficients of oleic acid for the ionic liquids studied in this work.

Ionic liquid	K_D
[C_2OHMIM][BF_4]	1.27
[BMIM][BF_4]	1.44
[OMIM][BF_4]	1.65
[DMIM][BF_4]	1.31
[$(C_6)_3C_{14}P$][BF_4]	1.02
[BMIM][PF_6]	1.14
[OMIM][PF_6]	1.50
[EMIM][$EtSO_4$]	1.10
[BMIM][DCA]	1.84
[EMIM][$MDEGSO_4$]	2.96
[$(C_6)_3C_{14}P$][NTf_2]	1.08
[BMIM][NTf_2]	0.86
[C_2][NTf_2]	0.85

The majority of the RTIL studied in this work show a selectivity towards the oleic acid in detriment of squalene as can be seen from the values of K_D listed in Table 3.1. Taking into account that the majority of RTIL studied are dipolar hydrogen-bond acceptor solvents [9] it is not surprising that they show a higher affinity towards oleic acid (an equal hydrogen-bond acceptor with the carbonyl group as well as a hydrogen-bond donor with the hydroxyl group). A comparison of the K_D data for the ionic liquids listed in Table 3.1 shows that both the cation and anion types had a reasonable effect on the fractionation of the model mixture. Figures 3.3 and 3.4 show, respectively, the influence of the cation and the anion type on the partition of oleic acid between the ionic liquid and oil phases. A relatively wider variation of the K_D with the anion class was observed. The ionic liquid with the 2-(2-methoxyethoxy)-ethyl sulfate anion ([EMIM][$MDEGSO_4$]) gave the highest partition coefficient (K_D = 2.96) while the ionic liquids with the bis(trifluoromethylsulfonyl)-imide anion ([BMIM][NTf_2] and [C_2][NTf_2]) gave the lowest partition coefficients (K_D = 0.86 and 0.85, respectively).

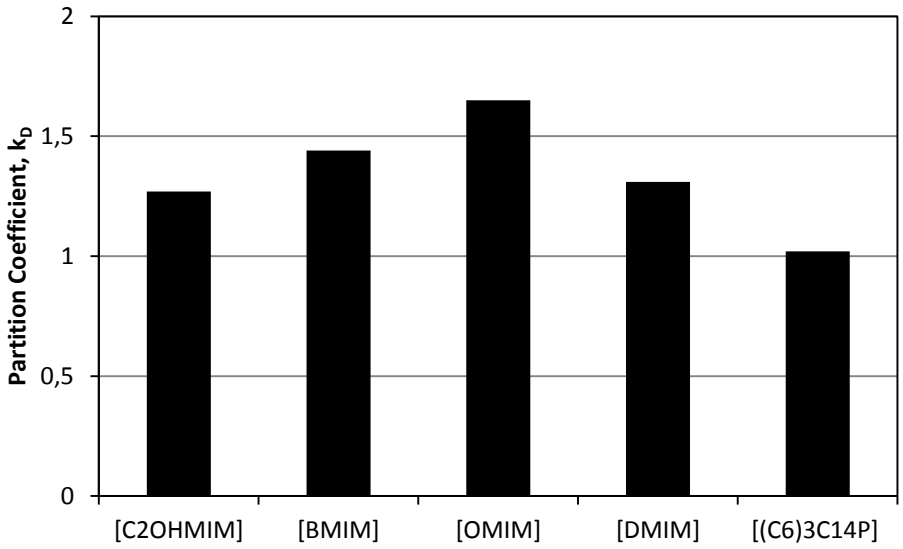

Figure 3.3 - Partition coefficient of oleic acid with A^+ $[BF4]^-$ ionic liquids.

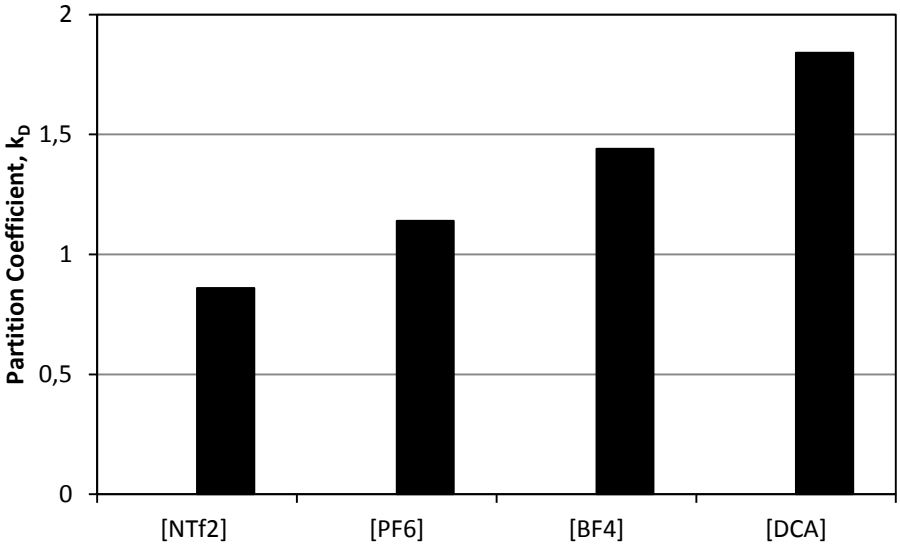

Figure 3.4 - Partition coefficient of oleic acid with $[BMIM]^+ X^-$ ionic liquids.

The influence of the proportions of model mixture and IL was also studied, and results are presented in Figure 3.5. In addition to the proportions shown in Figure 3.5, the proportion of 200 µL Mix/1 mL IL was also studied, but complete solubilisation occurred. It is seen that by increasing the relative proportion of IL, the partition coefficient also increases. In fact, by adjusting the proportions of model mixture and IL is possible to alter the selectivity towards squalene or oleic acid.

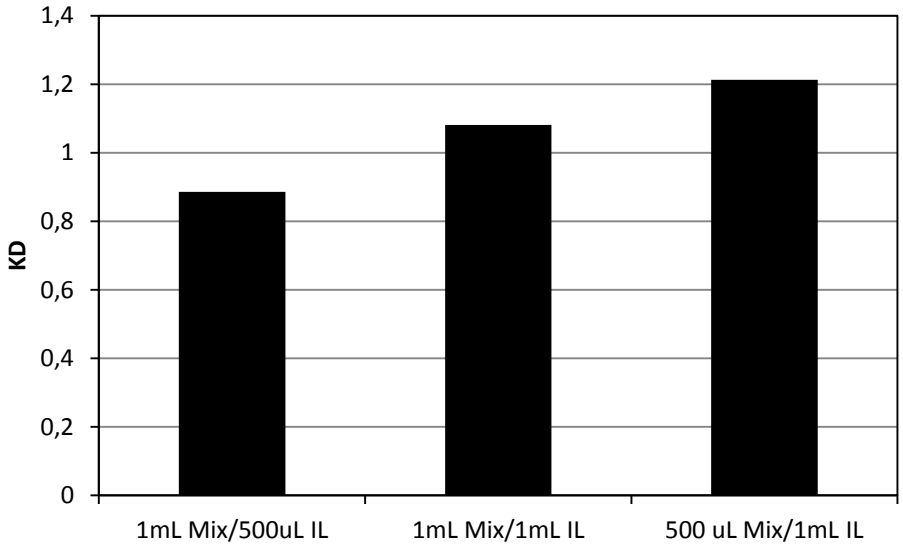

Figure 3.5 – Partition coefficient of oleic acid with different proportions of model mixture and $[(C_6)_3C_{14}P][NTf_2]$.

The effect of the type of cation and anion on the fractionation of the oil mixture can be explained by the change on the polarity or solvent strength of the room temperature ionic liquid

and thus on the affinity of the RTIL towards oleic acid or squalene. The most polar ionic liquids show more affinity towards the oleic acid, while the least polar ones have more affinity towards squalene.

The empirical scale of solvent polarity as suggested by Reichardt [10] was used to evaluate the polarity of the RTIL studied in this work. Reichardt used the large negative solvatochromism of the standard betaine dye no. 30 (2,6-diphenyl-4-(2,4,6-triphenylpyridinium-1-yl)phenolate) to determine spectroscopically an empirical scale of solvent polarity, called the $E_T(30)$ scale. The $E_T(30)$ values are simply defined as the molar transition energies of the betaine dye measured in solvents of different polarity at room temperature (298 K) and normal pressure (0.1 MPa), according to equation 3.2,

$$E_T(30)/(\text{kcal mol}^{-1}) = h\, c\, \tilde{\nu}_{max}\, N_A = (2.8591 \times 10^{-3})\, \tilde{\nu}_{max}/\text{cm}^{-1} = 28591/(\lambda_{max}/\text{nm}) \qquad (3.2)$$

where $\tilde{\nu}_{max}$ is the wavenumber and λ_{max} the wavelength of the maximum of the long-wavelength, solvatochromic, intramolecular charge-transfer absorption band of the standard betaine dye, and *h*, *c*, and N_A are the Planck's constant, the speed of light, and Avogadro's constant, respectively. According to this scale, high $E_T(30)$ values correspond to high solvent polarity.

The scale can be made dimensionless, by using a normalized E_T^N scale. This scale ranges from 0.0 for tetramethylsilane (the least polar solvent) to 1.0 for water (the most polar solvent). E_T^N is defined according to equation 3.3,

$$E_T^N = [E_T(\text{solvent}) - E_T(\text{TMS})] / [E_T(\text{water}) - E_T(\text{TMS})] = [E_T(\text{solvent}) - 30.7] / 32.4 \qquad (3.3)$$

Table 3.2 presents the E_T^N polarity ranges for several groups of ionic liquids for which $E_T(30)$ values were available in the literature [9], [11]-[14]. For some of the ionic liquids studied in this work no information was available in the literature. In addition, a close inspection of Table 3.2 shows a non-negligible discrepancy of the E_T^N values for some ionic liquids. These deviations are probably linked to the fact that the E_T^N values reported in the literature have been determined at different temperatures and different solvatochromic indicator dyes. These effects are further studied in Chapter 4, where a new technique to probe ionic liquids polarities is developed.

Ionic liquids of the imidazolium type with a 1-alkyl-3-methyl- substitution pattern, $[R^3mim]^+X^-$, have E_T^N values ranging from 0.53 to 0.75. The increase of the length of one of the 1,3-alkyl substituents causes a small decrease in the E_T^N values; alternation of the anion has a small

influence on the E_T^N value. In comparison, the tetraalkylphosphonium salts are less polar with values (E_T^N = 0.35 - 0.44) that cover a similar range to less polar organic solvents (e.g., acetone, E_T^N = 0.36 [14], dimethylformamide, E_T^N = 0.40, and dimethyl sulfoxide, E_T^N = 0.44 [9]). For the A^+ $[BF4]^-$ ionic liquids studied in this work (see Figure 3.3) the trihexyltetradecylphosphonium salt, $[(C_6)_3C_{14}P][BF_4]$, had the lowest partition coefficient of all. For the 1-alkyl-3-methylimidazolium salts, $[R^3mim][BF_4]$, in general, the longer the alkyl chain, the more affinity towards squalene was observed. By looking at the effect of the anion class, and for the same cation [BMIM], affinity towards oleic acid grows in the anion sequence $[NTf_2]$ < $[PF_6]$ < $[BF_4]$ < [DCA] (see Figure 3.4), partially resembling the trend of polarities of these RTIL (see Table 3.2).

Table 3.2 - Solvent polarity of RTIL determined by solvatochromism (Reichardt's method).

Ionic liquid	E_T^N	Reference
$[R_4P]^+ X^-$ RTIL (R = Methyl, 1-Butyl, 1-Octyl, 1-Dodecyl; X = Cl, Br, I)	0.35 - 0.44	[11]
$[R^3mim]^+ X^-$ RTIL[&]	0.53 - 0.75	-
[EMIM] $[BF_4]$	0.71	[12]
[EMIM] $[NTf_2]$	0.68; 0.69	[13], [14]
[EMIM] [DCA]	0.65	[13]
[BMIM] $[PF_6]$	0.67 - 0.69	[12-17]
[BMIM] $[BF_4]$	0.67 - 0.68	[12], [16]
[BMIM] $[NTf_2]$	0.60 - 0.64	[13-16]
[BMIM] [DCA]	0.63	[13]
[OMIM] $[BF_4]$	0.67	[17]
[OMIM] $[NTf_2]$	0.63	[15]
[OMIM] $[PF_6]$	0.60	[17]
$[C_2OHMIM]$ $[NTf_2]$	0.93	[16]
Non-ionic solvents		
Water	1.00	[9]
Dimethyl formamide	0.40	[9]
n-Heptane	0.05	[9]

[&] R^3: generic group on position 3 of the imidazolium ring

3.4 - Conclusions

Fractionation of a mixture of oleic acid / squalene using room temperature ionic liquids as the extracting agent has been investigated for a range of imidazolium, phosphonium and ammonium based ionic liquids. It was shown that it is possible to adjust the fractionation of the oil mixture by adequately choosing the type of anion and cation of the room temperature ionic liquid. This effect could be explained by the change in the polarity or solvent strength of the RTIL. It was also shown that by altering the proportions of ionic liquid and mixture to be extracted is possible to further adjust the fractionation.

3.5 - References

[1] L.C. Branco, J.G. Crespo, C.A.M. Afonso, Highly selective transport of organic compounds by using supported liquid membranes based on ionic liquids, Angew. Chem., Int. Ed. 41 (2002) 2771-2773.

[2] E. Miyako, T. Maruyama, N. Kamiya, M. Goto, Use of ionic liquids in a lipase-facilitated supported liquid membrane, Biotechnol. Lett. 25 (2003) 805-808.

[3] M. Matsumoto, Y. Inomoto, K. Kondo, Selective separation of aromatic hydrocarbons through supported liquid membranes based on ionic liquids, J. Membr. Sci. 246 (2005) 77–81.

[4] A.P. Ríos, F.J. Hernández-Fernández, H. Presa, D. Gómez, G. Víllora, Tailoring supported ionic liquid membranes for the selective separation of transesterification reaction compounds, J. Membr. Sci. 328 (2009) 81–85.

[5] P. Scovazzo, J. Kieft, D. Finan, R.D. Noble, C.A. Koval, Gas Separations Using Non-Hexafluorophosphate [PF6] - Anion Supported Ionic Liquid Membranes, J. Membr. Sci, 238 (2009) 57-64.

[6] M. Earle, U. Frohlich, S. Huq, S. Katdare, R. Lukasik, E. Bogel, N. Plechkova, K. Seddon, Base Stable Ionic Liquids, WO2006072785, 2006.

[7] L.A. Blanchard, J.F. Brennecke, Recovery of organic products from ionic liquids using supercritical carbon dioxide, Ind. Eng. Chem. Res. 40 (2001) 287-292.

[8] S. Keskin, D. Kayrak-Talay, U. Akman, Ö. Hortaçsu, A Review of ionic liquids towards supercritical fluid applications, J. Supercrit. Fluids, 43 (2007) 150–180.

[9] C.F. Poole, S.K. Poole, Extraction of organic compounds with room temperature ionic liquids, J. Chromatogr. A, 1217 (2010) 2268–2286.

[10] C. Reichardt, Polarity of ionic liquids determined empirically by means of solvatochromic pyridinium N-phenolate betaine dyes, Green Chem. 7 (2005) 339–351.

[11] W.B. Harrod, N.J. Pienta, Solvent polarity scales. 1. Determination of E_T and π^* values for phosphonium and ammonium melts, J. Phys. Org. Chem. 3 (1990) 534–544.

[12] S. Park, R.J. Kazlauskas, Improved preparation and use of room temperature ionic liquids in lipase-catalyzed enantio- and regioselective acylations, J. Org. Chem. 66 (2001) 8395–8401.

[13] C. Chiappe, D. Pieraccini, Determination of Ionic Liquids Solvent Properties Using an Unusual Probe: The Electron Donor−Acceptor Complex between 4,4‘-bis(Dimethylamino)-benzophenone and Tetracyanoethene, J. Phys. Chem. A 110 (2006), 4937-4941.

[14] K.A. Fletcher, S. Pandey, Solvatochromic Probe Behavior Within Neat and Cosolvent Added Room-Temperature Ionic Liquid Solutions, in H.C. Dulong, R.W. Bradshaw, M. Matsunaga, G.K. Stafford, P.C. Trulove (Eds.), 2002-19-Molten Salts XIII, Electrochemical Society, Pennsylvania, 2002, pp. 244-256.

[15] M.J. Muldoon, C.M. Gordon, I.R. Dunkin, Investigations of solvent–solute interactions in room temperature ionic liquids using solvatochromic dyes, J. Chem. Soc., Perkin Trans. 2 (2001) 433–435.

[16] S.V. Dzyuba, R.A. Bartsch, Expanding the polarity range of ionic liquids, Tetrahedron Lett. 43 (2002) 4657–4659.

[17] J.G. Huddleston, G. Broker, H. Willauer, R.D. Rogers, Ionic Liquids - Industrial Applications to Green Chemistry, ACS Symposium Series, American Chemical Society, Washington, DC, 2002, pp. 270–288.

Chapter 4

Ionic Liquids Polarities Measurements[2]

[2] Chapter partially accepted for publication as: Ricardo M. Couto, Catarina Lourenço, João C. Lima, Pedro C. Simões, Luis C. Branco; Studies of the influence in acetonitrile polarity using imidazolium Ionic Liquids as additives; Journal of Chemical and Engineering Data

4.1 - Introduction

When analyzing the results obtained for the separation of the model mixture of oleic acid/squalene with RTILs, presented in Chapter 3, it was realized that the separations being observed were related to the polarity of the RTILs. However, very few of the RTILs studied had their polarity already published in the literature. As a way of rationalizing the results obtained, it was decided to explore not only the polarity of the RTILs used in this work but also of a few others available in the laboratory.

The polarity or strength of a solvent is a well-accepted concept but suffers from a rather vague definition. Reichardt [1] proposed a practical definition of the solvent polarity (later accepted by IUPAC [2]) as the "overall solvation capability (or solvation power) for (i) educts and products, which influences chemical equilibria; (ii) reactants and activated complexes (''transition states''), which determines reaction rates; and (iii) ions or molecules in their ground and first excited state, which is responsible for light absorptions in the various wavelength regions. This overall solvation capability depends on the action of all, nonspecific and specific, intermolecular solute–solvent interactions, excluding such interactions leading to definite chemical alterations of the ions or molecules of the solute".

These interactions involve several distinct and different intermolecular forces with the consequence that no single probe molecule or macroscopic physical parameter is capable of providing a suitable scale of solvent polarity.

A considerable amount of ionic liquids (ILs) polarities measurements have been reported already [3]. Different probes have been explored, such as Nile Red [4]-[6], pyrene [6], dansylamide [6], 1-pyrenecarbaldehyde [6], Michler's ketone [7], DAP [8], [Cu(acac)(tmen)][BPh_4] [9], [Cu(acac)(tmen)][X] (X=BPh_4 or ClO_4) [10], and Coumarin-153 [11]. The measurement techniques employed have been mainly UV/Vis spectroscopy [4], [7], [9], [10] or fluorescence spectrometry [5], [6], [8], [11]. Despite of several polarity studies already reported using different probes, the largest number of approaches have undoubtedly been done based on solvatochromism of betaine dye nº. 30 (commonly known as Reichardt's dye) studied by UV/Vis spectroscopy [3], [6], [9], [10], [12]-[15].

Rani and coworkers [16] have shown that when comparing solvatochromic polarity values, it is important to always compare values from the same solvatochromic dye in order to avoid deviations due to the different interactions of different probes with the solvents being used. For that reason, we have chosen to work with betaine dye nº. 30, in order to have the widest range of data already published to compare with our results.

Reichardt [1] used the large negative solvatochromism of the standard betaine dye no. 30 as a UV/Vis spectroscopic indicator of solvent polarity. The long-wavelength intramolecular charge-transfer (CT) absorption band of betaine dye nº. 30 was used as a solvent-dependent reference process to define empirically a solvent polarity scale, called the $E_T(30)$ scale. $E_T(30)$ values are simply defined as the molar transition energies of the betaine dye measured in solvents of different polarities at room temperature (298 K) and normal pressure (0.1 MPa), according to equation 4.1,

$$E_T(30)/(\text{kcal mol}^{-1}) = h\, c\, \tilde{\nu}_{max}\, N_A = (2.8591 \times 10^{-3})\, \tilde{\nu}_{max}/\text{cm}^{-1} = 28591/(\lambda_{max}/\text{nm}) \qquad (4.1)$$

where $\tilde{\nu}_{max}$ is the wavenumber and λ_{max} is the maximum wavelength and h, c, and N_A are the Planck's constant, the speed of light, and Avogadro's constant, respectively. According to this scale, high $E_T(30)$ values correspond to high solvent polarity.

The scale can be made dimensionless, by using a normalized E_T^N scale. This scale ranges from 0.0 for tetramethylsilane (the least polar solvent for which $E_T(30)$ values are experimentally available) to 1.0 for water (the most polar solvent). E_T^N is defined according to equation 4.2,

$$E_T^N = [E_T(\text{solvent}) - E_T(\text{TMS})] / [E_T(\text{water}) - E_T(\text{TMS})] = [E_T(\text{solvent}) - 30.7] / 32.4 \qquad (4.2)$$

Despite of this simple procedure widely described in several papers [3], [6], [9], [10], [12]-[15], soon it was realized that most RTILs used in this work present difficulties in the dissolution of Reichardt's dye. Either the dye would not dissolve in the RTIL or it would be needed to add a large amount of the dye for the RTIL to acquire a measurable band in the region of the visible spectrum. In order to overcome this problem, it was needed to find an alternative solution. Thus, it was decided to probe the RTILs polarities by an indirect method. Instead of measuring the polarity of the RTIL, it was measured the change in polarity induced by the addition of small quantities of RTIL to common organic solvents of well known polarity.

Although many authors have explored the polarity of RTILs, little work has been done to explore the RTILs effect in the polarity of other organic solvents. Baker and co-workers [15] have explored the influence of water content and temperature in RTILs polarities, and found that the presence of small quantities of water increases the polarity of the RTIL. Rani and co-workers have also studied the deviation in polarity caused by the presence of common impurities [16]. The reverse effect of the one studied in this chapter, i.e., the influence of the addition of small quantities of solvents to ILs has been investigated [17]. Recently, some

specific cases of addition of small quantities of RTILs to common organic solvents, such as [BMIM][PF_6] to propylene carbonate [18] or [BMIM][Cl] to acetonitrile, dimethylsulfoxide or N,N-dimethylformamide [19] have been also reported.

4.2 - Materials and Methods

All RTILs used in this work are from Solchemar Lda (>98% purity). Acetonitrile was HPLC grade (Scharlau). Ethanol, tetrahydrofuran (THF), predried THF, toluene, isopropanol, dioxan and chloroform were all p.a. in purity and from Sigma Aldrich. Betaine dye nº. 30 was from Sigma-Aldrich (>90% purity). Molecular structures of solvents and betaine dye are presented in Figure 4.1, while those of RTILs anions and cations are presented in Figure 4.2.

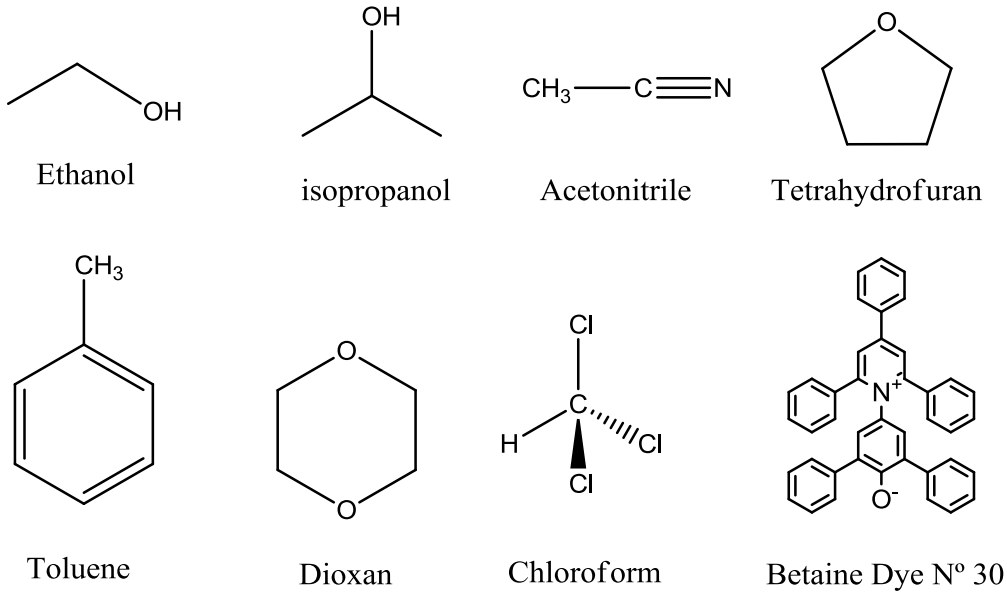

Figure 4.1 – Molecular structures of solvents and probe (betaine) used in this work.

The water content of all ILs used in this work was measured by Karl Fischer titration with a Metrohm 831 KF Coulometer.

4.2.1 - UV/Visible Spectroscopy

A solution of 20 mg betaine dye nº. 30 in 100 mL of the appropriate solvent was prepared as stock solution for the measurements. From this stock solution, 2.4 mL were placed in a quartz cell of 10 mm path length. The appropriate volume (2, 4, 6, 8 or 10 µL) of the ionic liquid to be measured was added and the cell was agitated for complete dissolution. The exceptions were [BMIM][Cl], [BDMIM][Cl], [BDMIM][BF_4], [C_3OMIM][PF_6] and [C_5O_2MIM][PF_6] which are solid at ambient temperature, and additions had to be measured in mass. In the cases of [DMG][Cl] and [C_3OMIM][Cl] dilutions had to be made with the solvent being studied before the addition, as very small amounts of these ILs would completely decolorize the Reichardt's

dye solution. Measurements were performed in a Perkin Elmer Lambda 35 UV/Vis Spectrometer. The results are the average of at least two measurements at room temperature (298 K).

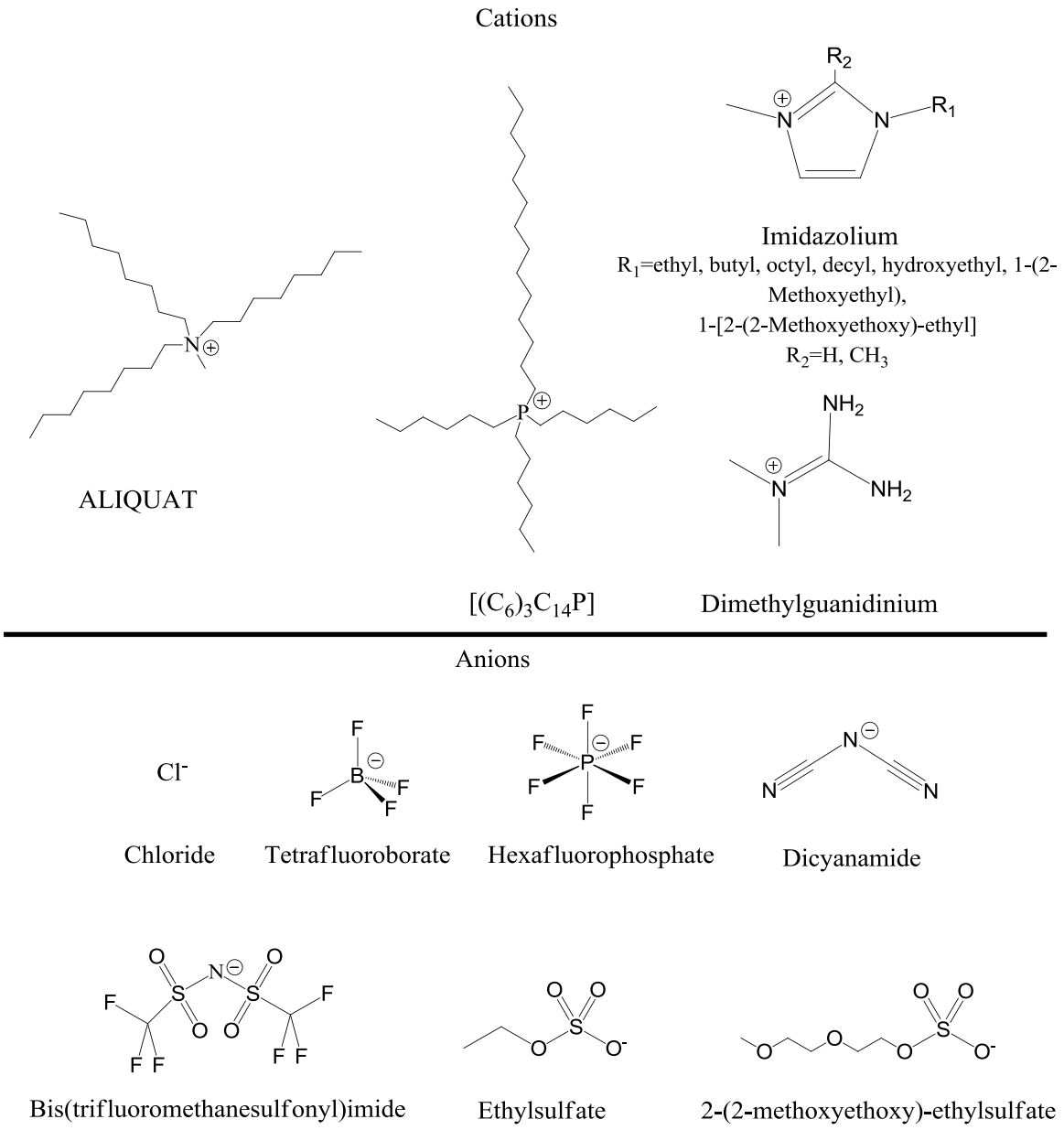

Figure 4.2 – Molecular structures of ionic liquids cations and anions used in this work.

4.3 - Results

For the polarity studies were selected thirty-one commercially available RTILs based on ammonium ([ALIQUAT]), phosphonium ([$(C_6)_3C_{14}P$]), imidazolium ([RMIM]), 1-butyl-2,3-dimethylimidazolium ([BDMIM]) and guanidinium ([DMG]) cations combined with ethylsulfate ([$EtSO_4$]), 2-(2-methoxyethoxy)-ethylsulfate ([$MDEGSO_4$]), chloride ([Cl]), tetrafluoroborate ([BF_4]), hexafluorophosphate ([PF_6]), dicyanamide ([DCA]) and bis(trifluoromethanesulfonyl)imide ([NTf_2]) anions. R substituents in imidazolium cations were ethyl, butyl, octyl, decyl, hydroxyethyl, 1-(2-Methoxyethyl), 1-[2-(2-Methoxyethoxy)-ethyl]. This selection of RTILs included, besides the RTILs used in Chapter 2, more hydrophobic or hydrophilic cations and anions in order to elucidate its influence in the polarity studies.

In Table 4.1 are presented reference values from the literature and the values obtained in this work by UV-Vis spectroscopy for the addition of Reichardt's dye to pure [BMIM][BF_4] RTIL. Although the two measurements made in this work present differences between themselves, these are in accordance with the values reported in literature, validating in this way our experimental procedure.

Table 4.1 – Wavelength values obtained and calculated $E_T(30)$ and E_T^N, from literature and this work, for pure [BMIM][BF_4] with addition of Reichardt's dye.

λ	$E_T(30)$	E_T^N	Reference
542.19	52.73	0.680	[12]
545.00	52.50	0.673	[10]
546.05	52.36	0.669	This Work
541.75	52.78	0.681	This Work

However, it was realized that it is very difficult to get Reichardt's dye to solubilize in most RTILs, or when it solubilizes it is needed to add large amounts to have the RTIL acquire some coloring. In view of these difficulties, it was decided to try to measure the RTILs polarities by an indirect method, in which a very small quantity of RTIL is added to a solution of Reichardt's dye and the deviation in the solvent polarity is measured. In this way, it should be possible to construct a table of relative polarities of the RTILs studied, based on the amount of deviation induced by the addition of a similar quantity of RTIL.

The solvent for which it was found that this method works best is acetonitrile, and thus it is also the solvent for which more results were obtained. In Table 4.2 are presented the values obtained by UV/Vis spectroscopy of the addition of RTILs to a solution of betaine dye (0.36 mM) in

acetonitrile. This table includes the mole fraction of RTIL in acetonitrile ($X_{RTIL/ACN}$), the corresponding volume or mass of RTIL added, the number of moles of RTIL per mole of betaine dye ($\mu_{RTIL/Betaine}$), the wavelength of the maximum of the intramolecular CT absorption band of the betaine dye, the respective E_T^N and $E_T(30)$ values. Water content for the ionic liquids was found to be between 9 and 250 mg/g.

Table 4.2 – Effects in polarity of the addition of ionic liquids to acetonitrile.

Mixture (ACN + RTIL)	**$X_{RTIL/ACN}$ x10^{-4}**	**Vol. RTIL (µL)**	**$\mu_{RTIL/Betaine}$**	**Wavelength (nm)**	**$E_T(30)$**	**E_T^N**
ACN	0	0	_____	626.1	45.67	0.462
[ALIQUAT][Cl]	4.94	10	22.41	624.4	45.79	0.466
[ALIQUAT][DCA]	4.45	10	20.20	623.1	45.89	0.469
$[(C_6)_3C_{14}P][Cl]$	2.22	6	10.06	624.3	45.80	0.466
$[(C_6)_3C_{14}P][BF_4]$	3.54	10	16.08	624.7	45.77	0.465
$[(C_6)_3C_{14}P][NTf_2]$	2.99	10	13.56	625.4	45.72	0.464
$[(C_6)_3C_{14}P][DCA]$	3.56	10	16.15	624.7	45.77	0.465
$[EMIM][NTf_2]$	3.39	4	15.37	531.9	53.76	0.712
$[EMIM][EtSO_4]$	4.55	4	20.65	623.1	45.89	0.469
$[EMIM][MDEGSO_4]$	3.24	4	14.72	621.7	45.99	0.472
[BMIM][Cl]	2.24	1.8 mg	10.17	622.6	45.93	0.470
$[BMIM][PF_6]$	4.16	4	18.89	621.3	46.02	0.473
$[BMIM][BF_4]$	4.31	4	19.55	620.9	46.05	0.474
$[BMIM][NTf_2]$	4.51	6	20.49	618.1	46.26	0.480
[BMIM][DCA]	4.50	4	20.42	622.7	45.91	0.470
[OMIM][Cl]	3.80	4	17.27	622.7	45.92	0.470
$[OMIM][PF_6]$	3.15	4	14.32	626.1	45.67	0.462
$[OMIM][BF_4]$	3.42	4	15.52	622.5	45.93	0.470
$[OMIM][NTf_2]$	3.64	6	16.52	618.0	46.26	0.480
[OMIM][DCA]	3.37	4	15.29	621.4	46.01	0.473
$[C_{10}MIM][BF_4]$	4.52	6	20.53	561.9	50.88	0.623
[BDMIM][Cl]	4.84	4.2 mg	21.96	623.5	45.85	0.468
$[BDMIM][BF_4]$	4.71	5.2 mg	21.37	624.6	45.77	0.465
$[BDMIM][NTf_2]$	4.29	6	19.46	624.3	45.80	0.466
$[C_2OHMIM][PF_6]$	4.73	4	21.46	564.0	50.70	0.617
$[C_2OHMIM][BF_4]$	5.31	4	24.12	623.0	45.90	0.469

Table 4.2 – (continued) Effects in polarity of the addition of ionic liquids to acetonitrile.

Mixture (ACN + RTIL)	$X_{RTIL/ACN}$ x10^{-4}	Vol. RTIL (µL)	$\mu_{RTIL/Betaine}$	Wavelength (nm)	$E_T(30)$	E_T^N
$[C_3OMIM][Cl]$	0.23	0.16	1.05	623.4	45.87	0.468
$[C_3OMIM][PF_6]$	3.80	5.0 mg	17.24	621.3	46.02	0.473
$[C_3OMIM][BF_4]$	4.98	4	22.60	618.7	46.22	0.479
$[C_5O_2MIM][Cl]$	4.49	4	20.38	620.9	46.05	0.474
$[C_5O_2MIM][PF_6]$	3.09	4.7 mg	14.04	620.0	46.11	0.476
[DMG][Cl]	0.26	0.6	1.16	624.5	45.78	0.465

All ionic liquids were added pure to acetonitrile, with the exceptions of [DMG][Cl] and $[C_3OMIM][Cl]$, which were first diluted in acetonitrile and then added to the solution with Reichardt's dye. The volumes indicated in the table for these two cases are the volumes of pure RTIL present in the solution added.

Figure 4.3 plots the effects in E_T^N values of acetonitrile of the addition of RTILs by anion, for the cations $[(C_6)_3C_{14}P]$, [BMIM] and [OMIM], whereas Figure 4.4 plots the effects in E_T^N values of acetonitrile by the addition of RTILs by cation, for the anions [Cl], $[BF_4]$, $[PF_6]$ and $[NTf_2]$.

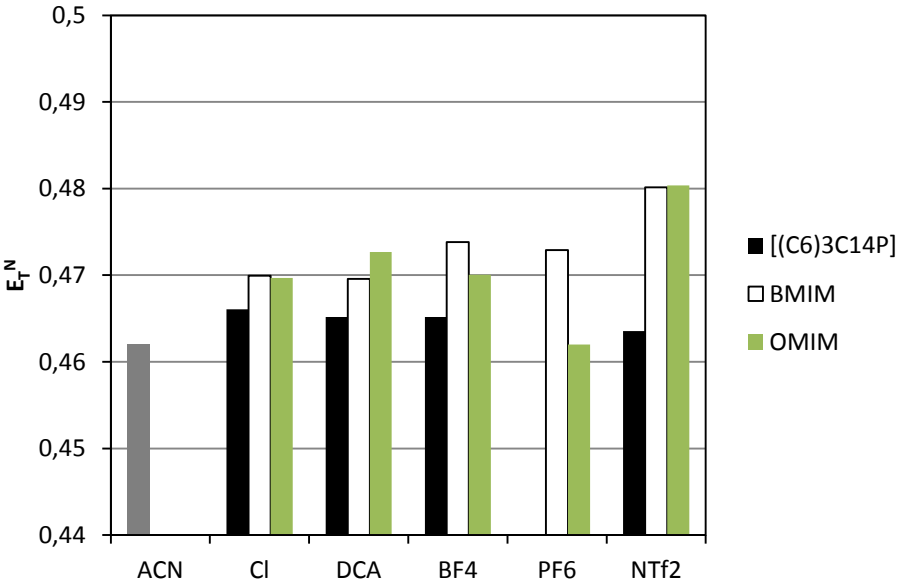

Figure 4.3 - Anion effect in E_T^N values of acetonitrile.

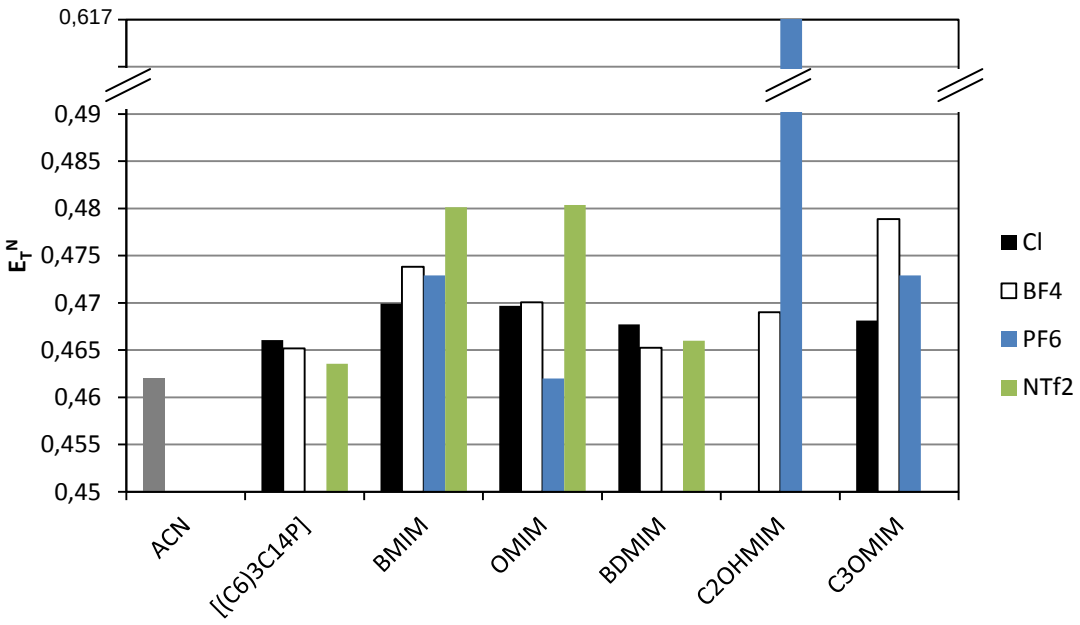

Figure 4.4 - Cation effect in E_T^N values of acetonitrile.

From Figures 4.3 and 4.4 it is apparent that the influence in polarity is linked mainly to the cation. The cation $[(C_6)_3C_{14}P]$ has consistently the lowest polarity with the three anions plotted in Figure 4.3. This is an obvious consequence of its structure with four long arms without any functionalisation. Secondly, [OMIM] has a polarity effect in acetonitrile similar or lower than [BMIM], which indicates that the longer side chain of [OMIM] leads to a lower polarity.

Except for $[C_2OHMIM][PF_6]$ (which has an E_T^N value of 0.617), the range of polarities plotted in Figures 4.3 and 4.4 is very limited (from 0.463 to 0.484), about 2% of the total polarity scale range. So, it is seen that although the addition of RTILs to acetonitrile leads to measureable deviations in polarity, these are still considerably low for most cases, as would be expected, since acetonitrile is much more abundant in the solutions prepared. Of the cases studied, the only exceptions are $[EMIM][NTf_2]$(E_T^N=0.712), $[C_2OHMIM][PF_6]$ (E_T^N=0.617) and $[C_{10}MIM][BF_4]$ (E_T^N=0.623). It is, however, foreseeable that with continuous addition of RTIL, the polarity values should stabilize in a plateau. On the other hand, with sufficient addition of RTILs, the solution becomes colorless, rendering it impossible to measure a polarity value. In some cases, this threshold is so low that it was needed to dilute the RTILs to obtain measurable values, as in the cases of $[C_3OMIM][Cl]$ and [DMG][Cl].

From the polarity studies (Table 4.2), we can conclude that the acetonitrile polarity increases with the addition of ionic liquid. Specifically, acetonitrile polarity increases with the addition of RTILs containing [BMIM] as cation in the following sequence $[Cl] < [PF_6] \approx [BF_4] < [NTf_2]$,

which is in agreement with the expected polarity of these anions [3]. Surprisingly, though, the [DCA] anion presents an effect in acetonitrile polarity very similar to the [Cl] anion. This might be due to the structural similarities of acetonitrile and the [DCA] anion, which would lead to a minor disruption of the supramolecular arrangement of the solvent.

As for the [OMIM] cation series, polarity of acetonitrile is found to increase in the following sequence $[PF_6]$< [Cl]≈$[BF_4]$< [DCA]< $[NTf_2]$. This could be an effect introduced by the longer alkyl side chain.

On the other hand, it is possible to observe that the substitution of the acidic proton for a methyl group in the imidazolium ring, as is the case of [BDMIM] when compared with [BMIM], has a considerable reduced effect in the acetonitrile polarity (see Figure 4.4). In fact, it is needed to add more than five times the amount of [BDMIM][Cl] (3.4×10^{-5} mol) to obtain the same effect as with [BMIM][Cl] (6.3×10^{-6} mol).

The presence of oxygen atoms in the side chain of imidazolium rings apparently confers to acetonitrile an increase in polarity identical to that introduced by RTILs with longer side chains without oxygen atoms. For instance, we can observe that $[C_2OHMIM][BF_4]$ (a side chain with two carbon atoms and one oxygen atom) has a similar effect in polarity as $[OMIM][BF_4]$ (a side chain with eight carbon atoms).

Figure 4.5 presents the ranges of effects in acetonitrile polarity arranged by anions and cations, to help visualize the observed effects. Again, with this image is apparent that the deviations in acetonitrile polarity are mainly dictated by the cation present in the RTIL studied. All the anions studied seem to cover almost the whole range of values obtained, with the exception of $[EtSO_4]$ and $[MDEGSO_4]$, for which there is only one example of each. The cations studied seem to increase the effect in polarity deviation in the order $[(C_6)_3C_{14}P]$<[BDMIM]<[ALIQUAT]<[EMIM]<[BMIM]. [OMIM] and $[C_3OMIM]$ cover a range too wide to be included in this generalization, while [DMG] and $[C_{10}MIM]$ are present in only one example of each. $[C_5O_2MIM]$ presents an effect greater than [EMIM], but it is not clear if it should be considered in the same range or higher than [BMIM].

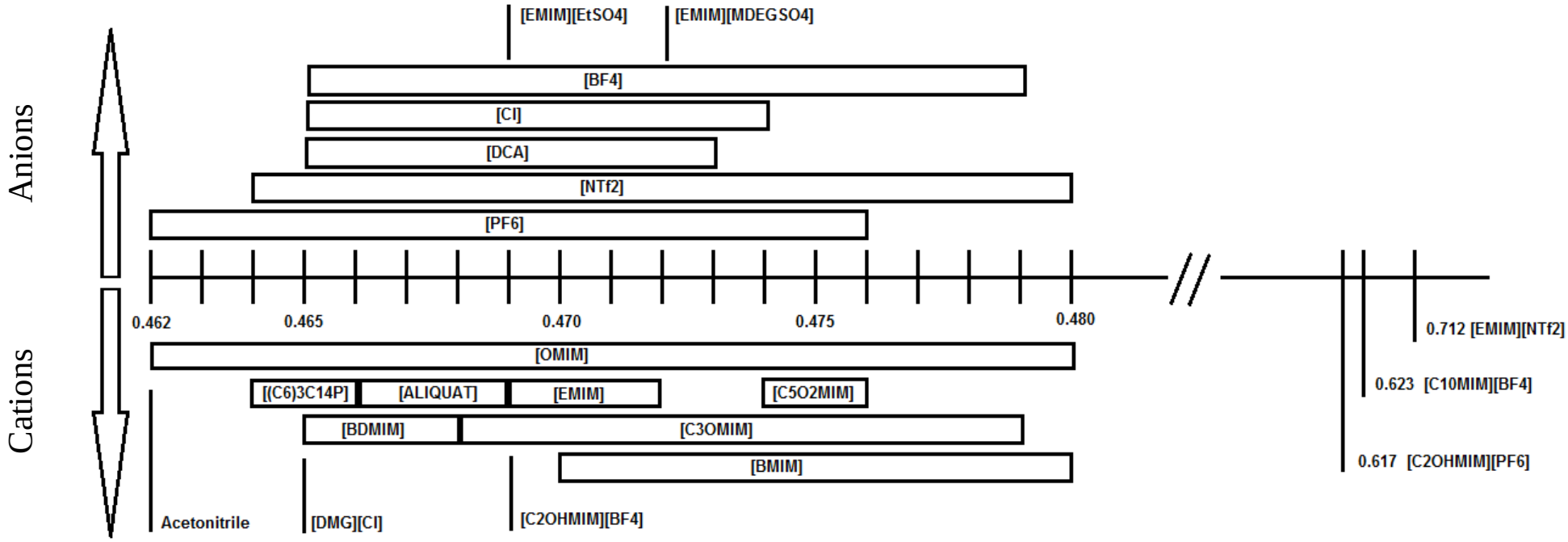

Figure 4.5 – Range of effects in acetonitrile polarity for individual anions and cations, in E_T^N values.

Figure 4.6 plots the effect in E_T^N values of the continuous addition of RTILs to acetonitrile. This plot shows that the increment in acetonitrile polarity is linearly dependent with the addition of RTIL based on [BF_4] anion. The same trend was observed for all RTILs tested.

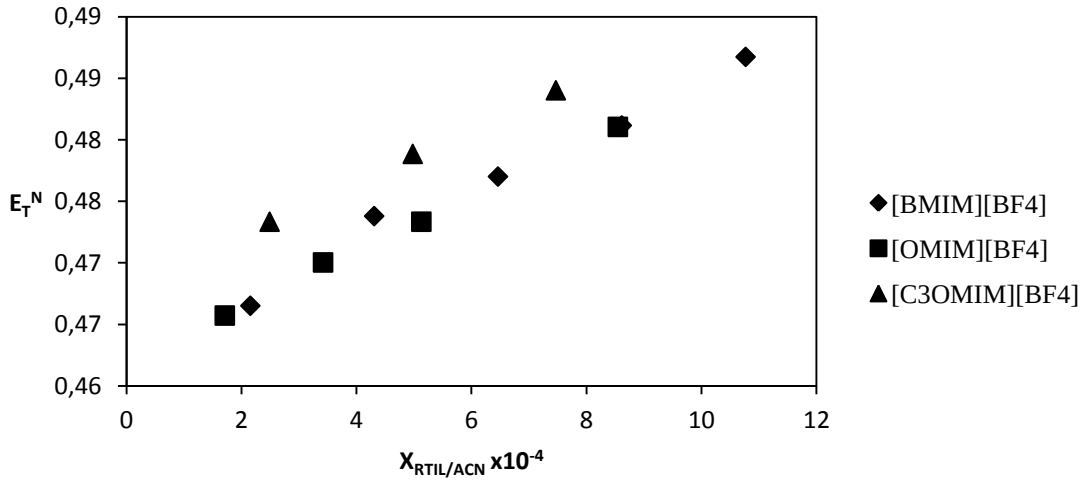

Figure 4.6 – Effect in E_T^N values of acetonitrile by the continuous addition of ionic liquid to acetonitrile.

In Table 4.3 are presented the values obtained by UV/Vis spectroscopy of the addition of RTILs to a solution of betaine dye (0.36 mM) in ethanol. This table includes the mole fraction of RTIL in ethanol ($X_{RTIL/EtOH}$), the corresponding volume of RTIL added, the number of moles of RTIL per mole of betaine dye ($\mu_{RTIL/Betaine}$), the wavelength of the maximum of the intramolecular CT absorption band of the betaine dye, the respective E_T^N and $E_T(30)$ values.

Table 4.3 – Effects in polarity of the addition of ionic liquids to ethanol.

Mixture (EtOH + RTIL)	$\mathbf{X_{RTIL/EtOH}}$ **x10^{-4}**	**Vol. RTIL (µL)**	$\boldsymbol{\mu_{RTIL/Betaine}}$	**Wavelength (nm)**	$\boldsymbol{E_T(30)}$	$\boldsymbol{E_T^N}$
EtOH	0	0	_____	550.5	51.94	0.655
[EMIM][$EtSO_4$]	5.08	4	20.65	548.5	52.13	0.661
[EMIM][$MDEGSO_4$]	5.44	6	22.09	546.5	52.32	0.667
[BMIM][PF_6]	4.65	4	18.89	548.5	52.13	0.661
[BMIM][BF_4]	4.81	4	19.55	549.5	52.03	0.658
[BMIM][NTf_2]	5.05	6	20.49	548.5	52.13	0.661
[BMIM][DCA]	5.03	4	20.42	549.5	52.03	0.658
[OMIM][PF_6]	5.29	6	21.47	548.0	52.17	0.663
[OMIM][BF_4]	5.73	6	23.28	548.5	52.13	0.661
[C_{10}MIM][BF_4]	5.06	6	20.53	545.5	52.41	0.670
[C_2OHMIM][BF_4]	5.94	3	24.12	551.0	51.89	0.654

When comparing the E_T^N values obtained for the addition of RTILs to ethanol with those obtained for the addition of RTILs to acetonitrile, it is seen that the value in ethanol is always higher for ethanol than acetonitrile. This is directly related to the higher polarity of ethanol.

Figure 4.7 plots the effects in E_T^N values of ethanol by the addition of RTILs by anion, for the cations [BMIM], [OMIM], [C_{10}MIM] and [C_2OHMIM] whereas Figure 4.8 plots the effects in E_T^N values of ethanol by the addition of RTILs by cation, for the anions [BF_4], [PF_6], [NTf_2] and [DCA].

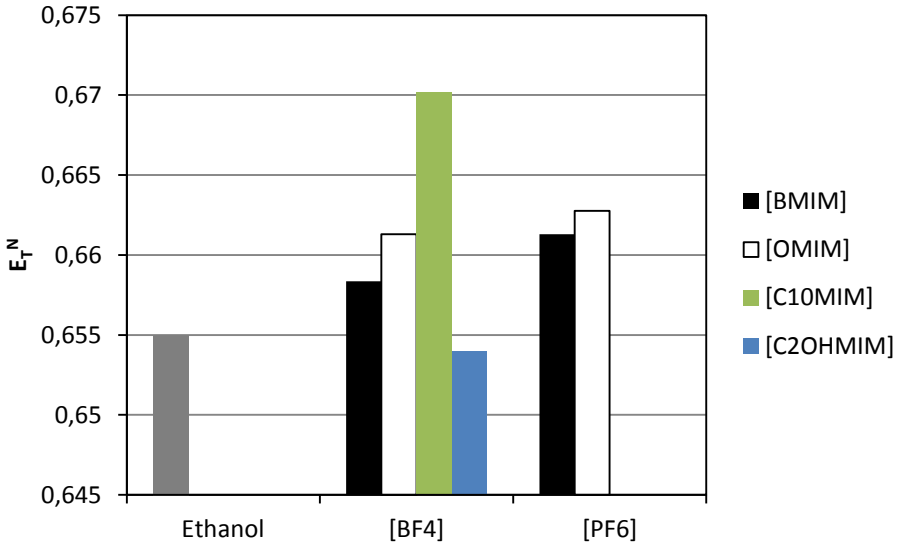

Figure 4.7 - Anion effect in E_T^N values of ethanol.

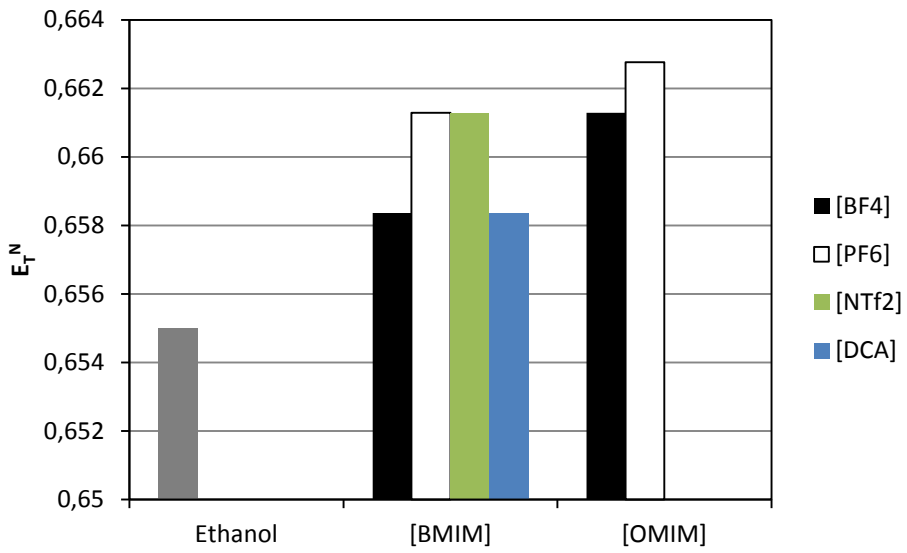

Figure 4.8 - Cation effect in E_T^N values of ethanol.

As with acetonitrile, the effect in polarity is more linked to the cation than to the anion. Specifically, we can see that the effect in polarity increases with the increase of the alkyl side chain for the imidazolium ring, as can be seen in the sequence [BMIM]<[OMIM]<[C_{10}MIM] for the anion [BF_4]. The order of polarity effects introduced by the anions is slightly different than the one found in acetonitrile. Now, the polarity effect increases in the sequence [PF6]≈[DCA]<[BF4]≈[NTf2]. This might be due to the higher polarity of ethanol.

The addition of the RTIL [C_2OHMIM][BF_4] to ethanol is the only case observed in which the polarity decreased. This is quite probably due to the presence of hydroxyl groups both in ethanol and the cation. However, with continued addition, the polarity value surpasses that of pure ethanol.

It is interesting to notice that the only two cases of the cation [EMIM] studied – [EMIM] [EtSO4] and [EMIM] [$MDEGSO_4$] - have effects in polarity similar to [BMIM][PF_6], [BMIM][NTf_2] and [OMIM][BF_4] in the case of the anion [EtSO4] or to [C_{10}MIM][BF_4] in the case of the anion [$MDEGSO_4$]. This leads us to conclude that these two anions are very polar and thus present effects similar to imidazolium RTILs with longer alkyl side chains and less polar anions.

In Table 4.4 are presented the values obtained by UV/Vis spectroscopy of the addition of RTILs to solutions of betaine dye (0.36 mM) in tetrahydrofuran, pre-dried tetrahydrofuran, chloroform and isopropanol. This table includes the mole fraction of RTIL in the solvent ($X_{RTIL/Solvent}$), the corresponding volume of RTIL added, the number of moles of RTIL per mole of betaine dye ($\mu_{RTIL/Betaine}$), the wavelength of the maximum of the intramolecular CT absorption band of the betaine dye, the respective E_T^N and $E_T(30)$ values.

Table 4.4 – Effects in polarity of the addition of ionic liquids to tetrahydrofuran, chloroform and isopropanol.

	Mixture (Solvent + RTIL)	**$X_{RTIL/Solvent}$ x10^{-4}**	**Vol. RTIL (µL)**	**$\mu_{RTIL/Betaine}$**	**Wavelength (nm)**	**$E_T(30)$**	**E_T^N**
Tetrahydrofuran	THF	0	0	_____	759.0	37.67	0.215
	[BMIM][PF_6]	6.47	4	18.89	640.7	44.62	0.430
	[BMIM][BF_4]	6.70	4	19.55	660.1	43.31	0.389
	[OMIM][PF_6]	7.35	6	21.47	643.3	44.45	0.424
	[C_{10}MIM][BF_4]	forms emulsion					
Pre-dried Tetrahydrofuran	THF	0	0	_____	760.1	37.61	0.213
	[BMIM][PF_6]	6.47	4	18.89	652.4	43.82	0.405
	[BMIM][BF_4]	6.70	4	19.55	659.3	43.36	0.391
Chloroform	$CHCl_3$	0	0	_____	703.2	40.66	0.307
	[BMIM][PF_6]	forms emulsion					
	[BMIM][BF_4]	6.65	4	19.55	667.0	42.87	0.376
	[OMIM][PF_6]	7.30	6	21.47	649.5	44.02	0.411
	[C_{10}MIM][BF_4]	forms emulsion					
Isopropanol	i-PrOH	0	0	_____	593.0	48.21	0.541
	[BMIM][PF_6]	6.10	4	18.89	585.9	48.80	0.559
	[BMIM][BF_4]	6.31	4	19.55	588.2	48.61	0.553
	[OMIM][PF_6]	6.93	6	21.47	580.2	49.28	0.573
	[C_{10}MIM][BF_4]	6.63	6	20.53	577.4	49.52	0.581

Besides the solvents presented in Tables 4.2, 4.3 and 4.4, were also tested toluene and dioxan. However, these two solvents presented no measurable band in the region considered for the E_T^N scale, and thus were discarded of this study.

Figure 4.9 plots the effects in E_T^N values of tetrahydrofuran, pre-dried tetrahydrofuran, chloroform and isopropanol of the addition of all RTILs tested in these solvents.

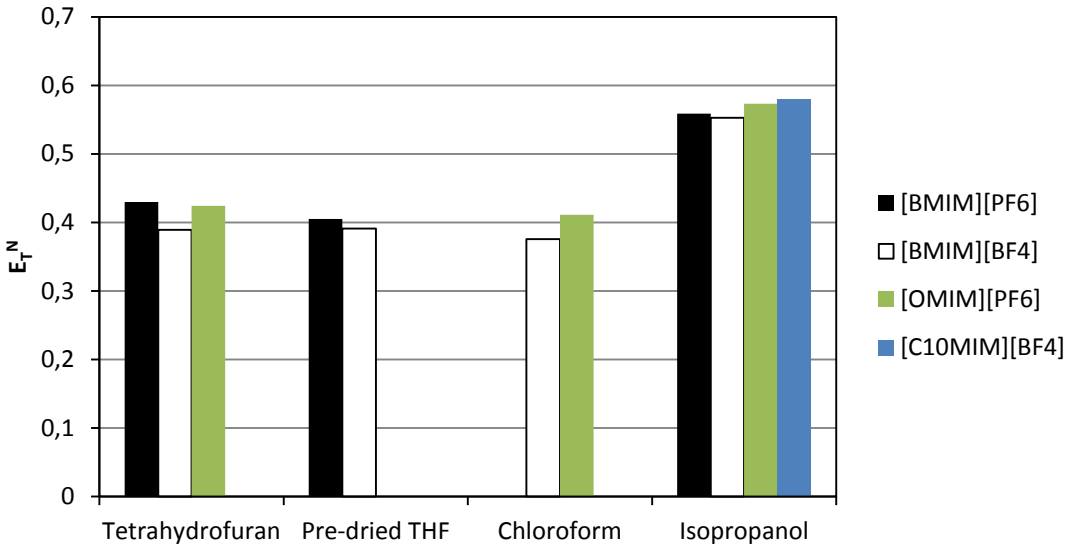

Figure 4.9 - Effect in ETN values of the addition of RTILs to tetrahydrofuran, pre-dried tetrahydrofuran, chloroform and isopropanol.

From Table 4.4 and Figure 4.9 it is seen that the difference between using pre-dried tetrahydrofuran or not is minimal. It is also seen that, despite chloroform having a higher E_T^N value, the values obtained after addition of RTIL are practically identical to those obtained with tetrahydrofuran. Isopropanol, on the other hand, has higher E_T^N values for all the RTILs tested.

For all the cases studied, the polarity of the solvent increased with the addition of RTIL, with the exception noted previously of the addition of $[C_2OHMIM][BF_4]$ to ethanol. In addition to this observation, we should also note that the most polar solvent used in this study was ethanol, with an E_T^N value of 0.655, which still leaves space to wonder if by using a more polar solvent the solvent polarity would decrease with the addition of RTIL.

Table 4.5 presents the effects of the addition of one specific RTIL, $[BMIM][BF_4]$, which was tested for all the solvents. We can see that the increase in polarity with the addition of $[BMIM][BF_4]$ follows generically the same trend as the polarities of the pure solvents, with the only exception of chloroform, which has a higher polarity than tetrahydrofuran when pure, but lower when $[BMIM][BF_4]$ is added. For the two tetrahydrofuran cases, the values are too close to discriminate between them.

Table 4.5 - Effects in polarity of the addition of [BMIM][BF_4] to different solvents.

Mixture (Solvent + [BMIM][BF_4])	$X_{RTIL/Solvent}$ x10^{-4}	Vol. [BMIM][BF_4] (μL)	$\mu_{RTIL/Betaine}$	Wavelength (nm)	$E_T(30)$	E_T^N Solvent	E_T^N Solvent + RTIL
Chloroform	6.65	4	19.55	667.0	42.87	0.307	0.376
Tetrathydrofuran	6.70	4	19.55	660.1	43.31	0.215	0.389
Pre-dried THF	6.70	4	19.55	659.3	43.36	0.213	0.391
Acetonitrile	4.31	4	19.55	620.9	46.1	0.462	0.474
Isopropanol	6.31	4	19.55	588.2	48.61	0.541	0.553
Ethanol	4.81	4	19.55	549.5	52.03	0.655	0.658

Figure 4.10 plots the effect of continuous addition of [BMIM][BF_4] to ethanol, tetrahydrofuran, pre-dried tetrahydrofuran, chloroform and isopropanol. As with acetonitrile (see Figure 4.6), the continuous addition results in a linear increase in polarity.

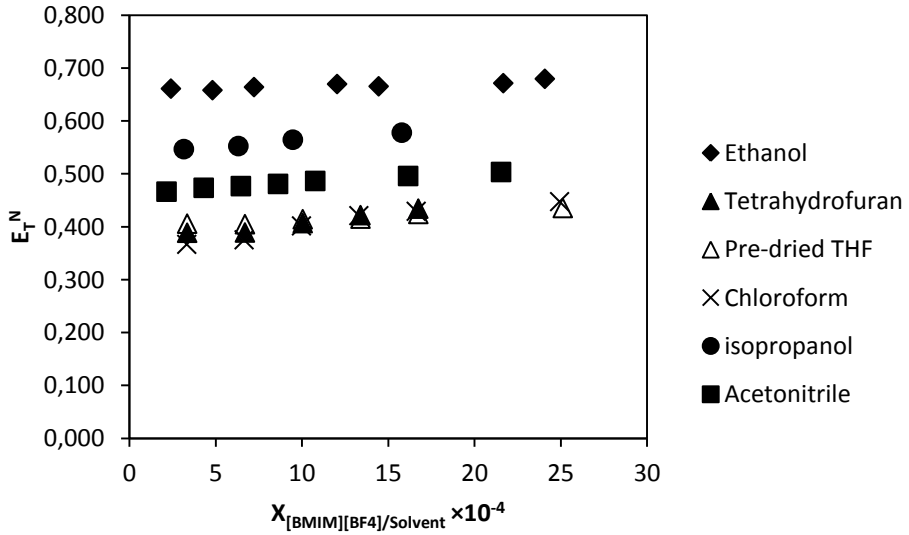

Figure 4.10 – Effect in E_T^N values of continuous addition of [BMIM][BF_4] to solvents.

When ordering the RTILs studied by the E_T^N values obtained in acetonitrile and ethanol, as presented in Table 4.6, one can see that there are discrepancies in the ordering. As the effect in E_T^N is the result of the addition of a very small quantity of RTIL to a solvent, one can assume that the effect observed is also very dependent on the solvent polarity, as this effect stems from the dissolution of the RTIL in that solvent and the consequent rearrangement of the supramolecular structure.

In Table 4.7 are presented the partition coefficients of oleic acid in the ionic liquids studied, as results from the extraction of the model mixture oleic acid/squalene 50% (w/w), presented in Chapter 3. If we compare Table 4.7 with Table 4.6, we can conclude that it follows the inverse order of the addition of RTILs to ethanol, with the exception of RTILs [EMIM][$MDEGSO_4$], [EMIM][$EtSO_4$] and [BMIM][NTf_2]. It is interesting to notice that these three exceptions include the two extreme values of partition coefficients found. For most cases, increasing polarity in ethanol is inversely related with the partition coefficient of oleic acid in the same RTIL.

The similarity in the ordering of the partition coefficients with that of the addition of RTILs to ethanol, whereas that is not true for acetonitrile, might be explained by the closer proximity of ethanol polarity to those of the RTILs studied. In fact, when we compare the published values of polarity for pure RTILs (Table 4.8) which were used in the partition studies, we see that these fall in the range 0.60-0.69, while that of ethanol is 0.655. On the other hand, the polarity of acetonitrile is 0.462, quite further away than ethanol. However, ethanol presents also less sensitivity to the addition of RTILs, and thus it results in less differentiation between the RTILs studied.

Table 4.6 – Ordered E_T^N values of common RTILs tested in acetonitrile and ethanol.

Acetonitrile		Ethanol	
[OMIM][PF_6]	0.462	[BMIM][DCA]	0.661
[EMIM][$EtSO_4$]	0.469	[OMIM][BF_4]	0.661
[C_2OHMIM][BF_4]	0.469	[BMIM][NTf_2]	0.661
[BMIM][DCA]	0.470	[OMIM][PF_6]	0.663
[OMIM][BF_4]	0.470	[EMIM][$EtSO_4$]	0.664
[EMIM][$MDEGSO_4$]	0.472	[BMIM][BF_4]	0.664
[BMIM][PF_6]	0.473	[C_2OHMIM][BF_4]	0.666
[BMIM][BF_4]	0.474	[EMIM][$MDEGSO_4$]	0.667
[BMIM][NTf_2]	0.480	[BMIM][PF_6]	0.667
[C_{10}MIM][BF_4]	0.623	[C_{10}MIM][BF_4]	0.670

Table 4.7 – Partition coefficients of oleic acid for the ionic liquids studied in this chapter and corresponding E_T^N value in ethanol.

Ionic Liquid	K_D	E_T^N in Ethanol
[EMIM][$MDEGSO_4$]	2.96	0.667
[BMIM][DCA]	1.84	0.661
[OMIM][PF_6]	1.5	0.663
[BMIM][BF_4]	1.44	0.664
[C_2OHMIM][BF_4]	1.27	0.666
[EMIM][$EtSO_4$]	1.1	0.664
[BMIM][PF_6]	1.14	0.667
[BMIM][NTf_2]	0.86	0.661

Table 4.8 - Solvent polarity of pure RTILs determined by solvatochromism (Reichardt's method) as found in published literature.

Ionic liquid	E_T^N	Reference
$[R^1R^2_3N]^+ X^-$ RTIL (R = Methyl, 1-Butyl, 1-Octyl, 1-Dodecyl,	0.39 - 0.62	[3]
$[R_4P]^+ X^-$ RTIL (R = Methyl, Ethyl, 1-Propyl, 1-Butyl, 1-Pentyl, 1-Hexyl, 1-Octyl, 1-Decyl, 1-Dodecyl; X = Cl, Br, CH_3COO, C_6H_5COO, CHES, MOPSO, BES, HSO_4, ClO_4)	0.35 - 0.44	[3]
$[R^3MIM]^+ X^-$ RTIL[&]	0.53 - 0.75	-
[EMIM] [BF_4]	0.71	[12]
[EMIM] [NTf_2]	0.68; 0.69	[7], [20]
[EMIM] [DCA]	0.65	[7]
[BMIM] [PF_6]	0.67 - 0.69	[7], [10], [12], [20], [21]
[BMIM] [BF_4]	0.67 - 0.68	[12], [21]
[BMIM] [NTf_2]	0.60 - 0.64	[7], [10], [20], [21]
[BMIM] [DCA]	0.63	[7]
[OMIM] [BF_4]	0.67	[22]
[OMIM] [NTf_2]	0.63	[10]
[OMIM] [PF_6]	0.60	[22]
[C_2OHMIM] [NTf_2]	0.93	[21]

[&] R^1, R^2: generic substituents in the ammonium molecule; R^3: generic group on position 3 of the imidazolium ring; CHES: 2-(Cyclohexylamino)-ethanesulfonate; MOPSO: 2-hydroxy-3-(4-morpholino)propanesulfonate; BES: 2-[N,N-bis(2-hydroxyethyl)amino]ethanesulfonate.

4.4 - Conclusions

This work intended to use the addition of RTILs to common organic solvents to probe their polarities by an indirect method, in order to try to find a correlation between the polarity and the results obtained with the extraction of the model mixture of oleic acid/squalene 50% (w/w) with RTILs.

It was seen that the influence in solvent polarity is more linked to the cation than the anion. For all the cases studied, the polarity of the solvent increased with the addition of RTIL and the continuous addition is linearly correlated to the increase in polarity. The only exception is $[C_2OHMIM][BF_4]$, which decreases the polarity of ethanol with the first addition, but with further additions it also increased the value of polarity. The increase in polarity in acetonitrile (the solvent with more RTILs studied) can be generically described following the cation sequence $[(C_6)_3C_{14}P]$<[BDMIM]<[ALIQUAT]<[EMIM]<[BMIM].

Ethanol presented the polarity scale more in accordance with the already published values for pure RTILs, which is also the sequence observed for the partition coefficients of oleic acid in the pure RTILs for the model mixture oleic acid/squalene. This is probably a result of closer polarity of ethanol to those of the pure RTILs. However, it was also seen that ethanol is less sensitive to the changes in polarity than acetonitrile.

4.5 - References

[1] Reichardt, C. Empirical Parameters of the Polarity of Solvents *Angew. Chem. Int. Ed.* **1965**, *4*, 29–40.

[2] Muller P.; Glossary of terms used in physical organic chemistry (IUPAC Recommendations 1994) *Pure Appl. Chem.* **1994**, *66*, 1077–1184.

[3] C. Reichardt; Polarity of ionic liquids determined empirically by means of solvatochromic pyridinium N-phenolate betaine dyes *Green Chem.* **2005**, *7*, 339–351.

[4] Carmichael, A. J.; Seddon, K. R.; Polarity study of some 1-alkyl-3-methylimidazolium ambient-temperature ionic liquids with the solvatochromic dye, Nile Red *J. Phys. Org. Chem.* **2000**, *13*, 591-595.

[5] Saha, S.; Mandal, P. K.; Samanta, A. Solvation dynamics of Nile Red in a room temperature ionic liquid using streak camera *Phys. Chem. Chem. Phys.* **2004**, *6*, 3106–3110.

[6] Fletcher, K. A.; Storey, I. A.; Hendricks, A. E.; Pandey, S.; Pandey, S. Behavior of the solvatochromic probes Reichardt's dye, pyrene, dansylamide, Nile Red and 1-pyrenecarbaldehyde within the room-temperature ionic liquid bmimPF6 *Green Chem.* **2001**, *3*, 210–21.

[7] Chiappe, C.; Pieraccini, D. Determination of Ionic Liquids Solvent Properties Using an Unusual Probe: The Electron Donor-Acceptor Complex between 4,4'-bis(Dimethylamino)-benzophenone and Tetracyanoethene J. Phys. Chem. A. **2006**, *110*, 4937-4941.

[8] Aki, S. N. K. V. K.; Brennecke, J. F.; Samanta, A. How polar are room-temperature ionic liquids? *Chem. Commun.* **2001**, 413-414.

[9] Wasserscheid, P.; Gordon, C. M.; Hilgers, C.; Muldoon, M. J.; Dunkin, I. R. Ionic liquids: polar, but weakly coordinating solvents for the first biphasic oligomerisation of ethene to higher a-olefins with cationic Ni complexes *Chem. Commun.* **2001**, 1186–1188.

[10] Muldoon, M. J.; Gordon, C. M.; Dunkin, I. R. Investigations of solvent-solute interactions in room temperature ionic liquids using solvatochromic dyes *J. Chem. Soc., Perkin Trans.* **2001**, *2*, 433-435.

[11] Karmakar, R.; Samanta, A. Solvation Dynamics of Coumarin-153 in a Room-Temperature Ionic Liquid *J. Phys. Chem. A* **2002**, *106*, 4447–4452.

[12] Park, S.; Kazlauskas, R. J. Improved Preparation and Use of Room-Temperature Ionic Liquids in Lipase-Catalyzed Enantio- and Regioselective Acylations *J. Org. Chem.* **2001**, *66*, 8395-8401.

[13] Crowhurst, L.; Mawdsley, P. R.; Perez-Arlandis, J. M.; Salter, P. A.; Welton, T. Solvent–solute interactions in ionic liquids *Phys. Chem. Chem. Phys.* **2003**, *5*, 2790–2794.

[14] Kaar, J. L.; Jesionowski, A. M.; Berberich, J. A.; Moulton, R.; Russell, A. J. Impact of Ionic Liquid Physical Properties on Lipase Activity and Stability *J. Am. Chem. Soc.* **2003**, *125*, 4125-4131.

[15] Baker, S. N.; Baker, G. A.; Bright, F. V. Temperature-dependent microscopic solvent properties of 'dry' and 'wet' 1-butyl-3-methylimidazolium hexafluorophosphate: correlation with ET(30) and Kamlet–Taft polarity scales *Green Chem.* **2002**, *4*, 165–169.

[16] Ab Rani, M. A.; Brant, A.; Crowhurst, L.; Dolan, A.; Lui, M.; Hassan, N. H.; Hallett, J. P.; Hunt, P. A.; Niedermeyer, H.; Perez-Arlandis, J. M.; Schrems, M.; Welton, T.; Wilding, R. Understanding the polarity of ionic liquids *Phys. Chem. Chem. Phys.* **2011**, *13*, 16831–16840.

[17] Mellein, B. R.; Aki, S. N. V. K.; Ladewski, R. L.; Brennecke, J. F. Solvatochromic Studies of Ionic Liquid/Organic Mixtures *J. Phys. Chem. B* **2007**, *111*, 131-138.

[18] Trivedi, S.; Sarkar, A.; Pandey, S. Solvatochromic absorbance probe behavior within 1-butyl-3-methylimidazolium hexafluorophosphate + propylene carbonate: Preferential solvation or solvent–solvent interaction? *Chem. Eng. J.* **2009**, *147*, 36–42.

[19] Yang, Q.; Xing, H.; Su, B.; Yu, K.; Bao, Z.; Yang, Y.; Ren, Q. Improved separation efficiency using ionic liquid–cosolvent mixtures as the extractant in liquid–liquid extraction: A multiple adjustment and synergistic effect *Chem. Eng. J.* **2012**, *181-182*, 334-342.

[20] K.A. Fletcher, S. Pandey, Solvatochromic probe behavior within neat and cosolvent added room-temperature ionic liquid solutions, in: H.C. Dulong, R.W. Bradshaw, M. Matsunaga,

G.K. Stafford, P.C. Trulove (Eds.), 2002-19-Molten Salts XIII, Electrochemical Society, Pennsylvania, 2002, pp. 244–256.

[21] S.V. Dzyuba, R.A. Bartsch, Expanding the polarity range of ionic liquids, Tetrahedron Lett. 43 (2002) 4657–4659.

[22] J.G. Huddleston, G. Broker, H. Willauer, R.D. Rogers, Ionic liquids – industrial applications to green chemistry, in: ACS Symposium Series, American Chemical Society, Washington, DC, 2002, pp. 270–288.

Chapter 5

Supported Ionic Liquids Membranes[3]

3 Chapter partially submited for publication as: Ricardo M. Couto, Tânia Carvalho, Luísa A. Neves, Rui M. Ruivo, Pedro Vidinha, Alexandre Paiva, Isabel M. Coelhoso, Susana Barreiros, Pedro C. Simões; Development of Ion-Jelly® Membranes; Separation and Purification Technology

5.1 - Introduction

In recent years ionic liquid membranes have gained relevance and were proven to effectively separate compounds of interest. The first approach was developed by Branco et al. [1], who proposed to use room temperature ionic liquids (RTILs) as bulk membranes, in a U-shaped tube, or as supported ionic liquid membranes (SILMs), by impregnating a porous membrane with the desired ionic liquid. With this approach it was possible to separate secondary and tertiary amines with very similar boiling points, which was not possible to do before either with other liquid membranes or by distillation. Since then, many substances have been separated with SILMs, such as hydrocarbons, alcohols, esters and gases [2]-[5].

There are mainly three approaches commonly used to immobilise RTIL in a porous support: (1) direct immersion, in which the membrane is soaked in the RTIL [5]-[8]; (2) pressure, in which the RTIL is spread over the membrane and a small pressure is applied to force it to flow into the membrane pores [9], [10]; (3) and vacuum, in which the air in the pores of the supporting membrane is removed with vacuum and then, still under vacuum, RTIL is spread over the membrane [1], [10]-[14]. In all the cases, excess RTIL has to be removed from the surface of the membrane, either by letting it drip, or by gently wiping it with absorbing tissue. In a study where the operational stability was assessed, it was found that the preparation method in which pressure is used, is the one which results in higher amounts of RTIL immobilized in the membrane and which also presents higher stability [10].

In this chapter is shown the development and application of SILMs in $scCO_2$ separations, based on the commercial reverse osmosis membranes studied in Chapter 2 and the ionic liquids studied in Chapters 3 and 4. However, difficulties arose in operation and poor results were obtained. Furthermore, it is known that RTILs are displaced from SILMs under operation, even at low differential pressure (above 2 bar) [14]. To try to overcome these difficulties, gel membranes, in which RTIL is blended with a polymer, have been prepared by several authors [15]-[17]. Membranes prepared in this way retain solubility characteristics identical to the liquid, which confer them identical permeabilities, but with improved mechanical properties. These membranes were effectively employed in the separation of gases such as carbon dioxide from nitrogen [15], [17], methane [16], [17], and hydrogen [17] or hydrogen from nitrogen [17].

In this work gel membranes were developed based on Ion-Jelly® (IJ), a new gel material developed in our research group, which is obtained by adding an ionic liquid to gelatine [18]. This material is a transparent and flexible polymer which can be moulded into a wide range of shapes, with the additional advantage of being obtained from a natural polymer. It was found that Ion-Jelly® can have very reasonable conductivities over a wide range of frequencies, leading to possible

application in electrochemical devices. Recently, microfibers of Ion-Jelly® have been produced by electrospinning to obtain high surface area conductive materials [19].
Two methods of preparation of Ion-Jelly® membranes were developed, which differ in the process employed for the spreading and jellification of the gel. The second method was developed to try to overcome homogeneity problems in the membrane.

The application of Ion-Jelly® membranes was studied on the separation/fractionation of two systems in $scCO_2$: the former model mixture of oleic acid and squalene, and the effluent stream coming from the transesterification conversion of edible sunflower oil to alkyl esters (i.e., biodiesel). In the reaction of transesterification, three molecules of methanol react with one molecule of triglyceride, in the presence of a catalyst, to yield one molecule of glycerol and three molecules of methyl ester. If this reaction is not complete, monoglycerol and diglycerol can also occur (see Figure 5.1).

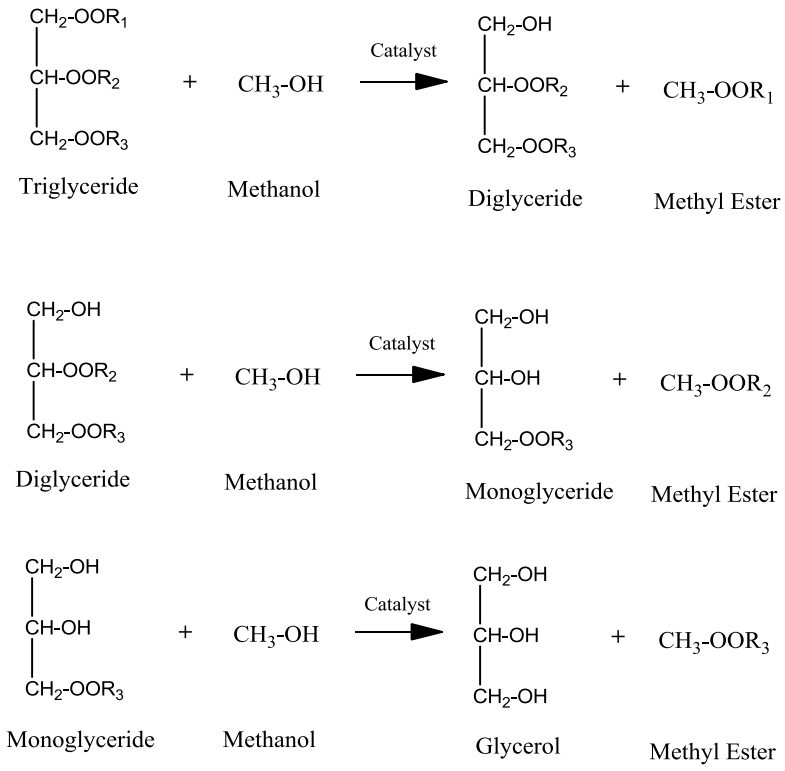

Figure 5.1 – Generic transesterification reaction.

To extend the possible range of applications of this kind of gel membranes, the application of the Ion-Jelly® membrane was also studied in the separation of low pressure gaseous systems.

5.2 - Materials and Methods

Ionic liquids 1-butyl-3-methylimidazolium tetrafluoroborate ([BMIM][BF_4]), 1-butyl-3-methylimidazolium bis(trifluoromethylsulfonyl)imide ([BMIM][NTf_2]), 1-ethyl-3-methylimidazolium dicyanamide ([EMIM][DCA]), 1-butyl-3-methylimidazolium dicyanamide ([BMIM][DCA]) and 1-butyl-3-methylpyrrolidinium dicyanamide ([BMPyr][DCA]) were purchased from Iolitec (99% purity). 1-ethyl-3-methylimidazolium 2-(2-methoxyethoxy)-ethylsulfate ([EMIM][MDEGSO4], trade name ECOENG 21M), was purchased from Solvent Innovation (≥98% purity). Trihexyl-tetradecyl-phosphonium bis(trifluoromethylsulfonyl)imide ([$(C_6)_3C_{14}P$][NTf_2], trade name CYPHOS IL 109, min 97% purity), was purchased from Cytec (purity). The anions and cations structures of these ionic liquids are presented in Figure 5.2. Gelatin was purchased from Panreac ref. 403 902. The gases used in the experiments were hydrogen (high-purity grade (99.999%), Air Liquide, France), oxygen (high-purity grade (99.999%), Praxair, USA), nitrogen (industrial grade (99.99%), Praxair, USA), methane (99.95%, Praxair, USA) and carbon dioxide (high-purity grade (99.998%), Praxair, USA). Carbon dioxide used in scCO_2 experiments was supplied by Air Liquide, France (99.995% purity). Methanol (p.a.) was supplied by Sigma-Aldrich. The edible sunflower oil used in the biodiesel experiments was from Fula®. Lipozyme® RM IM (*Rhizomucor miehei* lipase immobilized on an acrylic resin) was from Novozymes A/S, Bagsvaerd, Denmark.

Flat sheet reverse osmosis membranes used as supports for ionic liquids were cellulose acetate (CA) Ref. YMCFSP3001 and polyamide AD (AD) Ref. YMADSP3001 from Sterlitech Corporation, USA.

Cellulose supports used to make ion-jelly membranes were disks 4 cm in diameter cut from filter paper 1300/80 from Filter-Lab

CATIONS

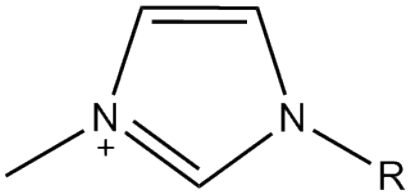

1-R-3-methylimidazolium
R= ethyl, butyl

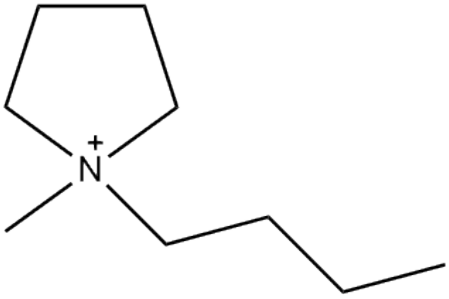

1-butyl-3-methylpyrrolidinium

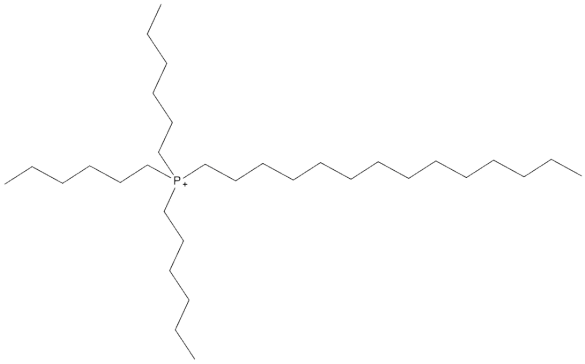

Trihexyl-tetradecyl-phosphonium

ANIONS

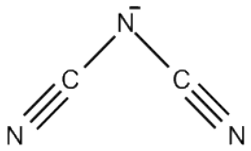

Dicyanamide

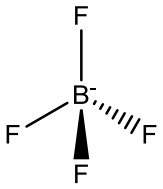

Tetrafluoroborate

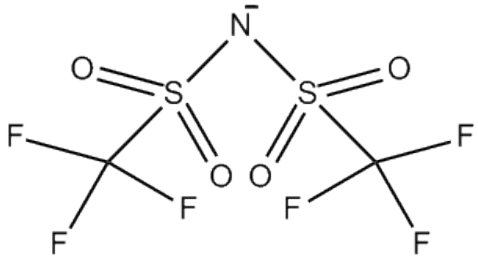

Bis(trifluoromethylsulfonyl)imide

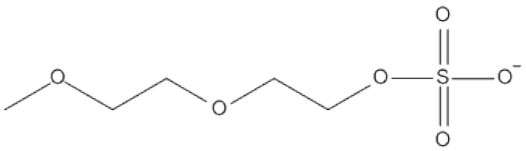

2-(2-methoxyethoxy)-ethylsulfate

Figure 5.2 – Structure of ionic liquids cations and anions used in this work.

5.2.1 - Oleic Acid and Squalene Analysis by Gas Chromatography

Prior to the GC analysis, oleic acid was methylated to the respective methyl ester form, by reaction with diazomethane, according to the method described elsewhere [20]. Methyl heptadecanoate (TCI Europe, Belgium, >97.0%) was used as the internal standard. The chromatograph was a Thermo Quest Trace GC 2000 with a flame ionization detector (FID); a TR-Biodiesel (F) column,

30 m × 0.25 mm and 0.25 μm film thickness, from Thermo-Scientific was used. Helium was used as carrier at a constant flow of 2 $mL \cdot min^{-1}$. The oven temperature was set at 393 K for 0.5 min, then to 493 K at 30 $K \cdot min^{-1}$ and holding for 1 min, and then to 523 K at 10 $K \cdot min^{-1}$ with a final holding time of 5 min. The injector was a PTV programmed to heat from 363 K to 533 K at 10 $K \cdot s^{-1}$, with a transfer time of 3 min and cleaning at 633 K with a split of 250 $mL \cdot min^{-1}$ for 20 min. Detector temperature was 553 K, respectively. Peak identification was carried out using known standards (FAME mix C8-C24, Supelco).

5.2.2 - Methyl Esters Analysis by Gas Chromatography

Prior to the GC analysis, methyl esters were derivatized with n-methyl-n-trimethylsilyltrifluoroacetamide (TCI Europe, Belgium, >90%) for better detection. (±)-1,2,4-Butanetriol (Sigma-Aldrich, ≥90%) and tricaprin (TCI Europe, Belgium, >98%) were used as internal standards. The gas chromatograph was a Thermo Quest Trace GC 2000 with a flame ionization detector (FID); a TR-Biodiesel (G) column, 10 m × 0.25 mm and 0.1 μm film thickness, from Thermo-Scientific was used. Helium was used as carrier at 3 $mL \cdot min^{-1}$ for 12 min, and then ramped to 5 $mL \cdot min^{-1}$ at 0.5 $mL \cdot min^{-1} \cdot min^{-1}$. The oven temperature was 353–453 K at 15 $K \cdot min^{-1}$, then to 503 K at 7 $K \cdot min^{-1}$, then to 638 K at 10 $K \cdot min^{-1}$ with a final holding time of 4 min. The injector was a true cold On-Column and detector temperature was 653 K.

5.2.3 - Preparation of Supported Ionic Liquid Membranes

Disks 4 cm in diameter were cut from CA or AD flat sheet membranes, and were deposited in the bottom of a high pressure stainless steel vessel. 1 mL of appropriate ionic liquid was spread on top of the membrane, and the vessel was closed. CO_2 was added to the vessel, at a pressure of 0.2 MPa, in order to force the ionic liquid to flow into the pores of the membrane. After one hour the vessel was opened and the excess ionic liquid remaining on top of the membrane was gently wiped with absorbing tissue. To make sure there was no remaining ionic liquid, the membrane was set upright and left to drip overnight.

5.2.4 - Preparation of Ion-Jelly® Membranes by evaporative casting-knife method

300 μl of ionic liquid were heated to 318 K under magnetic stirring, followed by the addition of 120 mg of gelatin. In order to obtain a homogenous solution 300 μL of water were added dropwise. The mixtures were kept stirring at 318 K until gelatin was completely solubilized (approximately 15 minutes). The solution was then spread over a cellulose support, in order to form thin films. Jellification occurred at room temperature. In some cases the thickness of the Ion-Jelly® layer

applied was controlled with a K101 Control Coater (RK Print Ltd.), equipped with a casting knife regulated to make films 0.5 and 1 mm thick.

5.2.5 - Preparation of Ion-Jelly® Membranes by glass plates pressed method

The preparation procedure was basically the same as the first method, differing only in the drying process. Now, the solution was spread over a cellulose support and pressed between two glass plates, in order to remove air bubbles and to form thin films of homogeneous thickness. The membranes were left to jellify overnight pressed between the glass plates, at room temperature. A blank membrane was prepared in a similar fashion but using 1020 µl of water and 120 mg of gelatin.

5.2.6 - Characterization of Ion-Jelly® Membranes

5.2.6.1 - Traction

The tensile properties of the membranes were tested with a tensile testing machine (MINIMAT firm-ware v.3.1) at room temperature. A full scale load of 20 N and maximum extension of 90 mm were used. Load extension graphs were obtained during testing and converted to stress-strain curves applying the following equations:

$$\text{stress} = \sigma = \frac{F}{A} \tag{5.1}$$

$$\text{strain} = \varepsilon = \frac{\Delta l}{L} \tag{5.2}$$

where F is the applied force (N); A is the cross-sectional area (m^2); Δl is the change in length (mm); L is the length between clamps (mm).

5.2.6.2 - Contact Angles

Contact angles were measured by the sessile drop method in a contact angle goniometer (CAM 100, KSV Instruments Ltd, Finland). In this method a drop of liquid is dropped with a syringe on top of the surface to evaluate and images are captured at short intervals for a certain duration of time. The angle between the surface and the tangent of the drop is measured on both sides of the drop. The contact angles of water and triglycerides in the Ion-Jelly® membranes were measured over a period of 10 seconds in intervals of 0.1 seconds.

5.2.6.3 - SEM Images

The membranes were characterized by Scanning Electron Microscopy (SEM) using a SEM DSM962 model from Zeiss. Samples were coated with 8 nm gold/palladium particles in a Q 150T ES from Quorum. For cross-section analysis the membrane samples were frozen and fractured in liquid nitrogen.

5.2.7 - $scCO_2$ Fractionation Experiments

For the fractionation experiments with the model mixture of squalene and oleic acid (50% in mass of each) we used the apparatus as described in Chapter 2. For the biodiesel experiments, a slight modification of the former configuration was used, in which two HPLC pumps (models 305 and 306, Gilson, USA) were employed, instead of using the single LDC pump, to pump separately the sunflower oil and the methanol flows. Furthermore, the separation vessel before the membrane cell was replaced by a high pressure packed-bed enzymatic tubular 316SS reactor (115 cm length, 9 mm I.D.) filled with Lipozyme RM IM, which converted sunflower triglycerides and methanol to methyl esters and glycerol. The reaction mixture (monophasic) exiting the packed-bed reactor was fed to the membrane cell for further fractionation. The enzymatic reactor is heated by means of a water bath recirculated through an external shirt using a heating circulator (MD, Julabo Labortechnik GmbH, Germany).

5.2.7.1 - Elemental Analysis

Elemental analysis of feed, retentate and permeate streams collected in the $scCO_2$ fractionation experiments was performed with a Flash EA 1112 CHNS series from Thermo Finnigan-CE Instruments, Italy.

5.2.8- Single Gas Permeabilities

The pure gas permeability of the Ion-Jelly® membranes for H_2, N_2, O_2, CH_4 and CO_2 was determined by using the experimental apparatus shown in Figure 5.3. This rig is composed by a stainless steel cell with two identical compartments separated by the supported liquid membrane. The effective membrane area was 4 cm^2. Each individual gas permeability was evaluated by pressurizing both compartments (feed and permeate) with the pure gas, and after opening the permeate outlet, establishing a driving force of around 0.07 MPa between the feed and the permeate compartments. The pressure change in both compartments over time was followed using two pressure transducers (Druck, PDCR 910 models 99166 and 991675, England). All measurements were performed at a constant temperature of 303 K by using a thermostatic bath (Julabo, Model EH, Germany).

The permeability of a pure gas through an ion-jelly membrane was calculated from the pressure data measured over time on both compartments (feed and permeate) as shown in Figure 5.3 according to the following equation [21]:

$$\frac{1}{\beta}\ln\left(\frac{[p_{feed}-p_{perm}]_0}{[p_{feed}-p_{perm}]}\right)=\frac{1}{\beta}\ln\left(\frac{\Delta p_0}{\Delta p}\right)=P\frac{t}{l} \qquad (5.3)$$

where p_{feed} and p_{perm} are the pressures in the feed and permeate compartments (Pa), respectively, P is the membrane permeability ($m^2\ s^{-1}$), t is the time (s), and l is the membrane thickness (m). The indicator 0 refers to the conditions at t=0. The geometric parameter β (m^{-1}) is characteristic of the geometry of the cell and is given by:

$$\beta = A\times\left(\frac{1}{V_{feed}}+\frac{1}{V_{perm}}\right) \qquad (5.4)$$

where A is the membrane area (m^2) and V_{feed} and V_{perm} are the volumes of the feed and permeate compartments (m^3), respectively. The β value calculated in this way for the test cell used in this work was 41.97 m^{-1}. The data can be plotted as $1/\beta\ \ln(\Delta p_0/\Delta p)$ versus t/l, and the gas permeability is obtained from the slope of this representation. The ideal selectivity ($\alpha_{A/B}$) can be calculated by dividing the permeabilities of two different pure gases (A and B) through a given membrane.

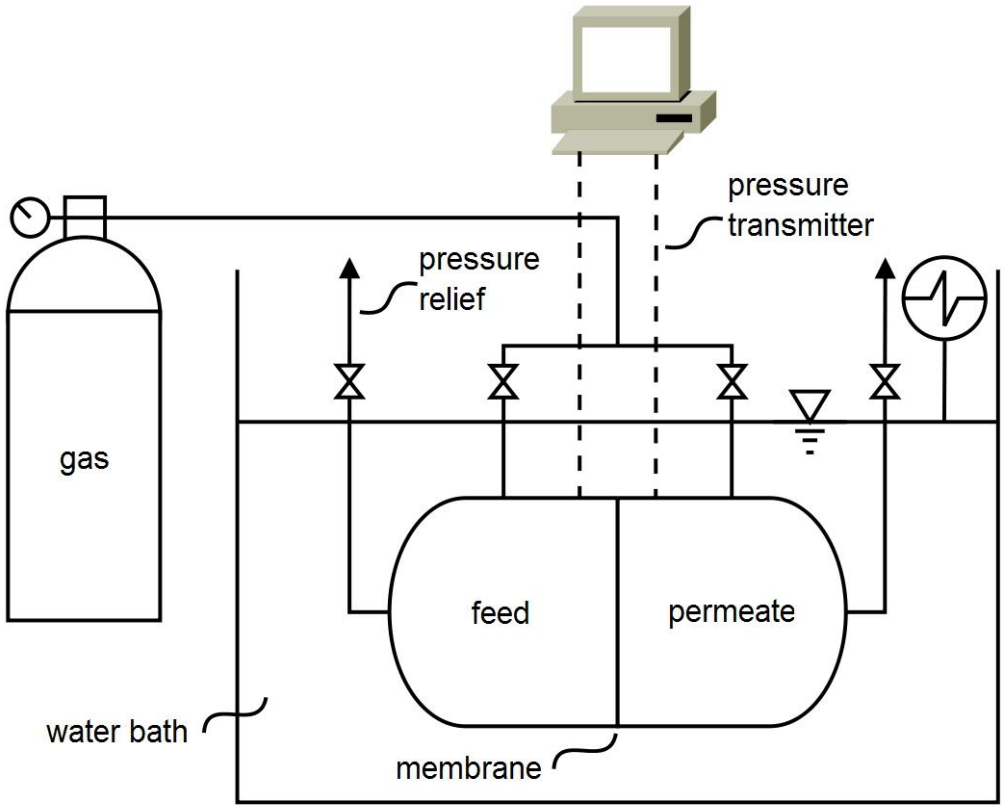

Figure 5.3 – Experimental set-up for measuring the permeability of the SILMs for a single gas.

5.3 - Results

5.3.1 - Supported Ionic Liquids Membranes

For this part of the work were chosen the best ionic liquids according to the screening made in Chapter 3 combined with the reverse osmosis membranes (RO) studied in Chapter 2. Since the ionic liquids with the [NTf_2] anion were the only ones that were selective towards squalene, we have chosen the RTILs [BMIM][NTf_2] and [$(C_6)C_{14}P$][NTf_2] combined with the RO membrane polyamide AD (which was the membrane with a better enrichment in squalene in the permeate side). In the same line of thought, we chose to combine the RTIL [BMIM][DCA] with the RO membrane of cellulose acetate, in order to create a SILM which would be selective towards oleic acid.

Table 5.1 shows the amounts of ionic liquid impregnated for each membrane studied, both in mass and in moles. From the replicas made for the impregnation of [BMIM][DCA] in the cellulose acetate membrane, it is seen that the method of impregnation is reproducible, with less than 10% variation . In addition, from the replica made with a longer time of impregnation (4.5 hours vs. 1 hour), we can conclude that a longer time of impregnation does not result in higher amounts of ionic liquid impregnated.

Table 5.1 – Amounts of ionic liquids impregnated in respective membranes and solubilities of CO_2 in ionic liquids reported in the literature at pressure and temperature conditions used in this work (18 MPa, 313 K).

Membrane	Ionic Liquid	Mass Impregnated (mg)	mmoles Impregnated	Solubility of CO_2 (Mole Fraction)
CA	[$(C_6)_3C_{14}P$][NTf_2]	43.78	0.057	0.847 [21]
CA	[BMIM][DCA]	131.84	0.642	0.531 [23]
CA*	[BMIM][DCA]	131.85	0.642	0.531
CA	[BMIM][DCA]	144.77	0.705	0.531
AD	[BMIM][NTf_2]	117.00	0.279	0.778 [22]

*: 4.5 hours of impregnation

In order to study the applicability of these membranes in high pressure processes, tests of permeability to $scCO_2$ were conducted, to assess the viability of creating pressure drops across

them and to be able to compare them with the results obtained in Chapter 2 with commercial reverse osmosis membranes

From the $scCO_2$ permeability results, plotted in Figure 5.4, it is seen that these membranes are much more permeable to $scCO_2$ than the corresponding RO membranes without the addition of RTILs. Also, it is seen that the permeabilities are similar for both RTILs studied. This result may indicate that the RTILs are functioning here as carriers for the $scCO_2$, increasing its flow across the membrane. From this reasoning, one could expect these results to be a consequence of the well known solubility of $scCO_2$ in RTILs. However, when comparing the amounts of RTIL impregnated in the membrane, we see that there are considerable differences in the number of moles impregnated, but this effect is not reflected in the permeabilities observed. Consequently, it is not possible to correlate directly the permeabilities obtained in this study with the solubilities of $scCO_2$ in RTILs.

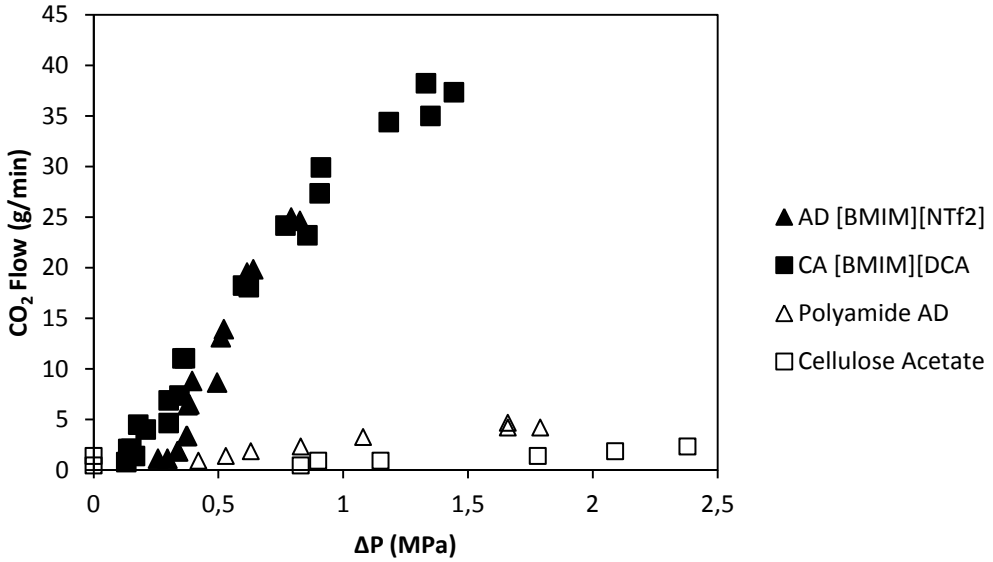

Figure 5.4 - $scCO_2$ permeability in commercial reverse osmosis membranes (see Chapter 2) and supported ionic liquids membranes at 18 MPa and 313 K.

Next, these membranes were evaluated for their performance in the separation of a model mixture of oleic acid/squalene (50% w/w). This is the same mixture which was used in Chapter 2 to evaluate the separation performance of commercial reverse osmosis membranes alone, in order to be able to compare results.

The performance of these membranes for fractionation of a model mixture was expressed in terms of selectivity of one component towards the other, $\alpha_{i/j}$, defined as:

$$\alpha_{i/j} = \frac{y_i/x_i}{y_j/x_j} \quad (5.5)$$

with $y_{i,j}$ and $x_{i,j}$ the mass fraction of component *i*, *j* in the permeate and retentate streams, respectively.

The selectivities towards the model mixture of squalene and oleic acid (50% w/w) obtained with these membranes are negligible, as can be seen from Figure 5.5 and Table 5.2. In fact, the slight enrichment that was obtained originally with the RO membranes is now lost. After testing the pairs best membrane/best ionic liquid, it was also tested the best membrane for the separation of oleic acid (cellulose acetate) with one of the best ionic liquids for the separation of squalene ($[(C_6)_3C_{14}P][NTf_2]$), in order to see if any difference in results could be obtained. But again, the selectivity was negligible, and the results only slightly higher than the cellulose acetate membrane impregnated with [BMIM][DCA]. The loss of selectivity observed for all the SILMs tested is probably the direct result of the higher permeability to $scCO_2$ presented by these membranes, which leads to a higher mass transfer across the membrane, but with the drawback of lower selectivity.

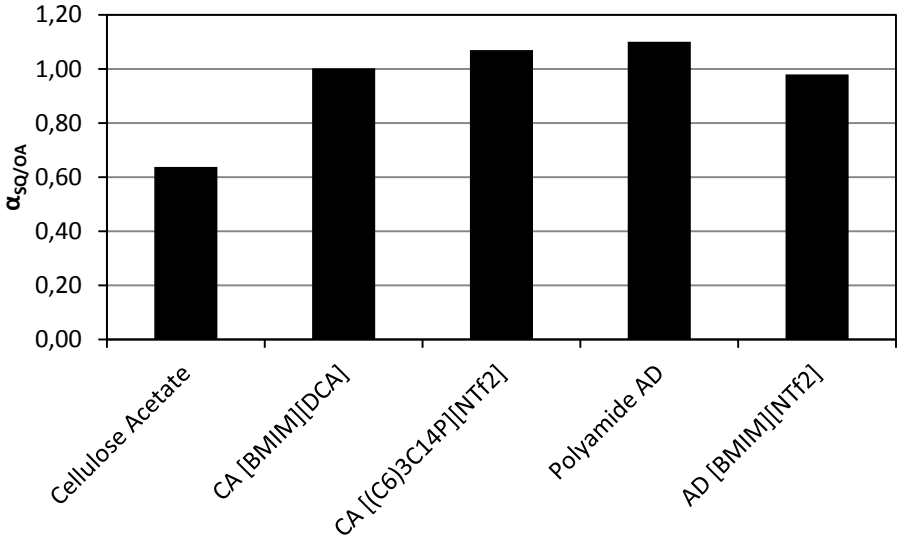

Figure 5.5 – Squalene selectivities with reverse osmosis membranes and their corresponding supported ionic liquid membranes at 18 MPa and 313 K.

Table 5.2 – Values obtained for diverse membranes in the fractionation of a model mixture of oleic acid and squalene.

Membrane	Ionic Liquid	Squalene Mass Fraction			Selectivity
		Feed	Retentate	Permeate	
Cellulose Acetate	———	0.53	0.61	0.50	0.64
	[BMIM][DCA]	0.51	0.59	0.59	1.00
	$[(C_6)_3C_{14}P][NTf_2]$	0.54	0.59	0.61	1.07
Polyamide AD	———	0.58	0.57	0.59	1.10
	$[BMIM][NTf_2]$	0.51	0.61	0.61	0.98

As the results obtained with SILMs for the fractionation of the model mixture of oleic acid and squalene were not good, it was decided to try to use these membranes to fractionate other system. As these membranes revealed to be fully permeable to oleic acid, a fatty acid, a mixture where fatty acids or similar components needed to be separated from other components was looked for.

In the transesterification reaction for the production of biodiesel, the products of interest are methyl esters, which are very similar to fatty acids, differing only in the fact that the carboxylic acid is now methylated. In this reaction, methyl esters need to be separated from glycerol (a subproduct of the reaction), unreacted triglycerides and methanol (the reactants) and monoglycerides and diglycerides (resulting from incomplete conversion of triglycerides). So, this looks like a promising system in which a membrane could be used for the fractionation of products and reactants. In Figure 5.6 are presented the results of the fractionation of the effluent stream of the enzymatic transesterification of sunflower oil to biodiesel with a SILM membrane composed of [BMIM][DCA] immobilized in a cellulose acetate membrane, at 20 MPa and 323 K.

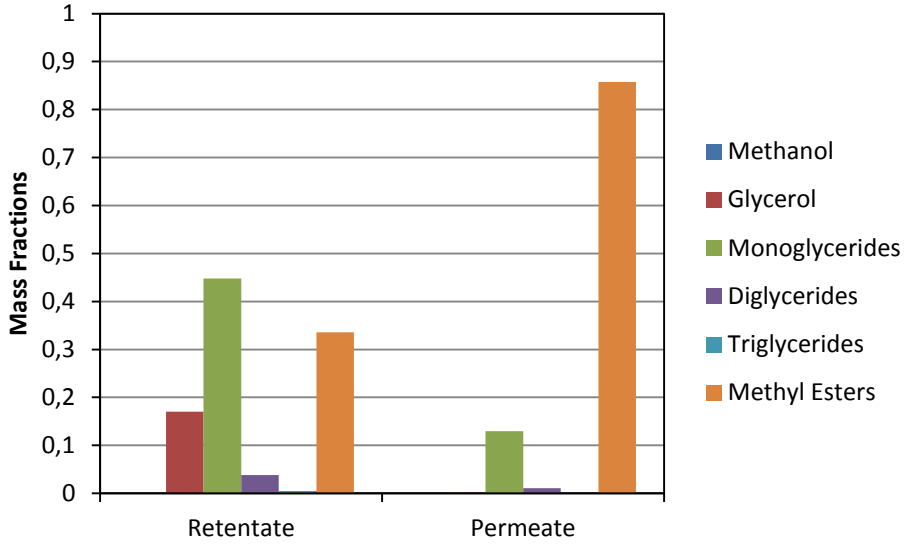

Figure 5.6 - Fractionation of effluent stream of enzymatic transesterification of sunflower oil to biodiesel with [BMIM][DCA] supported in cellulose acetate membrane. Operating conditions were 20 MPa and 323 K.

From Figure 5.6 it can be seen that triglycerides were almost completely converted to other products, being detected only a residual amount in the retentate stream. The small portion of diglycerides that were produced is mainly retained in the retentate side of the membrane, and methanol was not detected. There is also a considerable portion of monoglycerides, which are mainly retained by the membrane. As for the methyl esters, although they account still for 30% of the retentate fraction, they constitute about 85% of the permeate stream. The selectivity of methyl esters in relation to monoglycerides, $\alpha_{ME/MG}$, the two major constituents of both permeate and retentate, is 8.8, which is a considerable selectivity. On the other hand, glycerol was completely retained by the membrane. So, these membranes seem to be viable for application in an integrated process of enzymatic transesterification and fractionation in continuous operation.

As a consequence of the poor results obtained with the SILMs for the fractionation of the model mixture of oleic acid and squalene, it was decided to try to use gel membranes to overcome these problems. With gel membranes, it may be possible to reduce the solubility of $scCO_2$ in the RTILs, and consequently reduce its permeability across the membrane and increase its selectivity. Although it was not tested for these membranes, several authors report that RTILs are displaced from SILMs even at low pressure differences between permeate and retentate [14]. This problem was also related to the membrane compression occurring with the application of pressure and to the pore sizes of the membranes being used [24]. Gel membranes could also be a solution for this problem, as the gel polymerization entraps the RTIL and difficults its displacement.

5.3.2 - Development of Ion-Jelly® Membranes prepared by evaporative casting-knife method

5.3.2.1 - Traction

The stress-strain curves in Figure 5.7 indicate that the membrane prepared only with gelatine has a higher tolerance to stress than the ones prepared with Ion-Jelly®. It is also seen that the tolerance to stress in Ion-Jelly® membranes is very similar to that of cellulose alone, but the presence of Ion-Jelly® allows it to sustain higher strains. Additionally, by increasing the amount of Ion-Jelly® used, the tolerance to stress also increases.

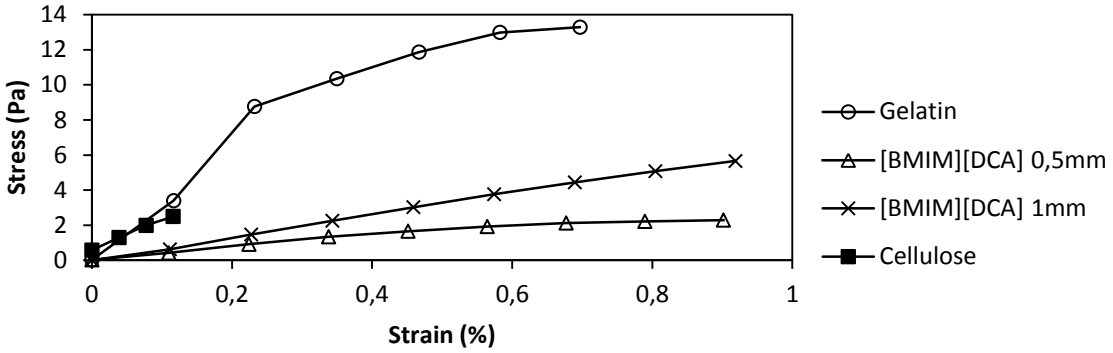

Figure 5.7 – Stress-strain curves of Ion-Jelly® membranes prepared by evaporative casting-knife method.

From Table 5.3 it is possible to observe, from the Young modulus, the difference in stiffness between spreading Ion-Jelly® over a cellulose support, or employing only gelatine. The Young modulus is the tangent modulus of the initial, linear portion of stress-strain curves, and increases with increasing stiffness of the material. It is seen that gelatine greatly increases the stiffness when compared with only the cellulose support. But, when ionic liquid is added to gelatine, the stiffness of the membrane is considerably reduced to values even below that of cellulose alone. Also, by using a higher amount of Ion-Jelly®, the membrane stiffness is even more reduced. This effect is visually apparent, as can be seen in Figure 5.8, where the pictures of a membrane prepared only with gelatine and another prepared with Ion-Jelly® are shown. While the membrane prepared with Ion-Jelly® has a smooth surface and is flexible, the one prepared only with gelatine is wrinkled and stiff.

Table 5.3 – Young modulus of Ion-Jelly® membranes

Membrane	Young Modulus (Pa)
Cellulose	16.7
Gelatin	26.2
[BMIM][DCA] 0.5 mm	3.9
[BMIM][DCA] 1 mm before $scCO_2$	1.9
[BMIM][DCA] 1 mm after $scCO_2$	5.6

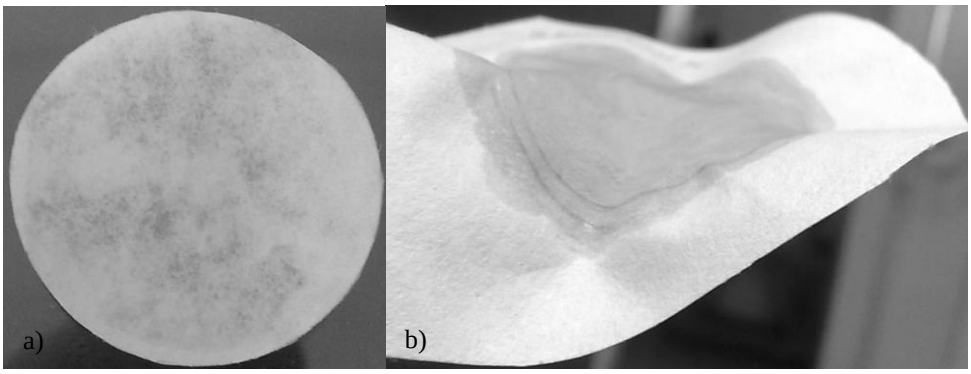

Figure 5.8 – Pictures of a) Ion-Jelly® based in [BMIM][DCA] membrane and b) gelatine membrane.

In Table 5.3 is also indicated the Young Modulus for an Ion-Jelly® membrane of [BMIM][DCA] with 1 mm thickness after being used in experiments with $scCO_2$. It is seen that the value increases which might indicate that Ion-Jelly® is being displaced from the membrane when submitted to high pressure conditions.

5.3.2.2 - Contact Angles

The curve profiles determined by sessile drop contact angle measurement (Figure 5.9) are typical of a porous material, which soaks the drop almost immediately upon contact. This observation is strengthened by the fact that the contact angle measured rapidly decreases to values below 90º either with polar or apolar liquids, consistent with a liquid being absorbed by a porous material [25]. Nevertheless, these membranes seem to be hydrophobic, as the contact angles for triglycerides and a model mixture of methyl oleate and squalene are around 20º while those for water are considerably higher, before the drop is absorbed.

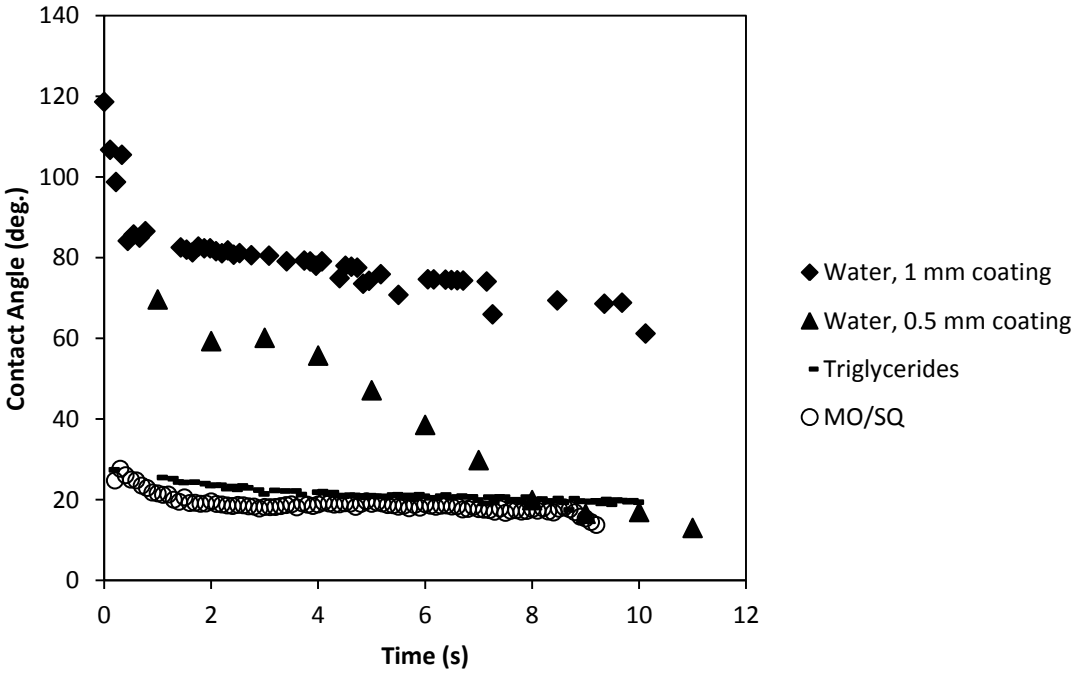

Figure 5.9 – Contact angles of [BMIM][DCA] Ion-Jelly® membranes prepared according to evaporative casting-knife method.

5.3.2.3 - $scCO_2$ Permeability Measurements

We have compared the permeability of $scCO_2$ at 18.0 MPa and 313K of Ion-Jelly® membranes and commercial reverse osmosis membranes. We can see in Figure 5.10 that the Ion-Jelly® membrane made with [EMIM][DCA] has similar permeability to $scCO_2$ as the commercial reverse osmosis membranes. However, the Ion-Jelly® membranes based in [BMIM][DCA] and [BMPyr][DCA] have considerably higher permeabilities, with pressure drops across the membrane as high as 2.0 MPa. Besides these membranes, it was also prepared one based in [EMIM][$MDEGSO_4$], but it was not possible to obtain a pressure drop across it, so it was discarded from further tests.

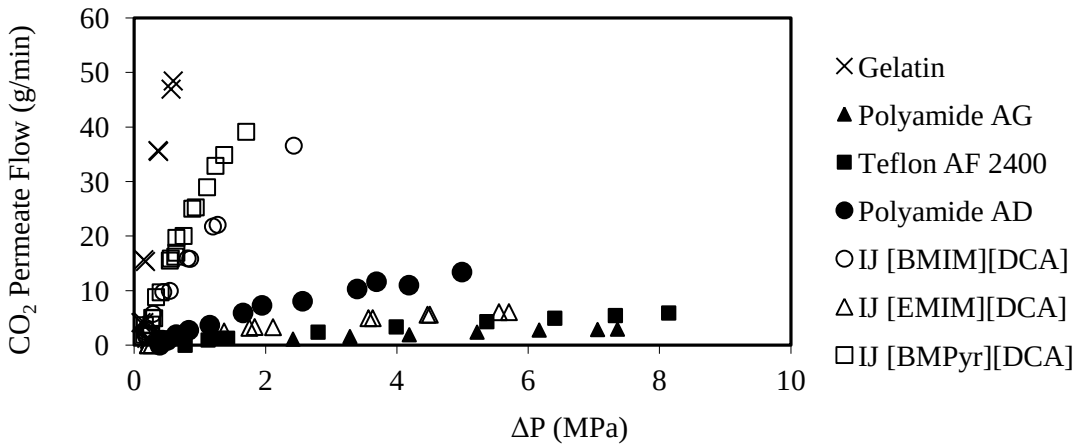

Figure 5.10 – $scCO_2$ permeability in commercial reverse osmosis membranes and Ion-Jelly® membranes without thickness control.

The membranes which were used to obtain the results presented in Figure 5.10 have no thickness control. When the thickness of the Ion-Jelly® layer is controlled with a casting knife, it is possible to increase the permeability by reducing the thickness of the ion-jelly layer, as is possible to observe in Figure 5.11, achieving permeability values as high as the membrane prepared only with gelatin. The thicknesses indicated below are the thicknesses at which the casting knife was set to spread the Ion-Jelly® while liquid. However, it was observed that after application the excess water present in Ion-Jelly® would evaporate and the Ion-Jelly® would be absorbed into the cellulose support, so that the final thickness of the membrane is much less than the thickness set for the casting knife. The thicknesses of the membranes were measured with a micrometer, and were in the range of 180-220 µm. However, it was found that in the same membrane fluctuations occurred, revealing that the distribution of Ion-Jelly® was not even. So, the thicknesses indicated here are to be interpreted as regarding the amount of Ion-Jelly® being impregnated in the membrane, and not the actual final thickness of the membrane.

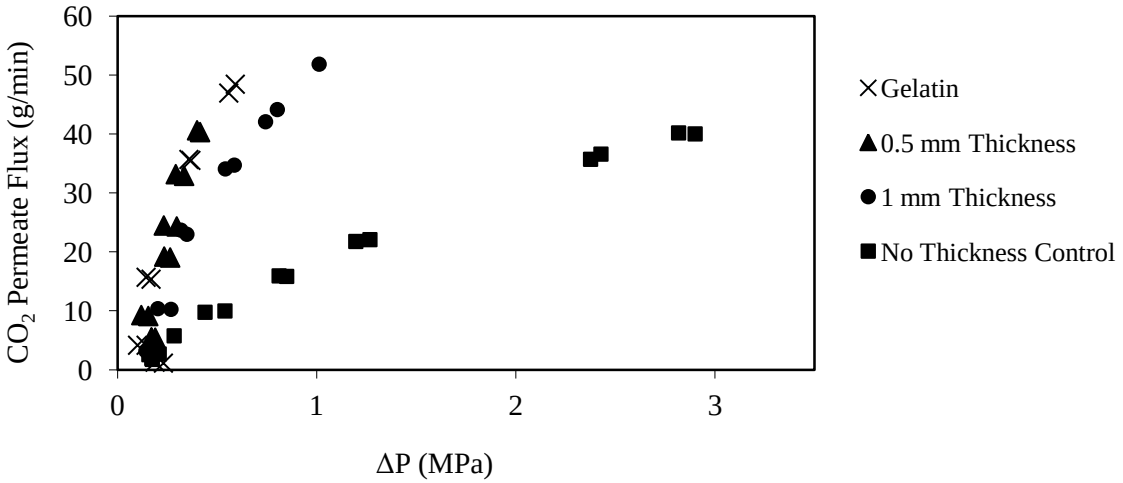

Figure 5.11 – $scCO_2$ permeability in [BMIM][DCA] Ion-Jelly® membranes with and without thickness control.

5.3.2.4 - SEM images

SEM images reveal that Ion-Jelly® forms a uniform and smooth surface on top of the cellulose support, as can be seen in Figure 5.12 a) and b). However, applying $scCO_2$, the Ion-Jelly® penetrates the cellulose support, covering the cellulose fibers (Figure 5.12 c) and d)). It is interesting to compare with the images of pure gelatine in Figure 5.12 e) and f), which show that the gelatine penetrates the cellulose support without the application of $scCO_2$, covering the cellulose fibers with a more compact and dense structure.

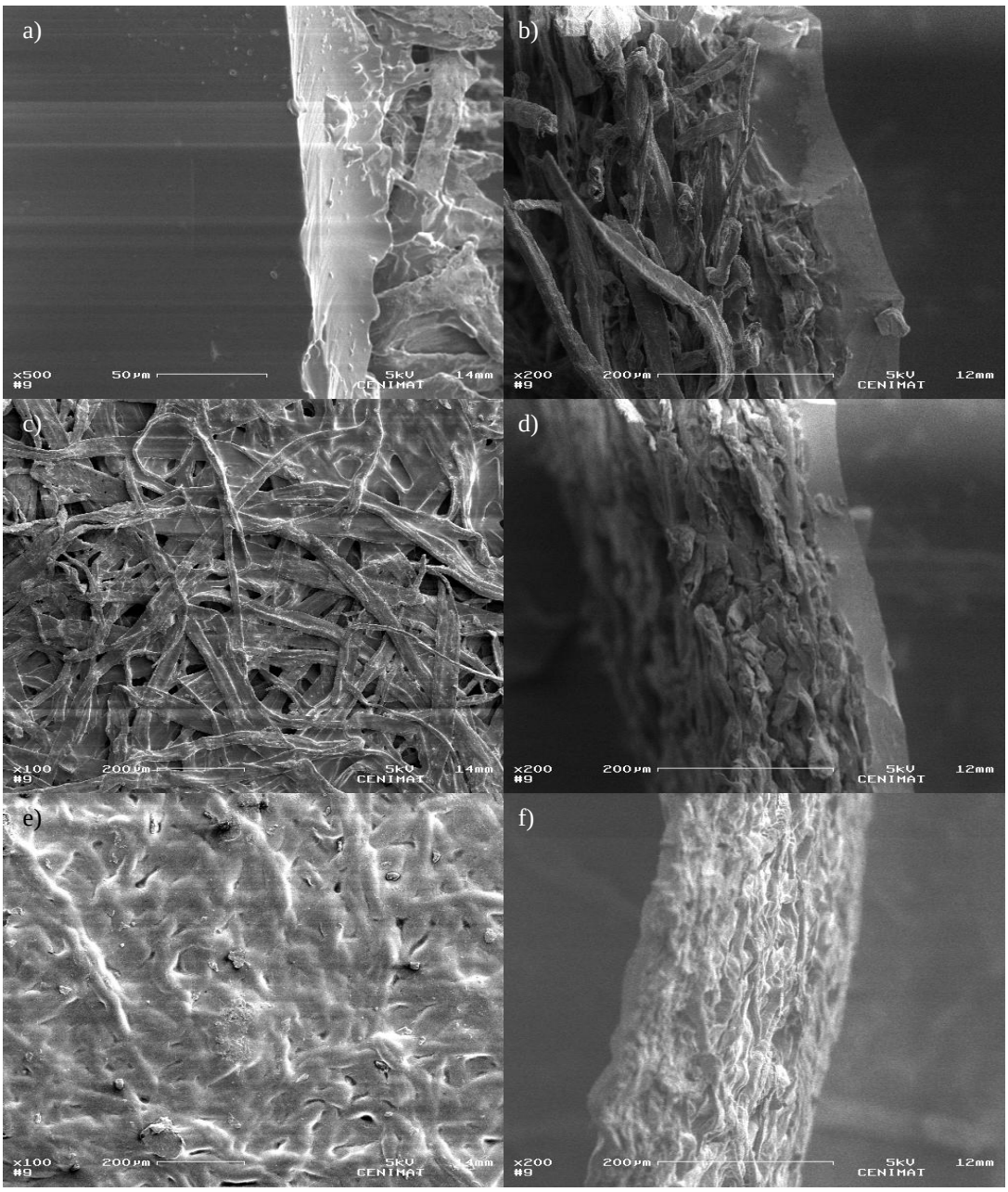

Figure 5.12 – SEM images of Ion-Jelly® membranes prepared by evaporative casting-knife method.

a) 1 mm casting knife thickness [BMIM][DCA] prior to $scCO_2$ tests (top view)

b) 1 mm [BMIM][DCA] prior to $scCO_2$ tests (cross section view)

c) 1 mm [BMIM][DCA] after $scCO_2$ tests (top view)

d) 1 mm [BMIM][DCA] after $scCO_2$ tests (cross section view)

e) Gelatin blank (top view)

f) Gelatin blank (cross section view)

5.3.3 - $scCO_2$ Fractionation Experiments

The application of the Ion-Jelly® membranes on the separation/fractionation of mixtures in supercritical carbon dioxide was studied for the particular cases of the model mixtures of oleic acid + squalene (50% w/w) and methyl oleate + squalene (40% / 60% w/w), in order to compare with the results presented in previous chapters.

In Figure 5.13 and Table 5.4 are presented the results for the fractionation of the model mixture of oleic acid + squalene (50% w/w), for three Ion-Jelly® membranes based in [EMIM][DCA], [BMIM][DCA] and [BMPyr][DCA]. It was found that the membrane with [EMIM][DCA] is slightly more selective towards squalene, while the one based on [BMPyr][DCA] is more selective towards oleic acid. However, as can be seen, the selectivities obtained are negligible.

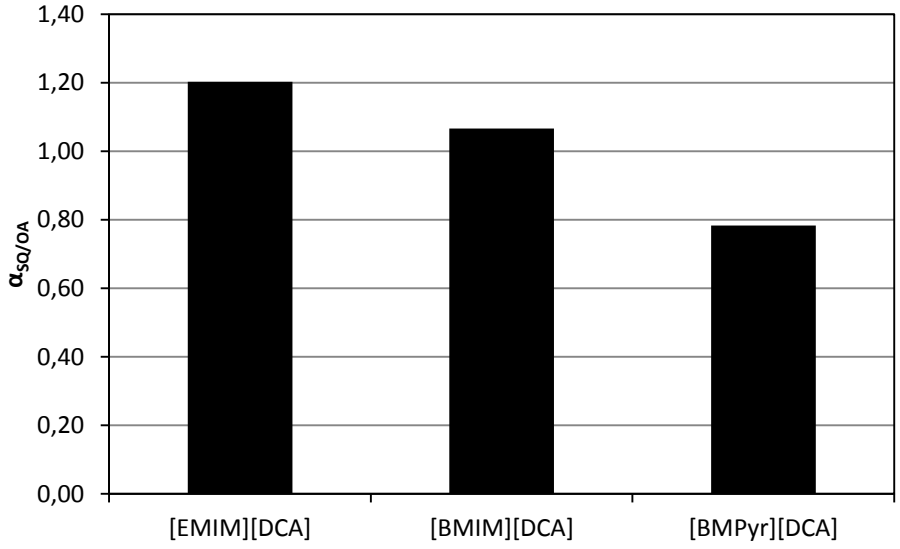

Figure 5.13 – Squalene selectivities with Ion-Jelly® membranes prepared according to evaporative casting-knife method at 18 MPa and 313 K.

Table 5.4 – Values obtained for diverse membranes in the fractionation of a model mixture of oleic acid and squalene and a model mixture of methyl oleate and squalene.

		Squalene Mass Fraction			
Mixture	Ionic Liquid	Feed	Permeate	Retentate	Selectivity
Oleic Acid / Squalene	[EMIM][DCA]	0.57	0.69	0.65	1.20
	[BMIM][DCA]	0.58	0.67	0.65	1.07
	[BMIM][DCA]	0.45	0.57	0.55	1.09
	[BMPyr][DCA]	0.49	0.75	0.79	0.78
Methyl Oleate/ Squalene	[BMIM][DCA] 0.5 mm	0.43	0.43	0.46	0.90
	[BMIM][DCA] 0.5 mm	0.42	0.38	0.37	1.01

As the fractionation of oleic acid and squalene presents several difficulties, it was decided to test these membranes with another model mixture which is known to be fairly easier to fractionate, methyl oleate and squalene [26]. The values obtained are plotted in Figure 5.14 and indicated in Table 5.4. However, both membranes tested presented also negligible selectivities.

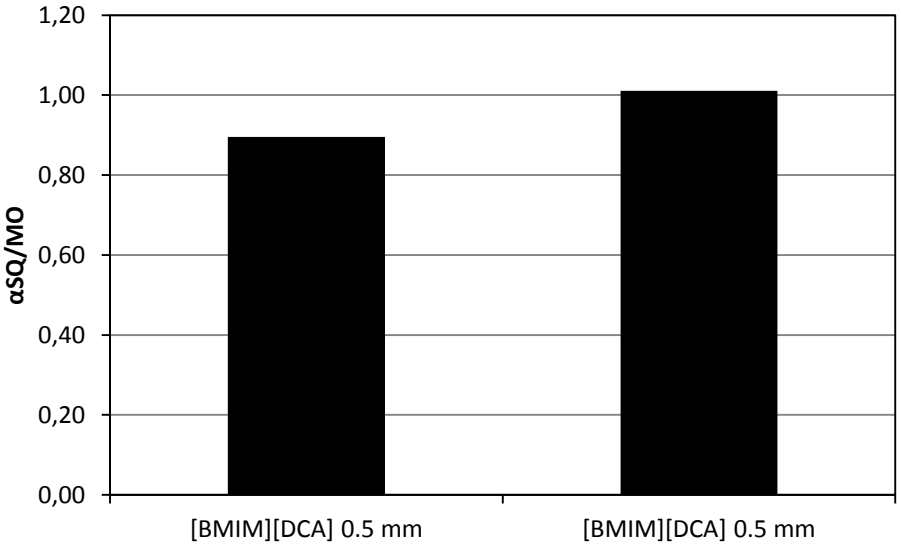

Figure 5.14 – Squalene selectivities with Ion-Jelly® membranes prepared by the evaporative casting-knife method at 18 MPa and 313 K.

From Figure 5.14 some discrepancies can also be seen in the results for two membranes prepared independently. These discrepancies led us to hypothesize that the production method was not reproducible, leading to defects in the production of the membranes. In fact, when looking at SEM images, some flaws in the surface of the Ion-Jelly® can be detected, as is signalled in Figure 5. 15.

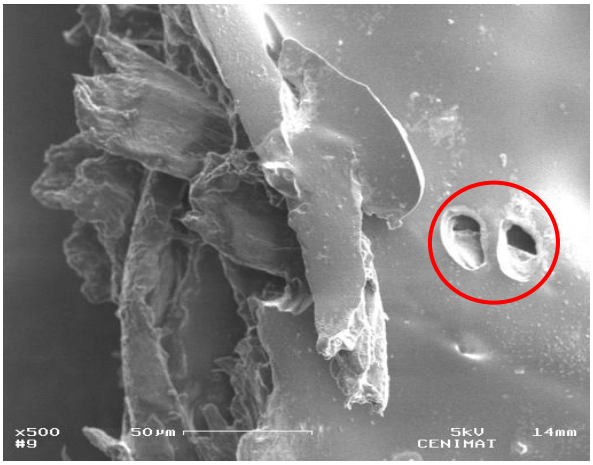

Figure 5.15 – SEM image of the surface of a [BMIM][DCA] membrane 0.5 mm in thickness. The red circle indicates two air bubbles which remained during the jellification process.

5.3.3.1 - Elemental Analysis

Taking into account that the SEM images revealed that the impregnation of Ion-Jelly® was not completely successful and there are flaws in the surface, it is also possible that some Ion-Jelly® is eroded from the surface during operation. To test this possibility elemental analysis of the feed, retentate and permeate streams of the $scCO_2$ fractionation experiments was performed to detect the eventual presence of nitrogen. In the high pressure systems studied in this work, the nitrogen element is present only in the gelatin, ionic liquid or cellulose support structure. So, if nitrogen is detected in the retentate or permeate streams, this should be indicative that the membrane was degraded under operation. As can be seen from Table 5.5, only trace amounts of nitrogen were found in the permeate and retentate streams, although a little higher than the nitrogen content present in the feed stream. After the $scCO_2$ fractionation experiments, the stainless steel porous plate which lies beneath the membrane was disassembled and washed with ethanol in an ultrasounds bath to remove the remaining portion of permeate remaining trapped inside the pores of the plate. After ethanol evaporation, a sample of remaining liquid was also analysed for the presence of nitrogen. It was found that this sample contained 6% nitrogen, which indicates that the membrane is being degraded and the remains of this erosion are being trapped in the porous plate.

Table 5.5 – Nitrogen detected by elemental analysis in several streams.

	Nitrogen Content (wt%)
Feed	0.11
Retentate	0.46
Permeate	0.67
Plate	6.06

By analysing together the results from elemental analysis (which show that the membranes are being degraded), those from traction experiments (which indicate that Ion-Jelly® is being displaced from the membrane), the SEM images (which show air bubbles and that Ion-Jelly® is penetrating into the cellulose fibers only after $scCO_2$ application) and the discrepancies observed in $scCO_2$ fractionation, it becomes obvious that these membranes are not uniform and the spreading method is not the best. Taking all this into account, it was decided to improve the spreading method and create a second generation of membranes.

5.3.4 - Development of Ion-Jelly® Membranes prepared by glass plates pressed method

To try to overcome the problems identified in the first generation of Ion-Jelly® membranes, a new approach to the spreading method of liquid Ion-Jelly® on the cellulose supports was developed. In order to eliminate air bubbles and to force the Ion-Jelly® layer to penetrate into the spaces between the cellulose fibers, it was decided to spread the Ion-Jelly® still liquid over the cellulose support, making sure the material covers completely the cellulose support, and immediately afterwards to press it between two smooth glass plates. In doing so, the air bubbles and the excess Ion-Jelly® are forced to flow out of the membrane surface, and the pressure applied also forces the Ion-Jelly® to penetrate into the cellulose support.

5.3.4.1 - Traction

The stress-strain curves shown in Figure 5.16 show that, as already observed with the membranes prepared by the evaporative casting-knife method, the membrane prepared only with gelatine had a higher tolerance to stress than the ones prepared with Ion-Jelly®. The behaviour of the [BMIM][DCA] membrane is very much like the one observed with the [BMIM][DCA] membrane 0.5 mm in thickness prepared by the evaporative casting-knife method. It is also possible to observe that the Ion-Jelly® membranes based in imidazolium ILs have a lower tolerance to stress than the cellulose support alone, whereas the Ion-Jelly® membrane based in pyrrolidinium RTIL has a higher tolerance to stress.

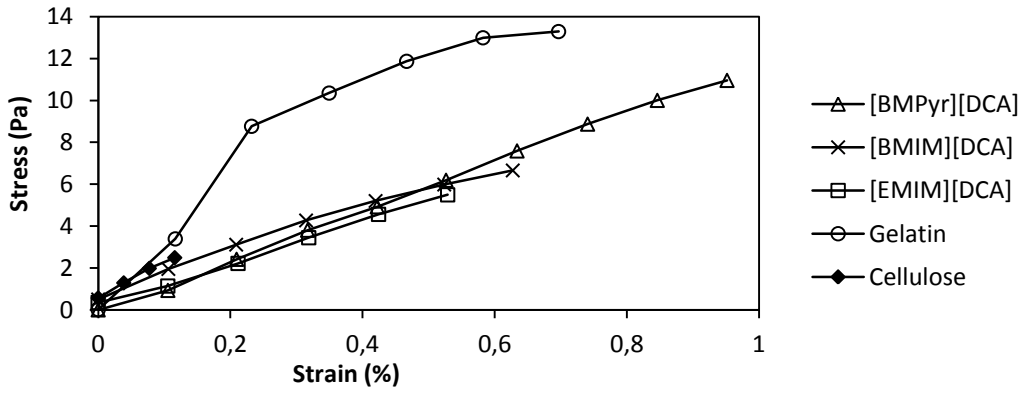

Figure 5.16 – Stress-strain curves of Ion-Jelly® membranes prepared by glass plates pressed method.

Comparing Table 5.6 with Table 5.3, we can see that the Young modulus is now considerably higher for these membranes. Also, the three different membranes tested present similar values between themselves. Already from these results we can see that these membranes are mechanically different from the ones prepared by the evaporative casting-knife method.

Table 5.6 – Young modulus of Ion-Jelly® membranes prepared by glass plates pressed method.

Membrane	Young Modulus (Pa)
Gelatine	26.2
Cellulose	16.7
[BMPyr][DCA]	11.9
[EMIM][DCA]	10.0
[BMIM][DCA]	9.8

5.3.4.2 - Contact Angles

The curve profiles determined by sessile drop contact angle measurement (Figures 5.17 and 5.18) continue to show the behaviour of a porous material [25]. However, now the contact angles values are higher for triglycerides while those of water remain identical for [BMIM][DCA] and [BMPyr][DCA], but lower for [EMIM][DCA]. We can therefore say that the [EMIM][DCA] membrane is more hydrophilic than the others, as it presents lower contact angles for water and higher contact angles for triglycerides.

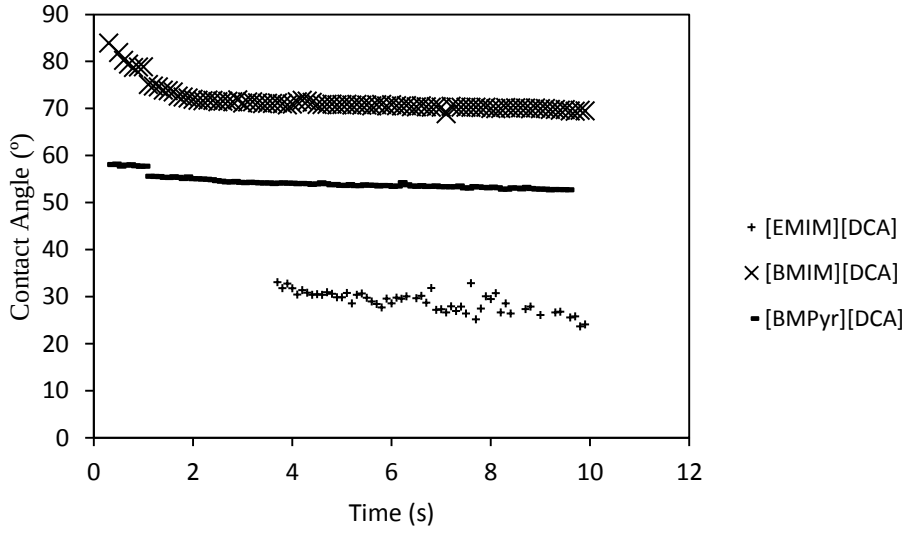

Figure 5.17 – Water contact angles in Ion-Jelly® membranes prepared by glass plates pressed method.

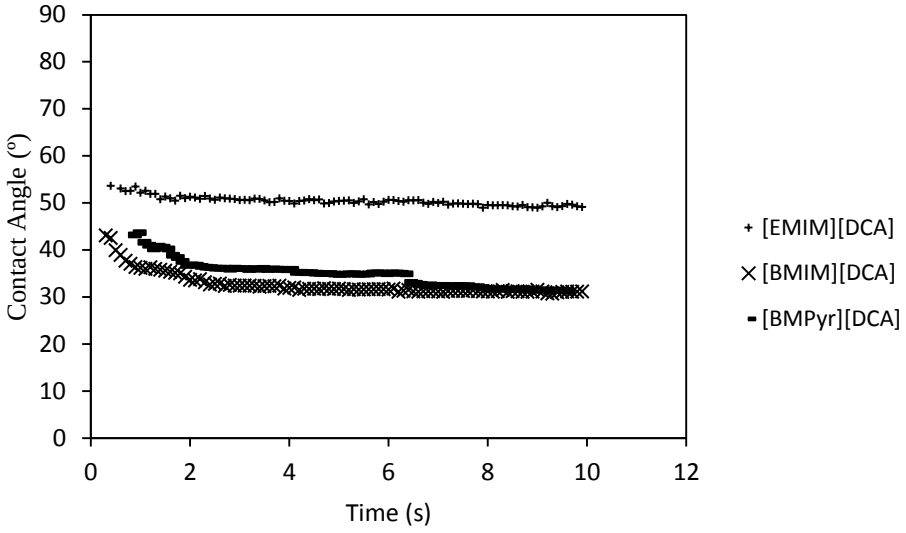

Figure 5.18 – Triglycerides contact angles in Ion-Jelly® membranes prepared by glass plates pressed method.

5.3.4.3 - $scCO_2$ Permeability Measurements

Comparing the values now obtained with the [BMIM][DCA] Ion-Jelly® membrane (Figure 5.19) with those prepared according to the evaporative casting-knife method, we see that the permeability has considerably decreased. It now presents values similar to commercial reverse osmosis membranes, although much higher pressure drops across the membrane can be obtained (up to 10 MPa). This is an indication that the Ion-Jelly® in this membrane is now much more homogeneous and that the previously observed high permeabilities to $scCO_2$ were probably the result of the presence of air bubbles, which allowed $scCO_2$ to flow through the membrane much more easily.

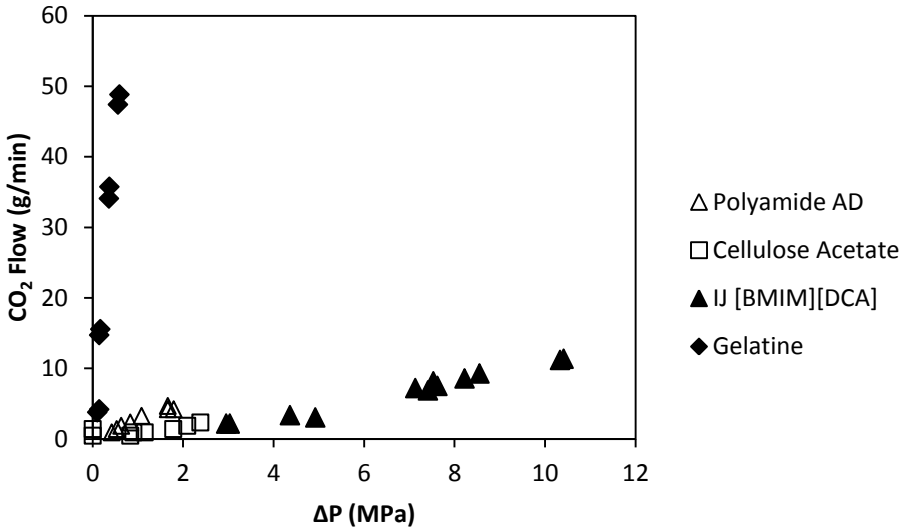

Figure 5.19 – $scCO_2$ permeability in commercial reverse osmosis membranes (see Chapter 2) and Ion-Jelly® membranes prepared by glass plates pressed method.

5.3.4.4 - SEM images

SEM images reveal that Ion-Jelly® now forms a thin layer on the surface of the cellulose fibers, as can be seen in Figure 5.20 a), c) and g), while permeating to the interior of the cellulose support and filling the empty spaces between the fibers. (Figure 5.20 b), d) and h)). The application of $scCO_2$ to the [BMIM][DCA] membrane, does not appear to have any significant effect in the membrane morphology, when comparing Figure 5.20 c) and d) with Figure 5.20 e) and f), respectively. This observation could indicate a better stability of these membranes.

These images are now remarkably different from those observed in the membranes prepared by the evaporative casting-knife method. We can now see that the Ion-Jelly® does not simply stay on top of the cellulose support but actually diffuses into it, covering the individual fibers and occupying the empty space between them, result which was obtained previously only upon the application of $scCO_2$. Although this result is much better than the one obtained previously, there can still be seen some pores between the fibers, which could result in poor performance of the membrane.

5.3.5 - $scCO_2$ Fractionation Experiments

The application of the Ion-Jelly® membranes prepared by the glass plates pressed method on the separation/fractionation of mixtures in supercritical carbon dioxide was studied for the particular case of the model mixture of oleic acid + squalene (50% w/w), in order to compare with the results obtained with the membranes prepared by the evaporative casting-knife method. Additionally, we studied its application to the fractionation of the effluent stream resulting from the transesterification conversion of edible sunflower oil to biodiesel.

In the case of the model mixture of oleic acid and squalene, little or no fractionation at all was achieved with the Ion-Jelly® membranes, as can be observed in Figure 5.21, where it is shown the selectivities of squalene towards oleic acid at different time intervals for the [BMIM][DCA] Ion-Jelly® membrane. This run was repeated again using a second [BMIM][DCA] Ion-Jelly® membrane to test the reproducibility of the method of preparation of the membranes.

The calculated selectivity obtained was 1.06. The upstream pressure and temperature were fixed at 18 MPa and 313 K, respectively. The transmembrane pressure drop was set at 6 MPa with a corresponding permeate flux of 3 $g \cdot min^{-1}$. Similar results, that is, no fractionation, were obtained for the other Ion-Jelly® membranes prepared by the glass plates pressed method.

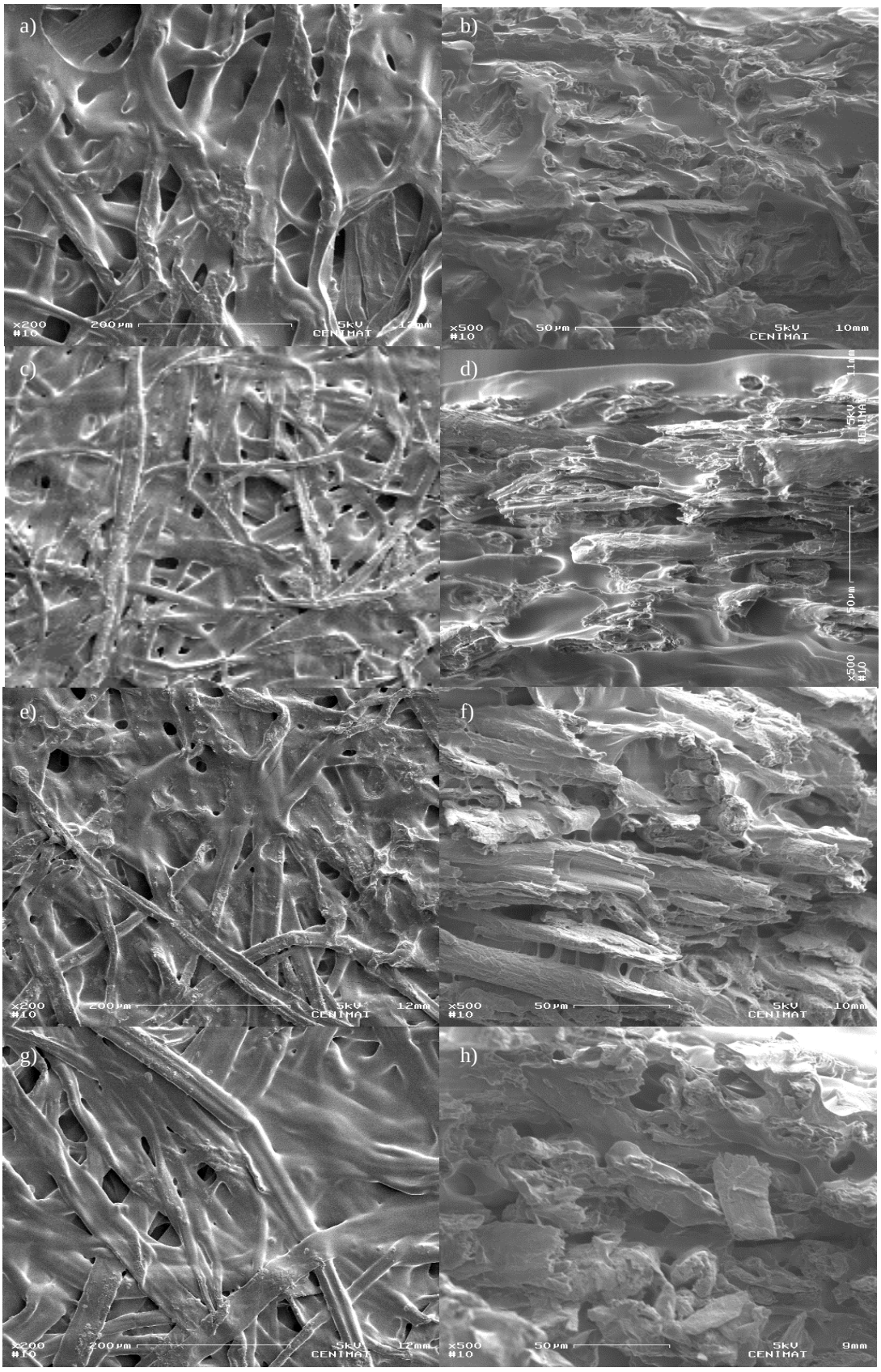
a)
x200
#10
200µm
5kV
CENIMAT
12mm
b)
x500
#10
50µm
5kV
CENIMAT
10mm
c)
d)
x500
#10
50µm
5kV
CENIMAT
e)
x200
#10
200µm
5kV
CENIMAT
12mm
f)
x500
#10
50µm
5kV
CENIMAT
10mm
g)
x200
#10
200µm
5kV
CENIMAT
12mm
h)
x500
#10
50µm
5kV
CENIMAT
9mm

Figure 5.20 – SEM images of Ion-Jelly® membranes prepared by glass plates pressed method.

a) [EMIM][DCA] (top view)

b) [EMIM][DCA] (cross section view)

c) [BMIM][DCA] before $scCO_2$ tests (top view)

d) [BMIM][DCA] before $scCO_2$ tests (cross section view)

e) [BMIM][DCA] after $scCO_2$ tests (top view)

f) [BMIM][DCA] after $scCO_2$ tests (cross section view)

g) [BMPyr][DCA] (top view)

h) [BMPyr][DCA] (cross section view)

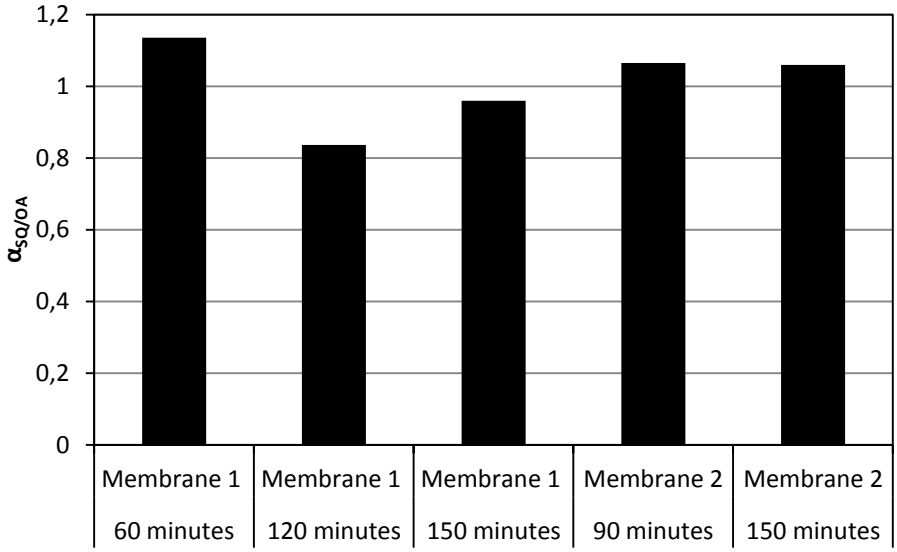

Figure 5.21 – Selectivity of squalene with [BMIM][DCA] Ion-Jelly® membranes prepared by the glass plates pressed method at 18 MPa and 313 K.

For the biodiesel fractionation experiments, two HPLC pumps pumped a combined flow of 291 $\mu L \cdot min^{-1}$ with a molar ratio of methanol : triglycerides of 9:1. Carbon dioxide was pumped at 50 $g \cdot min^{-1}$, 20 MPa and 323 K. The enzymatic reactor was filled with 23g Lipozyme RM IM. The membrane used in this experiment was of Ion-Jelly® based on [BMIM][DCA], and the transmembrane pressure drop was set at 1.2 MPa and a corresponding permeate flux of 15 $g \cdot min^{-1}$. The results obtained for this experiment are shown in Figure 5.22 in terms of mass fractions of main components in the liquid stream fed to the membrane and in the liquid fractions collected in the retentate and permeate collector vessels.

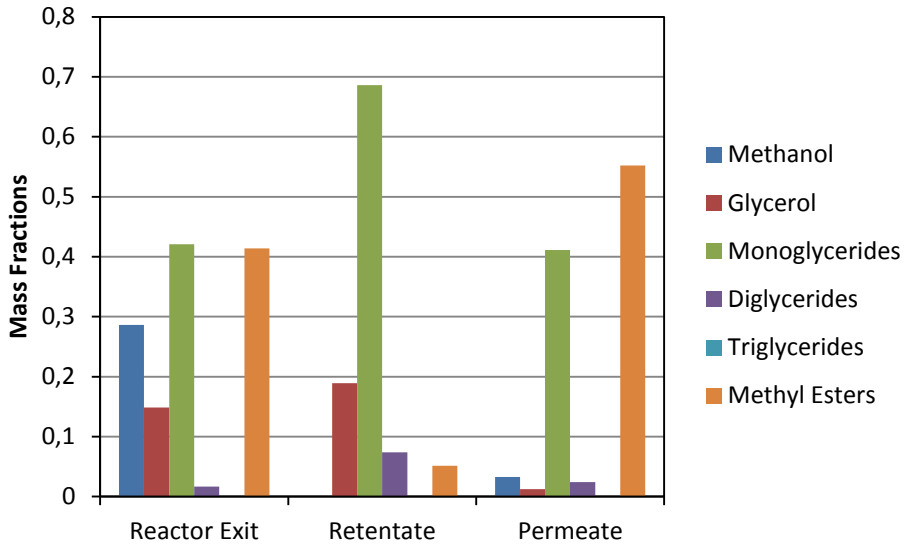

Figure 5.22 – Fractionation of effluent stream of enzymatic transesterification of sunflower oil to biodiesel with [BMIM][DCA] Ion-Jelly® membrane. Operating conditions were 20 MPa and 323 K.

The purpose of this experiment was to separate the methyl esters (the product of interest) from reagents and glycerol (the subproduct of the reaction).

The first observation that it is possible to make from Figure 5.22 is that the enzymatic transesterification of sunflower oil to biodiesel was not complete, since monoglycerides and diglycerides were identified at the effluent stream coming from the enzymatic reactor and fed to the membrane cell. However, no triglycerides were observed. The Ion-Jelly® membrane permeated preferentially the methyl esters and monoglycerides, while glycerol and diglycerides were retained. The monoglycerides, despite being concentrated to ca. 70 wt% in the retentate fraction, still permeated through the membrane. On the other hand, the selectivity of the membrane towards the methyl esters in detriment of glycerol, $\alpha_{ME/G}$, was 166 in our experiment, while that of methyl esters in detriment of monoglycerides $\alpha_{ME/MG}$, is 18.5. This result indicates that one could use this Ion-Jelly® membrane to achieve an efficient separation of the methyl esters from glycerol and other residual components. Methanol, on the other hand, was not detected in the retentate stream, and seems to completely permeate through the membrane.

5.3.5.1 - Elemental Analysis

Elemental analysis of the feed, retentate and permeate streams of the $scCO_2$ fractionation experiments of the model mixture of oleic acid and squalene was performed to detect the eventual presence of nitrogen. As can be seen from Table 5.7, only trace amounts of nitrogen were found in

the permeate and retentate streams, similar to the nitrogen content present in the feed stream. After the $scCO_2$ fractionation experiments, the stainless steel porous plate which lies beneath the membrane was disassembled and washed with ethanol in an ultrasounds bath to remove the remaining portion of permeate remaining trapped inside the pores of the plate. After ethanol evaporation, a sample of remaining liquid was also analysed for the presence of nitrogen. A small concentration of nitrogen (from 0.06 to 0.29 in mass percentage) was detected, although negligible. In face of all these results, we can say that the Ion-Jelly® membranes prepared according to the glass plates pressed method are much more stable than the ones prepared according to the evaporative casting-knife method.

Table 5.7 – Nitrogen detected by elemental analysis in several streams.

	Nitrogen Content (wt%)
Feed	0.06
Retentate	0.06
Permeate	0.07
Plate	0.29

5.3.6 - Single Gas Permeabilities of Ion-Jelly® Membranes Prepared by the Glass Plates Pressed Method.

To extend the possible range of applications of this kind of gel membranes we have also studied the application of Ion-Jelly® membranes in the separation of low pressure gaseous systems.

From Figure 5.23, where the gas permeabilities of the Ion-Jelly® membranes are plotted against the Lennard-Jones diameter of the gas molecules [27], it can be seen that the gas permeabilities are size dependent with the exception of CO_2. In fact, the biggest molecule (CO_2) has the highest permeabilities for all the membranes tested. Table 5.8 shows the permeabilities of the pure gases in the Ion-Jelly® membranes and the calculated ideal selectivities, $\alpha_{A/B}$. It is noticed that the ideal selectivities are not very high, with the highest value obtained for the CO_2/N_2 separation with the [BMIM][DCA] membrane ($\alpha_{CO2/N2}$ = 10), followed by the CO_2/N_2 separation with the [EMIM][DCA] membrane ($\alpha_{CO2/N2}$ = 6.67). From Table 5.8 it is also seen that an increase in the imidazolium side chain size in the cation results in a decrease in the gas permeabilities.

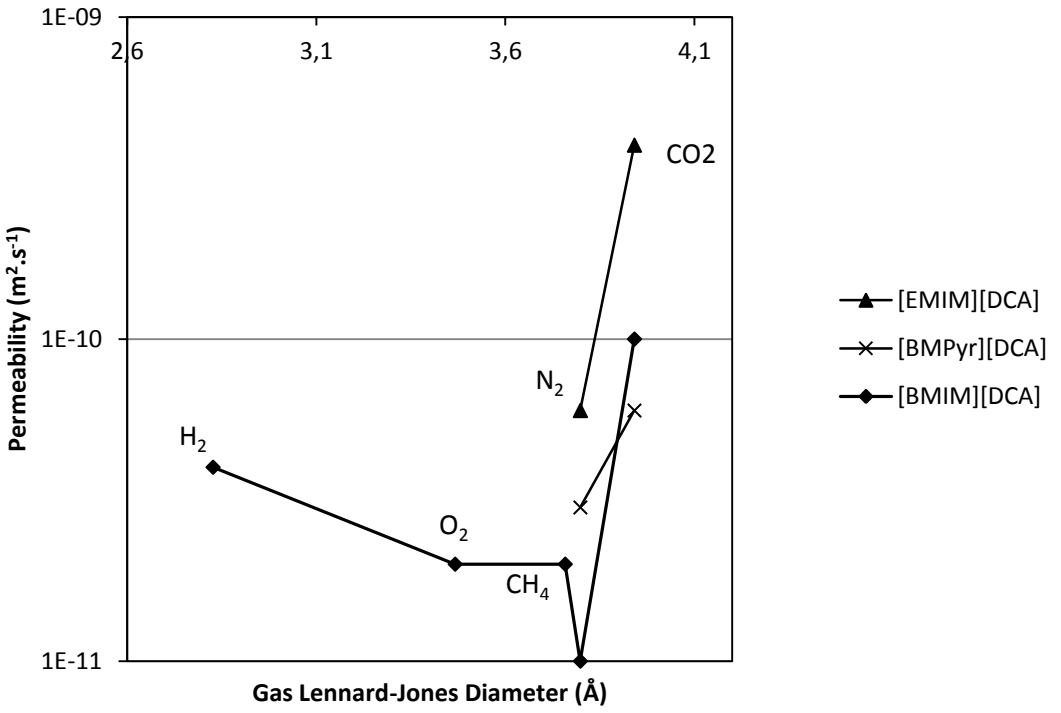

Figure 5.23 – Gas permeabilities of the Ion-Jelly® membranes as a function of the gas Lennard–Jones diameter.

Comparing our results with previously obtained results for SILMs, we can see the permeabilities are in the same order of magnitude, but with lower ideal selectivities [14].

For instance, when comparing [EMIM][DCA] Ion-Jelly® membrane with literature data for [EMIM][DCA] SILM, the permeability to CO_2 is slightly lower for the Ion-Jelly® case (480 and 610 barrer, respectively) whereas the selectivity for the CO_2/N_2 separation is 10 times lower (6,67 and 61, respectively) [5]. For the [BMIM][DCA] case, the permeability to CO_2 is even closer, with 200 barrer for the SILM [25] and 120 barrer for the Ion-Jelly® membrane, but the selectivity for the CO_2/N_2 separation is about 8 times lower (78 for the SILM and 10 for the Ion-Jelly® membrane). Furthermore, we can observe that these membranes have permeabilities and ideal selectivities similar to polymeric materials. For instance, the ideal selectivity for CO_2/CH_4 of the [BMIM][DCA] Ion-Jelly® membrane is similar to the one of natural rubber (4.6) [29].

Table 5.8 – Permeabilities of pure gases and calculated ideal selectivities.

RTIL used	Permeability ($m^{2}\cdot s^{-1}$)		Ideal Selectivity	
[EMIM][DCA]	CO_2	4.00×10^{-10}	CO_2/N_2	6.67
	N_2	6.00×10^{-11}		
[BMIM][DCA]	H_2	4.00×10^{-11}	CO_2/N_2	10
	O_2	2.00×10^{-11}	H_2/N_2	4
	CH_4	2.00×10^{-11}	CO_2/CH_4	5
	N_2	1.00×10^{-11}	CO_2/O_2	5
	CO_2	1.00×10^{-10}	CO_2/H_2	2.5
			H_2/O_2	2
			O_2/N_2	2
			CH_4/N_2	2
			H_2/CH_4	2
			O_2/CH_4	1
[BMPyr][DCA]	CO_2	6×10^{-11}	CO_2/N_2	2
	N_2	3×10^{-11}		

5.4 - Conclusions

In this Chapter SILMs and gel membranes with incorporated RTILS were developed, characterized and tested for the fractionation of several mixtures.

SILMs revealed much higher permeabilities to $scCO_2$ than the corresponding RO membranes alone. The slight selectivities that RO membranes presented to the model mixture of oleic acid and squalene has disappeared with the immobilization of RTILs. However, when one of these membranes was used in the fractionation of the products and reagents of a transesterification reaction it presented good results, retaining completely glycerol and triglycerides, and obtaining a permeate stream 85% rich in methyl esters.

In a first approach, gel membranes based in Ion-Jelly® were prepared with an evaporative casting-knife method. Contact angles measurements revealed that these membranes are porous and hydrophobic. $scCO_2$ permeability measurements showed that these membranes have higher permeability to $scCO_2$ than commercial reverse osmosis membranes, and that this permeability is related to the thickness of the Ion-Jelly® layer applied. SEM images showed that Ion-Jelly® forms a smooth, uniform layer on top of the cellulose support, and that it only penetrates the support when $scCO_2$ pressure is applied. The selectivities obtained with these membranes either for the model

mixture of oleic acid and squalene or the model mixture of methyl oleate and squalene are negligible. The evidences from elemental analysis, traction experiments, SEM images and from the discrepancies in $scCO_2$ fractionation revealed that the method of preparation of these membranes is not reproducible and presents flaws in the surface of the membranes, leading to the decision of altering the production method.

The glass plates pressed method of preparation of Ion-Jelly® membranes was developed to overcome the flaws in the membranes production method. The membrane of [EMIM][DCA] Ion-Jelly® prepared by this method revealed to be more hydrophilic than the membranes prepared with [BMIM][DCA] and [BMPyr][DCA]. The permeability to $scCO_2$ is now considerably lower than with the Ion-Jelly® membranes prepared with the previous method, and similar to the ones of commercial reverse osmosis membranes, although higher pressure drops can now be obtained. From SEM images is possible to see that Ion-Jelly® penetrates the cellulose support, covering the cellulose fibers and occupying the empty spaces between them, and that the application of $scCO_2$ presents no significative change in the membrane morphology. But these membranes still present no appreciable fractionation for the model mixture of oleic acid and squalene. In the fractionation of products and reactants from an enzymatic transesterification reaction, although this membrane presents a permeate less rich in methyl esters than that obtained with SILMs, it still presents very good retention factors for glycerol and monoglycerides. Elemental analysis shows that these membranes are not degraded with operation in $scCO_2$.

When testing the Ion-Jelly® membranes for the separation of gases, it was found that the permeabilities were similar to those reported in the literature for the corresponding SILMs. However, the selectivities are not significative when compared with those obtained with SILMs.

5.5 - References

[1] L. C. Branco, J. G. Crespo and C. A. M. Afonso; Studies on the Selective transport of Organic Compounds by Using Ionic Liquids as Novel Supported Liquid Membranes; Chem. Eur. J. 2002, 8, Nº. 17, 3865-3871.

[2] E. Miyako, T. Maruyama, N. Kamiya, M. Goto, Use of ionic liquids in a lipase-facilitated supported liquid membrane, Biotechnol. Lett. 25 (2003) 805-808.

[3] M. Matsumoto, Y. Inomoto, K. Kondo, Selective separation of aromatic hydrocarbons through supported liquid membranes based on ionic liquids, J. Membr. Sci. 246 (2005) 77–81.

[4] A.P. Ríos, F.J. Hernández-Fernández, H. Presa, D. Gómez, G. Víllora, Tailoring supported ionic liquid membranes for the selective separation of transesterification reaction compounds, J. Membr. Sci. 328 (2009) 81–85.

[5] P. Scovazzo, J. Kieft, D. Finan, R.D. Noble, C.A. Koval, Gas Separations Using Non-Hexafluorophosphate [PF6] - Anion Supported Ionic Liquid Membranes, J. Membr. Sci, 238 (2009) 57-64.

[6] Q. Gan, D. Rooney, M. Xue, G. Thompson, Y. Zou; An experimental study of gas transport and separation properties of ionic liquids supported on nanofiltration membranes; Journal of Membrane Science 280 (2006) 948–956.

[7] W. Zhao, G. He, L. Zhang, J. Ju, H. Dou, F. Nie, C. Li, H. Liu; Effect of water in ionic liquid on the separation performance of supported ionic liquid membrane for CO2/N2; Journal of Membrane Science 350 (2010) 279–285.

[8] Q. Gan, Y. Zou, D. Rooney, P. Nancarrow, J. Thompson, L. Liang, M. Lewis; Theoretical and experimental correlations of gas dissolution, diffusion, and thermodynamic properties in determination of gas permeability and selectivity in supported ionic liquid membranes; Advances in Colloid and Interface Science 164 (2011) 45–55.

[9] A. P. de los Ríos, F. J. Hernández-Fernández, F. Tomás-Alonso, J.M. Palacios, G. Víllora; Stability studies of supported liquid membranes based on ionic liquids: Effect of surrounding phase nature; Desalination 245 (2009) 776–782.

[10] F.J. Hérnandez-Férnandez, A.P. de los Ríos, F. Tomás-Alonso, J.M. Palacios, G. Víllora; Preparation of supported ionic liquid membranes: Influence of the ionic liquid immobilization method on their operational stability; Journal of Membrane Science 341 (2009) 172–177.

[11] R. Fortunato, C. A.M. Afonso, M.A.M. Reis, J. G. Crespo; Supported liquid membranes using ionic liquids: study of stability and transport mechanisms; Journal of Membrane Science 242 (2004) 197–209.

[12] R. Fortunato, C. A.M. Afonso, J. Benavente, E. Rodriguez-Castellón, J. G. Crespo; Stability of supported ionic liquid membranes as studied by X-ray photoelectron spectroscopy; Journal of Membrane Science 256 (2005) 216–223.

[13] P. Cserjési, N. Nemestóthy, K. Bélafi-Bakó; Gas separation properties of supported liquid membranes prepared with unconventional ionic liquids; Journal of Membrane Science 349 (2010) 6–11.

[14] L. A. Neves, J. G. Crespo, I. M. Coelhoso; Gas permeation studies in supported ionic liquid membranes; Journal of Membrane Science 357 (2010) 160–170.

[15] B. A. Voss, J. E. Bara, D. L. Gin, R. D. Noble; Physically Gelled Ionic Liquids: Solid Membrane Materials with Liquidlike CO2 Gas Transport; Chem. Mater. 2009, 21, 3027–3029.

[16] I.-N. Yoon, S. Yoo, S.-J. Park, J. Won; CO2 separation membranes using ion gels by self-assembly of a triblock copolymer in ionic liquids; Chemical Engineering Journal 172 (2011) 237– 242.

[17] J. C. Jansen, K. Friess, G. Clarizia, J. Schauer, P. Izák; High Ionic Liquid Content Polymeric Gel Membranes: Preparation and Performance; Macromolecules 2011, 44, 39–45.

[18] P. Vidinha, N. M. T. Lourenço, C. Pinheiro, A. R. Brás, T. Carvalho, T. Santos-Silva, A. Mukhopadhyay, M. J. Romão, J. Parola, M. Dionisio, J. M. S. Cabral, C. A. M. Afonso and S. Barreiros; Ion jelly: a tailor-made conducting material for smart electrochemical devices; Chem. Commun., 2008, 5842–5844.

[19] A. F.R. Pimenta, A. C. Baptista, T. Carvalho, P. Brogueira, N. M.T. Lourenço, C. A.M. Afonso, S. Barreiros, P. Vidinha, J. P. Borges; Electrospinning of Ion Jelly fibers; Materials Letters 83 (2012) 161–164.

[20] B.S. Furniss, A.J. Hannaford, P.W.G. Smith, A.R. Tachtell, Vogel's Textbook of Practical Organic Chemistry, fifth ed., Longmann Scientific & Technical, England, 1989.

[21] E.L. Cussler, Diffusion, second ed., Cambridge University Press, Cambridge, 1997.

[22] M. S. Manic, A. J. Queimada, E. A. Macedo, V. Najdanovic-Visak; High-pressure solubilities of carbon dioxide in ionic liquids based on bis(trifluoromethylsulfonyl)imide and chloride; J. of Supercritical Fluids 65 (2012) 1– 10.

[23] P. Carvalho, V. Álvarez, I. Marrucho, M. Aznar, J. Coutinho; High pressure phase behavior of carbon dioxide in 1-butyl-3-methylimidazolium bis(trifluoromethylsulfonyl)imide and 1-butyl-3-methylimidazolium dicyanamide ionic liquids; J. of Supercritical Fluids 50 (2009) 105–111.

[24] W. Zhao, G. He, F. Nie, L. Zhang, H. Feng, H. Liu, Membrane liquid loss mechanism of supported ionic liquid membrane for gas separation Journal of Membrane Science 411– 412 (2012) 73– 80.

[25] A. Clarke, T. D. Blake, K. Carruthers, A. Woodward; Spreading and Imbibition of Liquid Droplets on Porous Surfaces; Langmuir 2002, 18, 2980-2984.B.E. Poling, J.M. Prausnitz, J.P. O'Connell, The Properties of Gases and Liquids, fifth ed., McGraw-Hill International Editions, 2001.

[26] R. Ruivo, A. Paiva, P. Simões; Phase equilibria of the ternary system methyl oleate/squalene/carbon dioxide at high pressure conditions; J. of Supercritical Fluids 29 (2004) 77–85

[27] B. Poling, J. Prausnitz, J. O'Connel; The Properties of Gases and Liquids; 5th edition, McGraw-Hill, New York, 2001.

[28] P. Jindaratsamee, Y. Shimoyama, H. Morizaki, A. Ito; Effects of temperature and anion species on CO_2 permeability and CO_2/N_2 separation coefficient through ionic liquid membranes; J. Chem. Thermodynamics 43 (2011) 311–314.

[29] M. Mulder; Basic Principles of Membrane Technology; Kluwer Academic Publishers, 1st ed., Dordrecht, 1996.

Chapter 6

Conclusions and Future Work

In this thesis were explored fractionations of mixtures with supercritical carbon dioxide ($scCO_2$), room temperature ionic liquids (RTILs) and membranes. The first case tested was with commercial reverse osmosis (RO) membranes in $scCO_2$. Then, fractionations with RTILs were performed as a screening in order to choose adequate RTILs to produce supported ionic liquid membranes (SILMs). In view of the results obtained with the fractionations with RTILs was developed an indirect method to probe the polarity of RTILs, in order to explain the fractionations observed. Finally, SILMs and Ion-Jelly® membranes were developed and tested based on the knowledge obtained with the previous experiments.

In the experiments with RO membranes it was found that the permeability to $scCO_2$ is not dependent on the pressure applied on the retentate side of the membrane, in the range of 18 to 22 MPa. It was also found that all membranes are selective towards oleic acid, with polyamide AD being the less selective and cellulose acetate the more selective, although with lower permeate fractions obtained.

By coupling supercritical fluid extraction (SFE) in a countercurrent packed column with separation in Polyamide AD membrane it was possible to obtain an enrichment in squalene of 1.6 times.

When it was tried to separate a mixture analogous to the retentate of the column with membranes, it was very difficult to achieve results due to the impossibility of pumping liquids with high amounts of dissolved gas, and to the low contact times of the model mixture with the membrane in these conditions. In the cases in which it was possible to obtain permeate fraction, either there was no selectivity or this was negligible.

The fractionation of a model mixture using room temperature ionic liquids as the extracting agent was investigated for a range of imidazolium, phosphonium and ammonium based ionic liquids. It was shown that it is possible to adjust the fractionation of the oil mixture by adequately choosing the type of anion and cation of the room temperature ionic liquid. It was also shown that by altering the proportions of ionic liquid and mixture to be extracted is possible to further adjust the fractionation.

In order to explain the effects observed in the fractionation of a model mixture with RTILs, it was developed an indirect method to probe the polarity of RTILs. This method consisted in the addition of small quantities of RTILs to common organic solvents with a polarity probe dissolved, and the deviations in the polarity observed were related to the original polarity of the RTILs.

It was seen that the influence in solvent polarity is more linked to the cation than the anion. For all the cases studied, the polarity of the solvent increased with the addition of RTIL and the continuous addition is linearly correlated to the increase in polarity. The only exception is $[C_2OHMIM][BF_4]$, which decreases the polarity of ethanol with the first addition, but with further additions it also increased the value of polarity. The increase in polarity in acetonitrile (the solvent with more RTILs studied) can be generically described following the cation sequence $[(C_6)_3C_{14}P]$<[BDMIM]<[ALIQUAT]<[EMIM]<[BMIM].

Ethanol presented the polarity scale more in accordance with the already published values for pure RTILs. This is probably a result of closer polarity of ethanol to those of the pure RTILs. It was concluded that fractionation of oleic acid in RTILs increases with decreasing polarity. However, it was also seen that ethanol is less sensitive to the changes in polarity than acetonitrile.

SILMs developed in this work revealed much higher permeabilities to $scCO_2$ than the corresponding RO membranes alone. The slight selectivities that RO membranes presented to the model mixture of oleic acid and squalene have disappeared with the immobilization of RTILs. However, when one of these membranes was used in the fractionation of the products and reagents of a transesterification reaction it presented good results, retaining completely glycerol and triglycerides, and obtaining a permeate stream 85% rich in methyl esters. One could infer that if the transesterification reaction would be complete then the permeate would consist only in methyl esters and methanol.

In a first approach, gel membranes based in Ion-Jelly® were prepared with an evaporative casting-knife method. Contact angles measurements revealed that these membranes are porous and hydrophobic. $scCO_2$ permeability measurements showed that these membranes have higher permeability to $scCO_2$ than commercial reverse osmosis membranes, and that this permeability is related to the thickness of the Ion-Jelly® layer applied. Scanning electron microscopy (SEM) images showed that Ion-Jelly® forms a layer on top of the cellulose support, and that it only penetrates the support when $scCO_2$ pressure is applied. The selectivities obtained with these membranes either for the model mixture of oleic acid and squalene or the model mixture of methyl oleate and squalene are negligible. The evidences from elemental analysis, traction experiments, SEM images and from the discrepancies in $scCO_2$ fractionation of model mixtures revealed that the method of preparation of these membranes is not reproducible and presents flaws in the surface of the membranes, leading to the decision of altering the production method.

The glass plates pressed method of preparation of Ion-Jelly® membranes was developed to overcome the flaws detected with the former membranes production method. The membrane of

[EMIM][DCA] Ion-Jelly® prepared by this method revealed to be more hydrophilic than the membranes prepared with [BMIM][DCA] and [BMPyr][DCA]. The permeability to $scCO_2$ is now considerably lower than with the Ion-Jelly® membranes prepared with the previous method, and similar to the ones of commercial reverse osmosis membranes, although higher pressure drops can now be obtained. From SEM images it is possible to see that ion-jelly penetrates the cellulose support, covering the cellulose fibers and occupying the empty spaces between them, and that the application of $scCO_2$ presents no significative change in the membrane morphology. But these membranes still present no appreciable fractionation for the model mixture of oleic acid and squalene. In the fractionation of products and reactants from an enzymatic transesterification reaction, although this membrane presents a permeate less rich in methyl esters than that obtained with SILMs, it still presents very good retention factors for glycerol and monoglycerides. Elemental analysis shows that these membranes are not degraded with operation in $scCO_2$. It is thus proven that gel membranes can be used for fractionations in $scCO_2$ with stability.

When testing the Ion-Jelly® membranes for the separation of gases at low pressures, it was found that the permeabilities were similar to those reported in the literature for the corresponding SILMs. However, the selectivities are not significative when compared with those obtained with SILMs.

As future work to be conducted, the influence of feed and solvent flows in the separations with membranes could be tested. In view of the results obtained in Chapter 5, other mixtures could as well be tested with RO membranes (for example the products and reactants of the transesterification reaction).

In the coupling of membranes with SFE in a countercurrent packed column, other pressures, temperatures and membranes could be tested.

More RTILs should be tested for their influence in solvent polarity with ethanol, as this was the solvent which presented results more in accordance with published results for pure RTILs. Other polarity probes could as well be explored. The change in polarity observed in organic solvents with the addition of RTILs could be explored for the fractionation of mixtures.

Further tests with SILMs could be conducted concerning the coupling of an enzymatic reactor with SILMs, in order to optimize the process. Parameters like temperature, pressure, flow ratios, reactor geometry and enzyme content could be explored. Other SILMs could also be tested. Methanol could be replaced by ethanol and the separation of ethyl esters thus produced could be tested, being expected that the results should be similar to those obtained with methyl esters. These same tests are applicable also for IJ membranes.

There is probably still space to further improve the process of production of IJ membranes, in order to increase the reproducibility of the method and to facilitate the elimination of air bubbles. Better pressing equipment could be used, in order to apply more pressure in a more uniform way. The fluidity of the Ion-Jelly®, when it is still hot and liquid, could also be assessed in order to eliminate air bubbles. One approach which might be used could be to apply ultrasounds immediately before spreading the Ion-Jelly® on top of the cellulose layer.

Appendix

Complete E_T^N Tables

Table A.1 – E_T^N values for acetonitrile.

	E_T^N values							
Vol. RTIL Added (µL)	2	4	6	8	10	15	20	25
[ALIQUAT][Cl]	0.462	0.462	0.465		0.466			
[ALIQUAT][DCA]	0.466	0.465	0.466		0.469			
$[(C_6)_3C_{14}P][Cl]$	0.465	0.465	0.466					
$[(C_6)_3C_{14}P][BF_4]$	0.462	0.462	0.464		0.465			
$[(C_6)_3C_{14}P][NTf_2]$	0.465	0.465	0.463		0.464			
$[(C_6)_3C_{14}P]$ [DCA]	0.462	0.462	0.462		0.465			
$[EMIM][NTf_2]$	0.694	0.712	0.713		0.715			
$[EMIM][EtSO_4]$	0.462	0.469	0.473		0.482			
$[EMIM][MDEGSO_4]$	0.467	0.472	0.480		0.487			
[BMIM][Cl][a]	0.469	0.470	0.480					
$[BMIM][PF_6]$	0.466	0.473	0.477	0.482	0.486	0.497		
$[BMIM][BF_4]$	0.467	0.474	0.477	0.481	0.487	0.496	0.504	
$[BMIM][NTf_2]$	0.465	0.473	0.480		0.500			
[BMIM][DCA]	0.467	0.470	0.477		0.481			
[OMIM][Cl]	0.466	0.470	0.475		0.482			
$[OMIM][PF_6]$	0.462	0.462	0.466	0.470	0.473	0.482	0.492	0.496
$[OMIM][BF_4]$	0.466	0.470	0.473		0.481			
$[OMIM][NTf_2]$	0.473	0.477	0.480		0.491			
[OMIM][DCA]	0.469	0.473	0.477					
$[C_{10}MIM][BF_4]$	0.582	0.598	0.623	0.634				
[BDMIM][Cl][b]	0.463	0.468	0.469	0.472				
$[BDMIM][BF_4]$[c]	0.463	0.465	0.465	0.466				
$[BDMIM][NTf_2]$	0.465	0.465	0.466					
$[C_2OHMIM][PF_6]$	0.600	0.617	0.636		0.650			
$[C_2OHMIM][BF_4]$	0.466	0.469	0.473		0.481			
$[C_3OMIM][Cl]$[d]	0.467	0.472	0.466	0.468				
$[C_3OMIM][PF_6]$[e]	0.465	0.473	0.480	0.495				
$[C_3OMIM][BF_4]$	0.473	0.479	0.484					
$[C_5O_2MIM][Cl]$	0.470	0.474	0.480		0.488			
$[C_5O_2MIM][PF_6]$[f]	0.465	0.469	0.476	0.484				
[DMG][Cl][g]	0.462	0.462	0.462	0.462	0.464	0.465	0.465	

All ionic liquids were liquid at room temperature and added pure to acetonitrile. The exceptions were a-c, e, f which were solid at room temperature and d, g which were first diluted in acetonitrile and then added to the solution with Reichardt's dye. The amounts added for these cases are as follows: a) 1.1 mg; 1.8 mg; 5.7 mg; b) 1.3 mg; 4.2 mg; 6.5 mg; 13.2 mg; c) 1.9 mg; 5.2 mg; 6.5 mg; 8.1 mg; d) 0.1 µL; 0.12 µL; 0.14 µL; 0.16 µL; e) 1.4 mg; 5.0 mg; 7.7 mg: 16.6 mg; f) 0.5 mg; 1.6 mg; 4.7 mg; 8.6 mg; g) 0.02 µL; 0.07 µL; 0.2 µL; 0.3 µL; 0.4 µL; 0.5 µL; 0.6 µL.

Table A.2 - E_T^N values for Ethanol.

	E_T^N values							
Vol. RTIL Added (µL)	2	4	6	8	10	12	18	20
[EMIM][$EtSO_4$]	0.661	0.661	0.664					
[EMIM][$MDEGSO_4$]	0.664	0.658	0.667					
[BMIM][PF_6]	0.661	0.661	0.667					
[BMIM][BF_4]	0.661	0.658	0.664		0.670	0.666	0.672	0.680
[BMIM][NTf_2]	0.660	0.660	0.661	0.663	0.669	0.669	0.675[a]	
[BMIM][DCA]	0.658	0.658	0.661			0.669	0.672	
[OMIM][PF_6]	0.655	0.658	0.663					
[OMIM][BF_4]			0.661			0.666	0.667	
[C_{10}MIM][BF_4]	0.661	0.667	0.670	0.670				
[C_2OHMIM][BF_4]		0.654[b]	0.666	0.669	0.675[c]	0.681		

All ionic liquids were liquid at room temperature and added pure to ethanol. a: 14 µL; b: 3 µL; c: 9 µL.

Table A.3 - E_T^N values for Tetrahydrofuran.

	E_T^N values				
Vol. RTIL Added (µL)	2	4	6	8	10
[BMIM][PF_6]	0.416	0.430	0.435		
[BMIM][BF_4]	0.389	0.389	0.407	0.422	0.434
[OMIM][PF_6]	0.399	0.415	0.424	0.429	
[C_{10}MIM][BF_4]	Forms emulsion				

All ionic liquids were liquid at room temperature and added pure to tetrahydrofuran.

Table A.4 – E_T^N values for Pre-dried Tetrahydrofuran.

	E_T^N values							
Vol. RTIL Added (µL)	2	4	6	8	10	15	20	25
[BMIM][PF_6]	0.406	0.405	0.414	0.416	0.424	0.436	0.442	0.446
[BMIM][BF_4]	0.360	0.391	0.408	0.422	0.430	0.443		

All ionic liquids were liquid at room temperature and added pure to pre-dried tetrahydrofuran.

Table A.5 – E_T^N values for Chloroform.

	E_T^N values							
Vol. RTIL Added (μL)	2	4	6	8	10	15	20	25
[BMIM][PF_6]		Forms emulsion						
[BMIM][BF_4]	0.367	0.376	0.402	0.421	0.429	0.448	0.459	
[OMIM][PF_6]	0.332	0.389	0.411	0.427	0.443	0.459	0.468	0.475
[C_{10}MIM][BF_4]		Forms emulsion						

All ionic liquids were liquid at room temperature and added pure to chloroform.

Table A.6 – E_T^N values for isopropanol.

	E_T^N values			
Vol. RTIL Added (μL)	2	4	6	10
[BMIM][PF_6]	0.552	0.559	0.568	
[BMIM][BF_4]	0.547	0.553	0.565	0.578
[OMIM][PF_6]	0.552	0.562	0.573	0.585
[C_{10}MIM][BF_4]	0.555	0.568	0.581	

All ionic liquids were liquid at room temperature and added pure to isopropanol.